Analysis of the low molecular weight peptides of selected snake venoms

Dissertation

zur Erlangung des Doktorgrades der Naturwissenschaften

an der Fakultät für Mathematik, Informatik und Naturwissenschaften

der Universität Hamburg

vorgelegt von

Aisha Munawar (M. Phil)

aus Lahore, Pakistan

Hamburg 2012

Die vorliegende Arbeit wurde im Zeitraum von Juli 2009 bis September 2012 in der Arbeitsgruppe von Prof. Betzel am Institut für Biochemie und Molekularbiologie am Fachbereich Chemie der Universität Hamburg angefertigt.

Gutachter:

Herr Prof. C. Betzel

Herr Prof. A. Torda

Tag der Disputation: 26-11-2012

With love to my kids, Ahmad and Amna

Abstract

Snake venom peptidomes are valuable sources of pharmacologically active compounds. The peptidic fractions (peptides with molecular masses up to 10,000 Da) of the venoms of *Vipera ammodytes meridionalis* (Viperinae), the most toxic snake in Europe, *Bothrops jararacussu* (Crotalinae), an extremely poisonous snake in South America, *Naja mossambica mossambica* (Elapinae), a snake from Africa and *Notechis ater niger* (Acanthophiinae), distributed on the south coast of Australia having a very lethal venom, were analyzed. Liquid chromatography coupled to mass spectrometry (LC/MS), direct infusion electrospray mass spectrometry (ESI-MS) and matrix-assisted laser desorption/ionization time-of-flight mass spectrometry (MALDI-TOF-MS) were applied to characterize the peptides of the four snake venoms. 32 bradykinin-potentiating peptides (BPPs) were identified in the Crotalinae venom and their sequences were determined. 3 metalloproteinase inhibitors, 10 BPPs and a Kunitz-type inhibitor were observed in the Viperinae venom peptidome. 3 cytotoxins, 5 BBPs and one bradykinin inhibitor peptide were found in the Elapinae venom. Two neurotoxins, two Kunitz/BPTI type inhibitors and one natriuretic peptide were identified in the Acanthophiinae venom. Variability in the C-terminus of homologous BPPs was observed, which can influence the pharmacological effects. The data obtained so far shows a subfamily specificity of the venom peptidome in the Viperidae and Elapidae family: BPPs are the major peptide component of the Crotalinae venom peptidome lacking Kunitz-type inhibitors (with one exception) while the Viperinae and Acanthophiinae venom, in addition to BPP or natriuretic peptides, can contain peptides of the bovine pancreatic trypsin inhibitor family. The venoms of Elapidae family contain three finger toxins which have not been found in the Viperidae family and the absence of three finger toxin type of peptides in the Viperidae venom can mark the point of difference between the Elapidae and Viperidae family. Among the Elapidae family variations were also observed at the subfamily level. The Elapinae family contains cytotoxin type of three finger toxin, while that of Acanthophiinae venom lacks cytotxic peptides and instead contains neurotoxin type of three finger toxins. The Acanthophiinae family contains Kunitz/BPTI inhibitors which were not observed in the Elapinae venom. The MALDI-TOF mass spectrometry provided information for the post-translational phosphorylation of serine residues in *Bothrops jararacussu* venom BPP (SQGLPPGPPIP), which could be a regulatory mechanism in their interactions with ACE, and might influence the hypotensive effect. Homology between venom BPPs from Viperidae snakes and venom

natriuretic peptide precursors from Elapidae snakes suggests a structural similarity between the respective peptides from the peptidomes of both snake families. The Kunitz/BPTI type inhibitors isolated from the venoms of Viperinae and Acanthophiinae subfamily are also homologous to each other, but show variation of the reactive bond residues even within the same venom, suggesting that nature has engineered these peptides to perform a variety of functions by incorporating subtle mutations at convex and exposed binding loop. The results demonstrate that the venoms are rich sources of peptides influencing important physiological systems such as blood pressure regulation, hemostasis, and nervous system. The molecular models of the catalytic complexes of BPP-human ACE and Kunitz/BPTI-serine protease provide insights into the probable binding modes and interactions at the protein-ligand interface. The data can support pharmacological and medical applications.

Zusammenfassung

Die Peptidome von Schlangengifte sind wertvolle Quellen von pharmakologisch wirksamen Verbindungen. In der vorliegenden Arbeit wurden die peptidischen Fraktionen (Peptide mit einem Molekulargewicht von weniger als von 10,000 Da) der Gifte von *Vipera ammodytes meridionalis* (Viperinae), der giftigsten Schlange Europas, *Bothrops jararacussu* (Crotalinae), einer extrem giftigen Schlange aus Südamerika, *Naja mossambica mossambica* (Elapinae), der gefährlichsten Schlange Afrikas und *Notechis ater niger* (Acanthophiinae), von der Südküste Australiens mit einem sehr tödlichen Gift, analysiert. Flüssigkeits-Chromatographie gekoppelt mit Massenspektrometrie (LC/MS), Elektrosprayionisations-Massenspektrometrie per direkter Probeninfusion (ESI-MS) und Matrix-Assisted Laser Desorption/Ionisation Time-of-Flight-Massenspektrometrie (MALDI-TOF-MS) wurden angewandt, um die Peptide der vier Schlangengifte zu charakterisieren. Im Gift der Crotalinae wurden 32 Bradykinin-potenzierende Peptide (BPPs) identifiziert und ihre Sequenzen wurden bestimmt. Im Peptidom des Viperinae-Gifts wurden 3 Metalloproteinase-Inhibitoren, 10 BPPs und ein Kunitz-Typ-Inhibitor beobachtet. Drei zytotoxische Komponenten, 5 BBPs und ein Bradykinin-Inhibitor-Peptid wurden im Elapinae-Gift gefunden. Zwei Neurotoxine, zwei Kunitz-/BPTI-Typ-Hemmstoffe und ein natriuretisches Peptid wurden im Acanthophiinae-Gift identifiziert. Eine Variabilität am C-Terminus von homologen BPPs, die die pharmakologischen Wirkungen beeinflussen kann, wurde beobachtet. Die erhaltenen Daten zeigen eine Spezifität der Gifte in den Unterfamilien im Peptidom der Viperidae- und Elapidaefamilie: BPPs sind die wichtigsten Peptidkomponenten des Crotalinae-Gift-Peptidoms. In diesem fehlen Kunitz-Typ Inhibitoren (mit einer Ausnahme), während das Gift von Viperinae und Acanthophiinae, zusätzlich zu BPPs oder natriuretischen Peptiden, Peptide der Bovin-Trypsin-Inhibitor-Familie enthalten können. Die Gifte der Elapidae-Familie enthalten sogenannte Dreifinger-Toxine (three finger toxins), die nicht in der Viperidae-Familie gefunden wurden. Das Fehlen von Dreifinger-Giftstoffen im Gift von Viperidae ist der entscheidende Unterschied zwischen dem Gift der Elapidae- und Viperidae-Familien.

Innerhalb der Elapidae-Familie wurden auch auf der Subfamilien-Ebene Unterschiede in der Zusammensetzung des Giftes beobachtet. Das Gift der Elapinae-Familie enthält Cytotoxin vom Typ des Dreifinger-Toxins, dies fehlt im Gift der Acanthophiinae welches stattdessen Neurotoxine vom Typ der Dreifinger-Toxine enthält. Die Acanthophiinae-Familie enthält Kunitz-/BPTI-Inhibitoren, die nicht im Gift der Elapinae-Familie gefunden werden konnten. Die

MALDI-TOF-Massenspektrometrie ergab einen Anhaltspunkt für die post-translationale Phosphorylierung von Serin im BPP aus dem Gift von *Bothrops jararacussu* (SQGLPPGPPIP). Dies könnte ein Regulationsmechanismus in ihren Interaktionen mit ACE sein und die blutdrucksenkende Wirkung beeinflussen. Die Homologie zwischen BPPs von Viperidae-Schlangen und den Vorstufen des natriuretischen Peptids im Gift von Elapidae-Schlangen verweist auf eine strukturelle Ähnlichkeit zwischen den jeweiligen Peptiden beider Schlangenfamilien. Die Kunitz-/BPTI-Typ-Inhibitoren, die aus den Giften der Viperinae und Acanthophiinae-Unterfamilie isoliert wurden, sind auch homolog zueinander, zeigen aber Unterschiede bei ihren reaktiven Bindungsstellen, selbst innerhalb desselben Giftes, was darauf hindeutet, dass durch Einbau von kleinen Mutationen an konvex und freiliegenden bindenden Loops diese Peptide verschiedene Funktionen haben. Die Ergebnisse zeigen, dass die Gifte von vier Schlangen reiche Quellen für Peptide sind, die wichtige physiologische Systeme wie Regulierung des Blutdrucks, Hämostase und das Nervensystem beeinflussen. Die molekularen Modelle der katalytischen Komplexe von BPP aus Schlangengiften mit menschlichem tACE und der Kunitz-/BPTI in Komplex mit Serinproteasen gibt Einblicke in die wahrscheinlichen Bindungsmodi und Wechselwirkungen an der Protein-Ligand-Schnittstelle. Die Daten können für pharmakologische und medizinische Anwendungen verwendet werden.

Table of Contents

List of Abbreviations

A	Absorbance
l	Length of Spectrophotometer Cell
C	Concentration
ACE	Angiotensin Converting Enzyme
AChR	Acetylcholine receptor
ACN	Acetonitrile
BPP	Bradykinin potentiating Peptide
ANP	A type natriuretic peptide
BNP	B type natriuretic peptide
CNP	C type natriuretic peptide
CID	Collision Induced Dissociation
CRISP	Cysteine-rich secretory proteins
2DE	2 Dimensional Eleophoresis
ε	Extinction coefficient
λ_{ex}	Excitation Wavelength
λ_{em}	Emission Wavelength
ESI	Electrospray Ionization
3FTx	Three Finger Toxin
FTC	Fluorescein thiocarbamoyl-casein
FITC	Fluorescein isothiocyanate
FTICR	Fourier Transform Ion Cyclotron Resonance
FPLC	Fast Protein Liquid Chromatography
GBL	Galactose binding Lectins
Hex	Hexoe
HexNAc	N-acetylhexoseamine
HPLC	High Performance Liquid Chromatography
HIV	Human immunodeficiency virus

HCl	Hydrochloric acid
MALDI-TOF	Matrix Assisted Laser Desorption Ionization- Time of Flight
MS	Mass spectrometry
M	Protein marker
NCBI	National Center for Biotechnology Information
NeuAc	N-acetylneuraminic
NMR	Nuclear Magnetic Resonance
NP	Natriuretic Peptide
PAGE	Polyacrylamide Gel Electrophoresis
PLA_2	Phospholipase A_2
QTOF	Quadruple Time of Flight
RPC	Reverse Phase Chromatography
SDS	Sodium Dodecyl Sulphate
SEC	Size Exclusion Chromatography
SVMP	Snake Venom Metalloproteinase
SVSP	Snake Venom Serine Proteinase
StmPr1	*Stenotrophomonas maltophilia* Protease 1
T	Temperature
Tris	Tris (hydroxymethyl) aminomethane
VEGFs	Vascular endothelial growth factors
NEGFs	Nerve endothelial growth factors
η	Viscosity
λ	Wavelength
WHO	World Health Organization

Symbols for Amino Acids

A	Ala	Alanine
R	Arg	Arginine
N	Asn	Asparagine
D	Asp	Aspartate
C	Cys	Cysteine
E	Glu	Glutamate
Q	Gln	Glutamine
G	Gly	Glycine
H	His	Histidine
I	Ile	Isoleucine
L	Leu	Leucine
K	Lys	Lysine
M	Met	Methionine
F	Phe	Phenylalanine
P	Pro	Proline
S	Ser	Serine
T	Thr	Threonine
W	Trp	Tryptophan
Y	Tyr	Tyrosine
V	Val	Valine
Z	Pyr	Pyroglutamate

Introduction

1.1: Snake venom

Snake venom is an exquisitely complex mixture of hundreds of compounds, as proteins, peptides, carbohydrates, nucleosides, amines, free amino acids and lipids. Protein and peptide components comprise 90–95% of the dry weight of the venom [1, 2]. Snakes use their venoms as an offensive weapon in incapacitating and immobilizing their prey, as a defensive tool against their predators, and to aid in digestion, and hence use it as a tool to survive in their particular environment. Venomous snakes in the family *Viperidae* and *Elapidae* have a complex mixture of distinct toxic proteins produced in the specialized venom glands located in the upper jaw, which they inject into the prey using fang [3].

Scientists all over the world, study snake venoms and toxins by focusing one or more of the following objectives, i) to determine the mode and mechanism of action of the toxins, ii) to develop antivenoms/antidotes to neutralize the adverse effects of snake venom envenomation, iii) to understand the physiological processes both at cellular and molecular level and to design novel medicines, iv) to develop archetypes of pharmacological agents based on the structure of the toxins, and v) to understand the ecological niche and evolutionary relationship of the snakes [4, 5].

By now a large number of snake venom proteins have been purified and characterized. Some of them exhibit enzymatic activities, whereas others are non enzymatic proteins and polypeptides. Based on their structures, they can be grouped into families (summarized in Fig. 1) [6]. The members of a single family show remarkable similarities in their primary, secondary and tertiary structures, but they often exhibit distinct pharmacological effects [7].

Venom proteins are subjected to accelerated Darwinian evolution [8], and variability of venom composition at the genus, species, subspecies, population and individual levels may endow snakes with the capability to adapt to different ecological niches [9].

In 1994 Marc Wilkins developed the concept of proteome and coined the term [10]. In 1997 he co-wrote and co-edited the first book on proteomics [11]. Proteomics analysis of snake venoms, also known as “snake venomics”, is greatly expanding the knowledge and understanding of these complex secretions, vital to snakes but potentially fatal to humans. The advancement of

proteomic tools, during the recent years, have accelerated the work in unraveling the venom composition, and therefore paving the way for a deeper understanding of their biological, functional and clinical implications [12][and references therein].

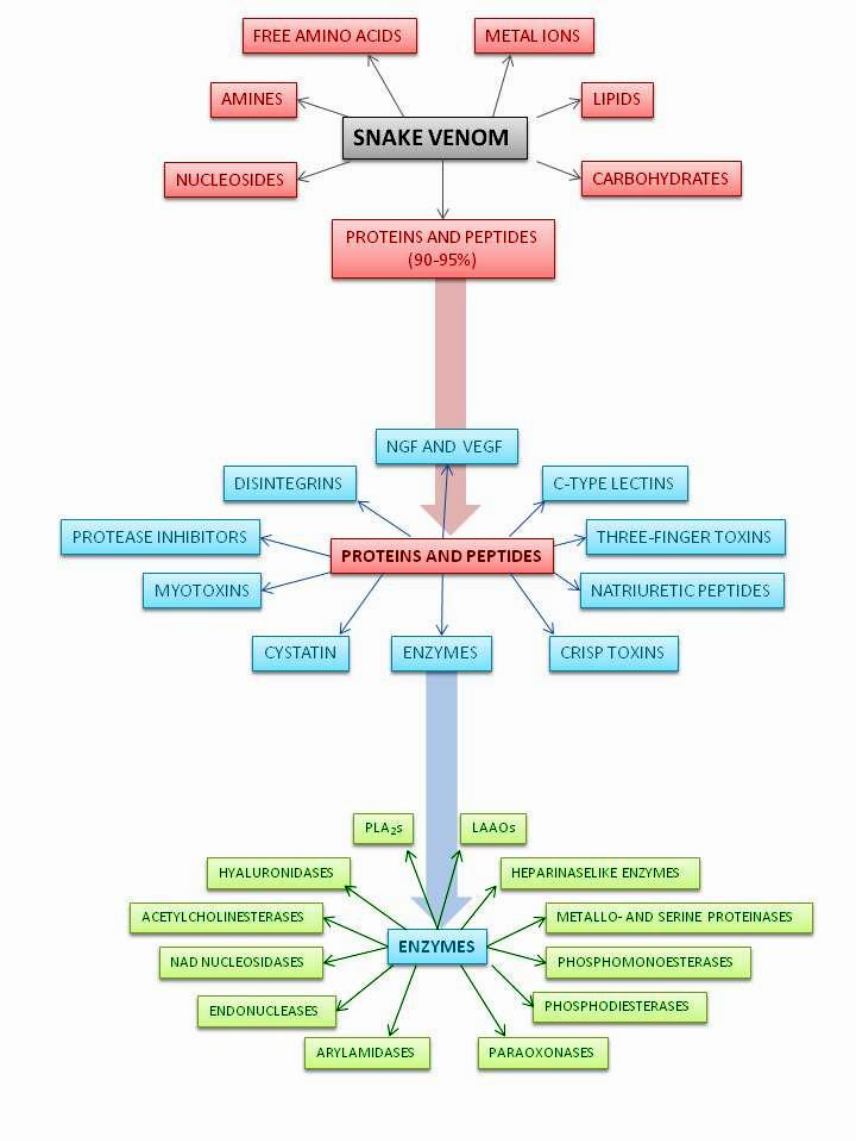

Fig. 1: Composition of the snake venom [6].

Snake venom consists of a wide range of proteins, with a complex proteome. Therefore it is not possible to visualize every component of a proteome using a single proteomic technique. Recent publications in the field of venomics have emphasized the need for multifaceted approaches to

maximize the protein coverage [6, 13]. Recently, the combinatorial peptide library approach (commercialized as Proteominer ^{TM}) has emerged as a powerful tool for mining below the tip of the iceberg, and complements the data gained using the snake venomics protocol towards a complete visualization of the venom proteome [14]. A general scheme of the steps to be followed in a snake venomic analysis is shown in Fig. 2.

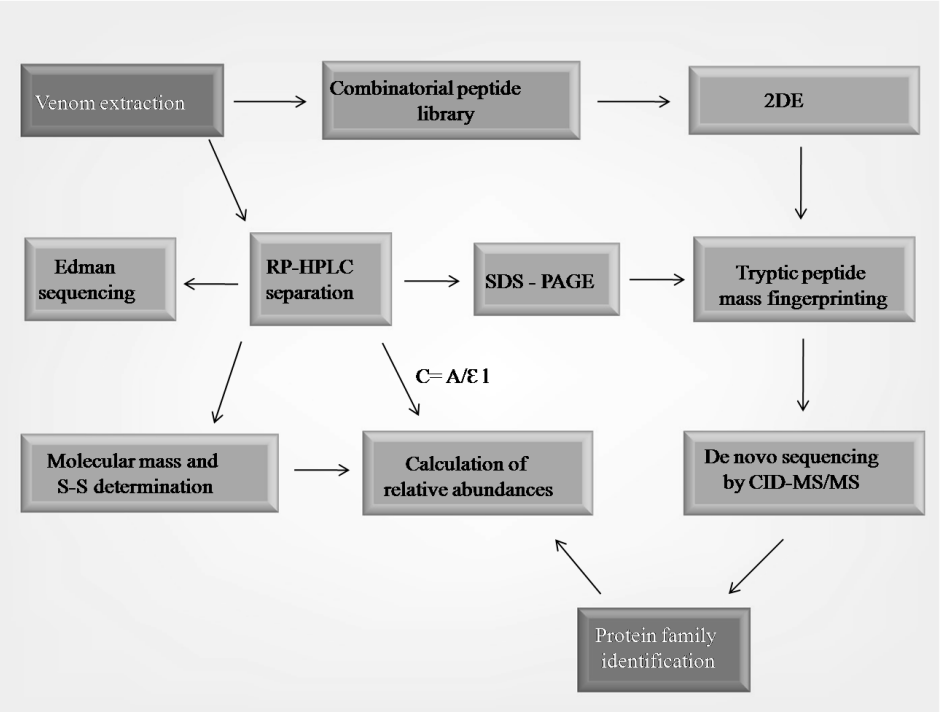

Fig. 2: Scheme of the steps typically performed in a snake venomics analyis. CID: Collision induced dissociation; RP-HPLC: Reverse phase HPLC [14].

The proteomic approach has given rise to a comprehensive understanding of the venom complexity, composition, and relative abundance of different protein families, and provides insights to investigators to focus on different issues and identification of novel proteins [15-26].

Studies have shown that the chemical composition of the venoms exhibit geographical variations and may be due to evolutionary environmental pressure acting on isolated populations [27]. Calvete et al. characterized the venom proteome of *Bothrops atrox* from different geographical

regions and vindicated the use of a venom signature as a tool to investigate the phylogeography of *Bothrops atrox* [28]. The snake venom composition is under genetic control and therefore proteome studies could serve as a tool to provide molecular markers for taxonomical purposes [12, 29-31]. However, besides varying between species, venom composition also differs within a species depending on age, season and temperature [27]. Fig. 3 illustrates variation of the venom composition between different species [5].

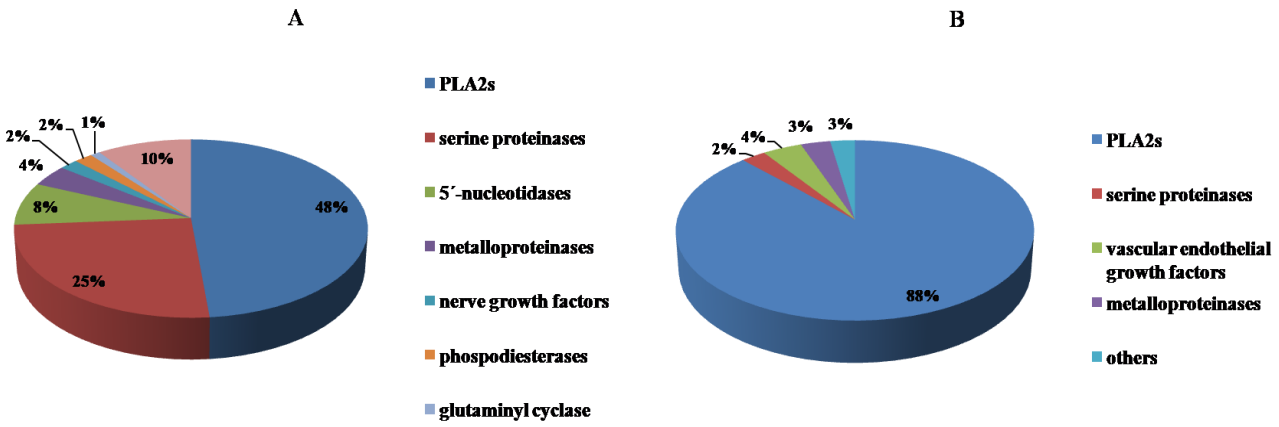

Fig. 3: Summary of the relative amounts of toxin families in the venoms of; (A) *C. d. terrificus venom*; (B) *C. d. collineatus venom* [5].

There is evidence that individual venom composition can vary through time likely due to the effects of gene regulation, a number of snakes show age related changes in venom composition [9]and references therein. This pattern is interpreted as reflecting ontogenetic changes in gene expression possibly related to diet differences between juvenile (eg. ectothermic prey such as frogs and lizards) and adults (e.g. endothermic prey, such as mammals), tuning the venom toxicity to deal with larger prey by adult snakes [32-34].

Characterizing the large molecular variability within all the major toxin families may contribute to a deeper understanding of the biological effects of the venoms, and poses exciting challenges for delineating structure-function correlations and for designing antivenom production strategies. Snake bite is still a serious threat in both developed and developing countries. Snake envenomation accidents represent a socio-medical problem of considerable magnitude with

about 2.5 million people bitten by snakes annually around the world, of which more than 100,000 lose their lives. The only effective treatment for systemic envenomation is intravenous administration of antivenom. However many of the antivenom have not achieved optimal protective effects. This is in part due to the fact that antiserum includes numerous antibodies with specificities not confined to the toxic target molecules [35], and also to the fact that the venom used as antigen for serum production may contain poorly immunogenic components, unable to induce production of protective antibodies. The WHO has only recently recognized snake bite as a "neglected tropical disease" [36, 37]. Therefore the knowledge of toxin composition of the venom is of great medical and biotechnological significance, to develop safe and more specific antivenoms, and studies are being carried out to use pooled venoms as a substrate for antivenom production, for designing novel polyvalent pan-generic antivenoms [38-50].

1.2: Chemical arsenal of the snake: nature's bio resource for drug design

Nature has been the traditional source and inspiration for drug discovery for thousands of years, among which snake venoms form a rich source of bioactive molecules [51].

Snakes have been used in Ayurevedic medicine since the seventh century B.C. to prolong life and treat arthritis and gastrointestinal ailments [52]. Cobra venom has been used since the 1930s to treat conditions as diverse as asthma, polio, multiple sclerosis, rheumatism, severe pain and trigeminal neuralgia [53].

Most venoms are delivered to their prey and consequently the venom peptides and proteins must be stable enough to reach their site of action before being degraded or excreted. This need has resulted in the recruitment of highly stable molecular scaffolds that are resistant to degradation by proteases [54, 55]. The stability is usually attained by disulfide bridges [56], and post-translational modification [57, 58].

Venom components can be used directly or as prototypes of drugs for the treatment of diseases which do not respond to currently available therapies [6, 59]. Some of these compounds have already found preclinical or clinical application for the treatment of hypertension, cardiovascular diseases, multiple sclerosis, diabetes and pain [57]. A well known example is the use of bradykinin-potentiating peptides (BPP), isolated from the *Bothrops jararaca* venom, which served as an antetype for the first orally-active inhibitor of the angiotensin-converting enzyme (ACE), named captopril [60-62]. BPPs, natriuretic peptides (NPs) and sarafotoxins (SRTXs)

exert profound effects on the cardiovascular system [63]. Snake venom NPs resemble their mammalian counterparts including atrial natriuretic peptides (ANPs), brain natriuretic peptides (BNPs) and C-type natriuretic peptides (CNPs). Mammalian NPs play a crucial role in natriuresis, diuresis and vasorelaxation [64]. A 38-residues peptide (DNP) was isolated from the *Dendroaspis angusticeps* (Green mamba) venom [65], which has been shown to possess vasodilator, natriuretic and diuretic properties, similar to those of the mammalian NPs [66] and references therein. A synthetic analogue of DNP is today a potent therapeutic agent for the treatment of acutely decompensated congestive heart failure [67]. Snake venom sarafotoxins and mammalian endothelins (ETs) are structurally and pharmacologically related peptides exhibiting a potent vasoconstrictor action. They act on the vascular system via identical receptors [68]. Endothelins are very potent vasoconstrictor substances [69]. Disintegrins, found in the venoms of Viperinae and Crotalinae snakes, are non-enzymatic peptides which selectively block integrin receptors. These receptors are located on the cell surface and mediate cell-cell and cell-matrix interactions [70, 71]. Disintegrins and their analogues have the potential to be used as pharmacological tools for the treatment of heart attacks, cancer, osteoporosis and diabetes [72]. A potent peptide antibiotic, cathelicidin-BF, was purified from the venom of *Bungarus fasciatus* [73]. Further research work based on structure activity relationship, is being carried out, to design novel and cost effective antimicrobial peptides with reduced haemolytic activity [74]. Textilinin-1, which is a 7 kDa Kunitz type serine protease inhibitor isolated from the venom of *P. textilis*, has been found to be a potent and selective inhibitor of plasmin. *In vitro* and *in vivo* studies have shown that this molecule is equally effective and has a better safety profile as compared to aprotinin, therefore it has been suggested as a lead candidate for the replacement of aprotinin as an anti-fibrinolytic agent [75].

The pharmaceutical industry has recognized the enormous potential inherent to venom peptides and has begun to exploit the selectivity and sensitivity fine tuned by evolution [76]. There are approximately 60 peptide drugs on the market with combined sales in 2010 of $ 13 billion [77]. Presently peptides share about 2% of the drugs in the market, and account for 50 % of the drugs in the pipelines of the drug manufacturers [78]. The drugs derived from snake venom, which have been approved or in clinical or preclinical trials are shown in table 1.

Table 1: Drugs derived from snake venom [78]

Drug	Source of venom protein	Molecular target	Function/ Disease	Company
Alfimeprase	Southern copperhead viper	Fibrin	Thrombolytic agent and catheter occlusion	Nuvelo Inc.
Contortrostatin	Southern copperhead viper	Integrin	Breast cancer	Pivotal Biosciences/University of California
Captopril	Brazillian arrowhead viper	Angiotensin converting Enzyme	ACE inhibitor, Antihypertensive	Bristol-Myers Squibb
Aggrastat	African Saw-scaled viper	Platelet glycoprotein IIb/IIIa receptor Inhibitors	Acute coronary syndrome (ACS), refractory ischaemia	Merck
Viprinex (ancrod)	Malaysian pit viper	Fibronogen inhibitor	Heparin-induced thrombocytopenia	Neurobiological Industries
Exanta; ximelagatran	Cobra Venom	Thrombin inhibitors	Atrial fibrillation and blood clotting after orthopedic surgery	AstraZeneca
Cenderitide	Eastern green mamba	Natriuretic peptide receptor	Congestive heart failure	Nile therapeutics
RPI-MN (α-cobrotoxin)	Cobra	nAChR	HIV	ReceptoPharm
RPI-78 (α-cobrotoxin)	Cobra	nAChR	Multiple sclerosis	ReceptoPharm

1.3: Evolution of the snake venom proteins

The advanced snakes (superfamily Colubroidea) constitute over 80% of the approximately 2,900 species of snake currently described and contain all the known venomous forms. Only about 20 % of the advanced snakes (Atractaspididae, Elapidae, Hydrophidae and Viperidae) have front-fanged delivery systems, and are typically regarded as of major medical interest [79]. The evolutionary studies of the venom are based on the variable nature of the venom. Venoms represent the critical innovation in ophidian evolution that allowed the advanced snakes to transition from a mechanical (constriction) to a chemical (venom) means of subduing and digesting prey larger than themselves [59, 80]. A great deal of work in mining the origin, evolution and phylogeny of the snake venom toxins was done by Fry and colleagues [81-87]. One of the important conclusions was that, the snake venom toxins evolved from recruitment events by which a body protein is recruited into the chemical arsenal of the snake. The toxins often undergo significant variations in sequence and structure, yet typically retain the molecular

scaffold of the ancestral protein [82]. It is believed that the original PLA_2, for example, had a role in digestion and that upon recruitment of this protein in the venom gland, the ancestral digestive enzyme evolved and through subtle mutations became toxic [84]. Studies on the origin and evolution of the snake venom proteome revealed that CRISPs and kallikrein toxins result from modification of salivary proteins, and that the toxin types, where the ancestral protein was extensively cysteine cross-linked, were the ones that flourished into functionally diverse, novel toxin multigene families [84].

The venomous snake families (Atractaspididae, Elapidae, Viperidae and Colubridae) consist of snakes with venoms that contain shared protein families. Despite of the fact that homologous toxins are found in the venom of these families, the venom of each family has distinct biological activity. The differences in biological characteristics are caused by the variation in amino acid sequence and relative abundance of the related proteins [13]. Viperidae venom toxins can be subdivided into two major groups, enzymatic and non enzymatic toxins. The enzymatic toxins consist of group II PLA_2s, serine proteases, metalloproteinases, LAAOs and glutaminyl cyclise. The non enzymatic toxins include C-type lectins, disintegrins, CNP, CRISPs, VEGFs, NEGFs, cystatin, BPP and Kunitz type protease inhibitors. The Elapidae snakes venom is characterized by a high post and presynaptic neurotoxicity, and contains a wide variety of group 1 PLA_2, 3FTx, CRISPs, Kunitz type protease inhibitors, NGFs, galactose-binding lectins, ANP, cystains and M12B peptidases The Atractaspididae snake venoms have a variety of peptide toxins that affect the cardiovascular system and the Colubridae snake venoms share some similar activities to both the Viperidae and Elapidae snakes [6].

Vipers and elapids are the most distantly related lineages among the Colubroidea, (Fig. 4) [88]. Fry et al. [83], studied eight toxin families, to investigate the origin and recruitment of toxin families into the venom proteome of these snakes. According to them the Kunitz type protease inhibitors, CRISP toxins, GBL toxins, M12B peptidases and NFG toxins were recruited at an early stage before the split of the lineage.

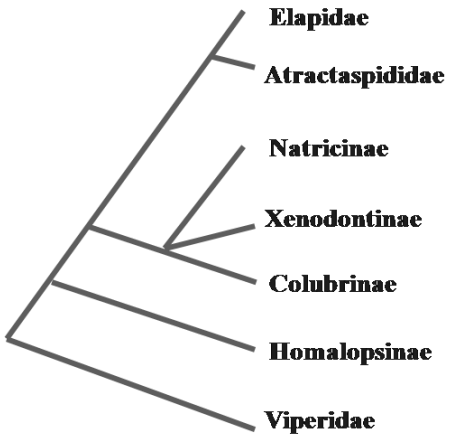

Fig. 4: Phylogeny of the major families of advanced snakes [88].

Three toxin families, lectin toxins, PLA_2, and the natriuretic peptides were recruited at two independent events. The Elapidae toxins belong to the "pancreatic-type" (group I) PLA_2 toxins, whereas the Viperidae toxins belong to the "synovial-type" (group II) PLA_2 toxins. The lectin protein family was recruited once before the split of the lineage, i.e. the GBL toxins and C-type lectins again in the Viperidae lineage subsequent to its split from the rest of the advance snakes. Hence the vipers contain both the C-type lectins and GBL, whereas all other lineages contain only GBL. On the contrary the actual points of recruitment of the group I PLA_2 and natriuretic toxin families remain unknown. Group I PLA_2 toxins have so far only been characterized and sequenced from elapid venoms. B. J. Fry has stated that the ANP/BNP natriuretic toxins may be another ancient recruitment at the base of the Colubridae tree, where as the CNP natriuretic toxins are an independent recruitment that occurred after the vipers split off from the remainder of the advanced snakes like that of the lectin toxins. The 3FTx family was recruited immediately after the vipers split from the remaining colubroid lineages. A number of other toxin families are presently known only from either elapids or the viperids and may have been recruited into the venom proteome later during the evolution of these lineages. Toxins molecular scaffolds sequenced only from Elapidae venoms include acetylcholinesterase, cobra venom factor, factor Xa prothrombin-activating toxins, factor V toxins, prokinecitin-like peptides, wapins, and toxins containing the SPRY domain. Current viperidae only toxins include myotoxic peptides, S1 peptidases, vascular endothelial growth factor-like toxins, and waglerins. Thus venoms evolved into complex and sophisticated secretions soon after the initial evolution of serous supralabial glands at the base of the colubroid radiation [89]. PII-disintegrins have been found only in the

viperidae venom, which evolved by the neofunctionalization of disintegrin-like domains of duplicated PIII-SVMP genes. Since PIII-SVMPs exist in all the five families of Colubroidea, it was concluded that disintegrins emerged after the split of Viperidae and Elapidae, but before the separation of Viperidae subfamilies [90].

1.4: Snake venoms analyzed in terms of the thesis

The following four snake venoms were selected from *Viperidae* and *Elapidae* snake family (Fig. 5), with different geographical distribution and habitat, to study their peptidic fractions in a comparative way.

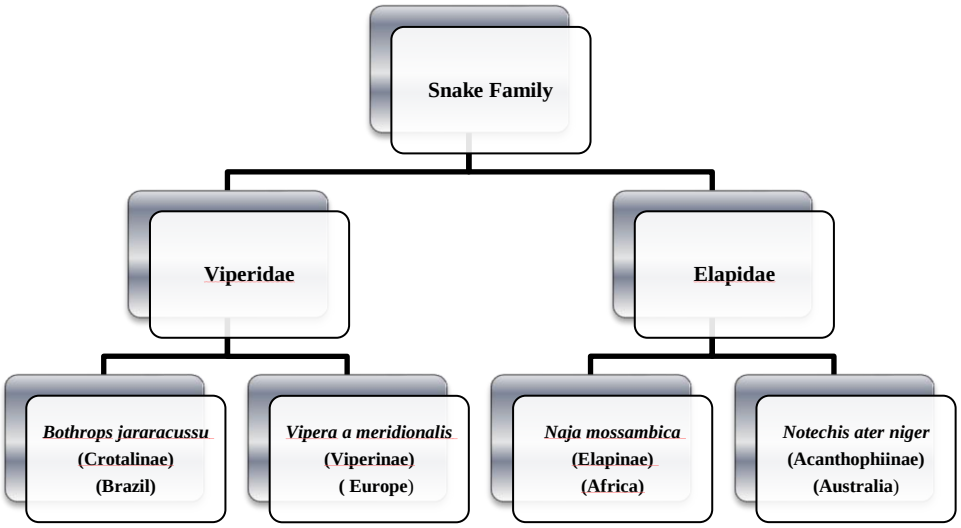

Fig. 5: Flow chart displaying the families and geographical distribution of snakes, the venom of which was analyzed in terms of the thesis.

1.4.1: *Bothrops jararacussu*

This snake is found in South America. It belongs to the subfamily Crotalinae and genus Bothrops. Fig. 5 shows a *Bothrops jararacussu* snake and its geographical distribution in South America. This snake has an exceptionally large venom output; up to 1000 mg (dry weight) venom can be obtained from a single milking [91]. The venom *B. jararacussu* is an enormous reservoir of pharmacologically active compounds.

Fig. 6: (A) *Bothrops jararacussu* snake; (B) Map illustrating the geographical distribution of *Bothrops jararacussu* (WHO venomous snake data base).

1.4.2: *Vipera ammodytes meridionalis*

This snake is from the biodiversity of Europe. It belongs to the subfamily Viperinae and genus Vipera. This snake is of public health significance and the most toxic European snake [92], with an unexplored venom peptidome. It is widely distributed in the eastern part of the continent, Fig. 6.

Fig. 7: (A) *V. a. meridionalis*; (B) Map illustrating the geographical distribution of the snake (WHO venomous snake data base).

1.4.3: *Naja mossambica mossambica*

This is a type of spitting cobra native to Africa, Fig. 7. It belongs to the family Elapidae, subfamily Elapinae and genus Naja. It is considered to be one of most dangerous snakes in Africa. Envenoming of the prey by this snake results in severe damage of the local tissue, and venom in the eyes can cause impaired vision or blindness [93].

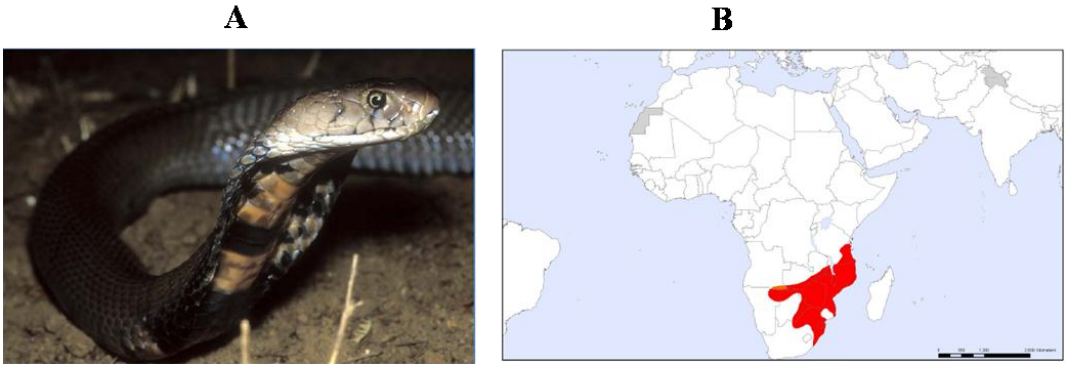

Fig. 8: (A) *Naja m mossambica*; (B) Map illustrating the geographic distribution of the snake (WHO venomous snake data base).

1.4.4: *Notechis ater niger*

This is an Elapidae snake (subfamily Acanthophiinae, genus Notechis). Snakes of this genus are distributed on the south coast of Australia (Fig. 8). The venom of this snake is highly lethal having neurotoxins, coagulants, haemolysins and myotoxins. Whereas the mainland snakes have a diet including lizards and frogs, the Kangaroo Island snakes of this species prefer to feed on mammals.

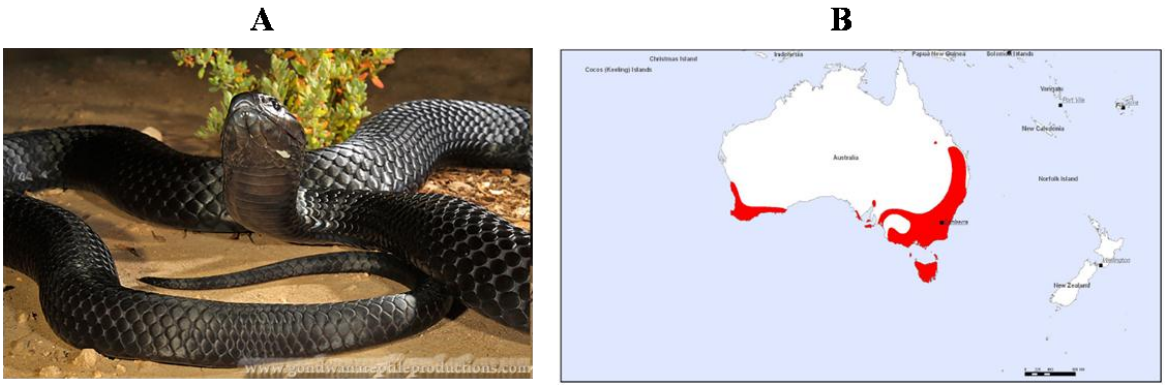

Fig. 9: (A) *Notechis ater niger*; (B) Map illustrating the geographical distribution of the snake (WHO venomous snake data base).

2: Aims and significance of the project

The advent of proteome technique has fostered the knowledge gained about the venom proteome composition, protein structure and function. However snake venom peptidomes are a so far mainly neglected/unexplored field and NCBI data base search shows that the snake venom peptide entries are much less as compared to the snake venom proteins. This can be ascribed to the difficulty in obtaining the venom to perform these studies, as the snake venom is very scarce and the peptides are present at a lower concentration as compared to the proteins. Another hypothesis might be that unlike the protein components of the venom, the peptide fractions can not be analyzed by high throughput approaches like 2-D gels followed by automated digestion and MS/MS sequencing. The peptides have to be purified prior to analysis. Purification of the peptides is a difficult task, due to high complexity and the similarity of chemical and physical properties. Also the de novo sequencing of non tryptic peptides is time consuming and difficult.

The main objectives of this study were:

- Isolation and identification of peptidic inhibitors of pharmacologically interesting enzymes.
- Development of analytical methods for the purification and characterization of these peptides.
- Molecular modelling and docking to build models of catalytic complexes, of selected peptidic inhibitors with enzymes of interest.

These investigations are of great significance as a better understanding of the snake venom peptides, engineered by nature over millions of years of evolution, would allow the development of new molecules with the potential to pinpoint a specific step of a physiological process such as coagulation, neurotransmission or blood pressure regulation, leading to new drugs with higher specificity. A comparative evaluation of the peptides, present in the snake venoms under study might shed light on the taxonomic and geographical variations in venom among these snakes. The optimization of the analytical methods for the purification and characterization of the peptides would aid in the further investigation of peptides from other snakes venoms.

3: Materials and methods

3.1: Collection of snake venom

Vipera ammodytes meridionalis venom was collected from snakes originating from the province Thrace, near the border between Greece and Bulgaria and provided by the Academy of Sciences, Sofia, Bulgaria. Crude venoms from *Bothrops jararacussu*, *Naja mossambica mossambica* and *Notechis ater niger* were obtained from [Instituto Butantan (São Paulo; Brazil)]. The venoms were filtered to remove potential mucosal contaminants, lyophilized and stored at -20 °C until required.

3.2: Liquid chromatography of crude venom and peptide fractions of *Vipera ammodytes meridionalis*

The crude venom was fractionated by size-exclusion chromatography. 50 mg of the venom (dry weight) were dissolved in 0.1 M ammonium acetate buffer, pH 5.0 and applied on a Superdex-75 column, (16 x 60). The chromatography was performed using the same buffer at a flow rate of 1 ml/minute. UV absorbance of the eluate was monitored at 220 and 280 nm. This step was repeated several times to fractionate about 150 mg of the venom. Fractions were collected and subjected to SDS-PAGE on a 15% glycine gel or on 18% Tris/Tricine gel under reducing and non-reducing conditions. The gels were stained with Coomassie Blue. Peptide fractions were further purified by liquid chromatography.

Further separations by HPLC or FPLC were performed on:

a) Mono-S Column:

   Liquid chromatography of the peptide fraction (Peak 6, Fig. 11) was performed on a Mono-S (5 x 50) cation-exchange column. Peptides were collected with a linear NaCl gradient (0 to1 M), at a flow rate of 1ml/minute, where buffer A was 0.05 M sodium acetate, pH 5 and buffer B was 0.05 M sodium acetate containing 1.0 M NaCl, pH5.

b) SOURCE 15RPC Column:

   To purify the peptides of the first peak eluting from the Mono-S column, a Source 15 RPC (4.6 x 100) column with a linear gradient of 0–60% consisting of solvent A (0.05% formic acid) and solvent B (0.05% formic acid in acetonitrile, ACN), at a flow rate of 1ml/minute, was used.

c) PerfectSil 300 ODS-C18 5µm

A C18 (4.6/250 mm) column with a linear gradient system of 0–70% consisting of solvent A (0.05% formic acid in H_2O) and solvent B (0.05% formic acid in acetonitrile), at a flow rate of 1ml/minute, was applied to isolate the peptides from peak 8 (Fig. 10).

d) LiChrosorb RP-C8 5µm

A C8 (4.6/150) column with a linear gradient of 0-70% consisting of solvent A (0.05% formic acid in H_2O) and solvent B (0.05% formic acid in acetonitrile) was used, at a flow rate of 1ml/minute, to isolate peptides from peaks 9-11 (Fig. 10).

3.3: Liquid chromatography of crude venom and peptide fractions of *Bothrops jararacussu*

The crude venom was fractionated by size-exclusion chromatography on a Superdex-75 column (10 x 300). A total of 200 mg venom was fractionated using the same buffer and elution conditions as mentioned above, by loading 20 mg (dry weight) of the venom. Peptide fractions were further purified by high pressure liquid chromatography.

a) PLRP Column

Fractions 4-9 obtained from a size exclusion column (Fig. 16), were subjected to further purification on a PLRP column with an asymmetric gradient of 3-60 % consisting of solvent A (20 mM ammonium carbonate) and solvent B (ACN), at a flow rate of 1 ml/ minute.

b) Chromolith C18 (100x4.6) Column

A Chromolith C18 column was used with an asymmetric gradient of 3-40%, consisting of solvent A (0.2% formic acid) and ACN as solvent B, at a flow rate of 2 ml/minute, to further purify the peptides after basic RPC, which showed inhibitory activity towards an angiotensin converting enzyme.

3.4: Liquid chromatography of crude venom and peptide fractions of *Naja mossambica mossambica*

A total of 200 mg venom was fractionated on Superdex-75 (10 X 300), as mentioned above. Peptide fractions were further separated by FPLC or HPLC.

a) Resource-S Column

   Liquid chromatography of peptide fractions (Peak 5, Fig. 38) was performed on a Resource-S 1ml cation-exchange column. Peptides were separated by a two segment NaCl gradient, 0 to 50% B, 35 CV, and 50-100, in 5 CV, at a flow rate of 1ml/minute, where buffer A was 0.05 M sodium acetate, pH 5.5 and buffer B was 0.05 M sodium acetate containing 1.0 M NaCl, pH 5.5.

b) Vydac C18 (150X4.6) Column

   Peptides (Peak 9, Fig. 38) were further separated by RPC, using a C18 column. A linear gradient of 0-75% B was used to elute the fractions, at a flow rate of 0.8 ml/ minute. 0.05% formic acid was used as solvent A and straight acetonitrile was used as solvent B.

3.5: Liquid chromatography of crude venom and peptide fractions of *Notechis ater niger*

A total of 300 mg venom was fractionated on a Superdex-75 (16 x 60) column, under the same conditions as the other venoms. Peptide fractions were further purified by HPLC.

a) SOURCE 5RPC (4.6 x 150) Column

   Peak 4 (Fig. 51) was fractionated on a SOURCE 5RPC column, by a linear gradient between 5-75%, at a flow rate of 1ml/minute, for 55 minutes. Solvent A was 0.1% formic acid and solvent B was straight acetonitrile.

b) Chromolith-C18 (100 x 4.6) Column

   In order to isolate peptides inhibiting ACE peak 4 (Fig. 51), was filtered through 3 KDa amicon membrane. The peptides present in the filtrate were fractionated on a C18 column, with a linear gradient of 0.3% B to 60 % B, at a flow rate of 1ml/minute, for 40 minutes. 0.2% formic acid was used as solvent A, and straight acetonitrile was used as solvent B.

3.6: Liquid chromatography of crude venom of *Agkistrodon bilineatus*

The crude venom was fractionated by size-exclusion chromatography, on a Superdex-75 column (16 x 60), under the same conditions as used for other venoms.

3.7: SDS-polyacrylamide gel electrophoresis (PAGE)

Polyacrylamide gel electrophoresis was performed using 15% glycine or 18% tricine SDS-polyacrylamide, according to the standard protocols [94, 95]. The 18% tricine gel was prepared

according to the protocol available at (http://www.fermentas.com/templates/files/tiny_mce/coa_pdf/coa_sm1891.pdf). The gels were 10 x10 cm and 0.7 mm thick. Before applying the samples to the gels, they were diluted 1:1 with sample buffer and heated to 85 ˚C for 5 minute. The voltage of the chamber was set to 120 V. The protein bands were stained with Coomassie Briliant Blue G250, and de stained with a 20 % acetic acid solution.

3.8: Inhibitory activity of snake venom peptides

The inhibitory activity of snake venom peptides was tested towards the following enzymes, using either chromogenic or fluorogenic substrates. All the assays were downsized to a volume of 100 µl, and the measurements were taken on the TECAN micro plate reader, at room temperature. The inhibitory activity of snake venom peptide was determined by incubating 20 µl of the snake venom fraction with the protease for 15 minutes, and then monitoring the residual protease activity by the addition of the corresponding substrate.

3.8.1: Angiotensin I-converting enzyme (ACE) assay

The ACE activity in the presence of venom peptides was determined by a fluorescence energy transfer assay using Abz-Phe-Arg-Lys (Dnp)-Pro-OH as a substrate [96]. 1 mg of the substrate was weighed and dissolved in 1ml DMSO. The exact concentration of the substrate was determined by taking four different volumes of the substrate stock solution, and constructing a standard curve spectrophometrically at 365 nm, using the molar extinction coefficient of the Dnp group (Ɛ_{356}= 17,300 M^{-1} cm^{-1}), according to the Beer's Lambert Law

$$A = \text{Ɛ}_{Dnp} \times l \times c$$

The stock solution of the enzyme was prepared by suspending 0.25 UN of ACE in 250 µl of the assay buffer (Dissolve 12.1 g Tris-base, 2.92 g NaCl and 1.36 mg $ZnCl_2$ in 1 liter of deionized water. Adjust the pH to 7.0 with HCl). Just before the assay an aliquot of the stock solution of ACE was diluted with assay buffer in a ratio of 1:3 (ACE: Buffer). An aliquot of the substrate stock solution was also diluted in a ratio of 1:3 (substrate: buffer). To determine the protease activity 2 µl of the dilute ACE solution was mixed with 96 µl of the buffer, the reaction was started by adding 2 µl of the freshly prepared substrate solution. The fluorescence measurements were made at λ_{ex}= 320 nm and at λ_{em}= 420 nm, for 5 minutes.

3.8.2: Subtilisin (StmPr1) assay

A bacterial subtilisin (StmPr1) was provided by Dr. Negm [97], to identify and isolate an inhibitor of this protease from snake venom, as a part of an internal collaboration. To determine the serine protease activity the chromophore tetrapeptide Suc-Ala-Ala-Pro-Phe-pNA was used, which is considered to be a non-specific serine protease substrate [98]. After incubation of a serine protease with the substrate nitroaniline is released. This absorbs at 405 nm. The amount of the released nitroaniline is a measure of the activity of the serine protease. A 50 mM stock solution of the substrate was prepared. Before the assay a working solution of the substrate was prepared by diluting 10 µl of the stock solution to 100 µl with the reaction buffer. To measure the protease activity, 10 µl of a diluted protein solution was mixed with 80 µl reaction buffer (20 mM Tris, 20 mM $CaCl_2$, 150 mM NaCl, pH 8), and the reaction was started by addition of 10 the assay 10µl of the diluted substrate solution. The absorbance was measured at 405 nm for four minutes.

3.8.3: Thrombin assay

The activity of thrombin was determined by using the substrate, Bz-Phe-Val-Arg-pNA [99]. A 20 mM stock solution of substrate was prepared by dissolving 6.82 mg in 500 µl of DMSO. The stock solution of the enzyme was prepared by dissolving 100 UN in 100 µl of the assay buffer (50 mM tris, 100 mM NaCl, pH=8). Just before the assay a working solution of the substrate was prepared by taking 20 µl of the stock solution and diluting to 100 µl with buffer, and that of the enzyme was prepared by diluting in the ratio of 2:5 (enzyme stock solution: buffer). 3µl enzyme was incubated with 84 µl buffer and 13 µl of the substrate working solution were added to start the reaction. Measurements were made by monitoring the absorbance at 405 nm for four minutes.

3.8.4: Trypsin assay

The activity of trypsin was monitored by using the same substrate as thrombin [99]. The assay buffer was also the same as for thrombin. A 0.143 mM stock solution of trypsin was prepared by dissolving 1.8 mg trypsin in 500 µl 1 mM HCl. The substrate stock solution was 20 mM. Prior to the assay a working enzyme solution was prepared by diluting 1.5 µl of the stock solution of the enzyme to 400 µl with the assay buffer. The substrate working solution was prepared by diluting 20 µl of the stock solution to 100 µl with the assay buffer. For the final assay 10 µl of enzyme

were incubated with 80 µl buffer and 10 µl of substrate were added to start the reaction. Measurements were made by monitoring the absorbance at 405 nm for four minutes.

3.8.5: Chymotrypsin assay

A stock solution of 40 mM of chymoyrypsin was prepared by dissolving 1 mg/ml in 1 mM HCl. The same substrate as that of subtilisin was used for chymotrypsin, and a stock solution of 30 mM was prepared in DMSO. Before starting the assay 2 µl of enzyme stock solution were diluted to 100 µl with buffer (50 mM tris, 10 mM $CaCl_2$, pH 8), and 10 µl of substrate stock solution were diluted to 100 µl to prepare a working solution. To do the assay 10 µl of enzyme solution was incubated with 70 µl buffer, and 20 µl substrate was added to start the reaction, and change of absorbance was monitored at 405 nm for 4 minutes.

3.8.6: Factor Xa assay

A 50 mM stock solution of the substrate, Z-D-Arg-Gly-Arg-pNA-HCl, was prepared by dissolving 9 mg in 250 µl DMSO [100]. The enzyme was supplied as 13 µl solution with a concentration of 3.8 mg/ml. The enzyme working solution was prepared by diluting 1 µl of the stock enzyme solution to 500 µl with the assay buffer (0.05 M Tris, 5 mM CaCl2, 200 mM NaCl, and pH 8.3). The substrate working solution was prepared by diluting 20 µl stock solution to 100 µl with assay buffer. To do the assay 5 µl of the working solution of the enzyme were incubated with 91 µl assay buffer, and 14 µl of the substrate working solution were added to start the reaction. Change of absorbance was monitored at 405 nm for four minutes.

3.8.7: Plasmin assay

A 50 mM stock solution of the substrate, Bz-Arg-pNA, was prepared by dissolving 10.9 mg in 500 µl DMSO [101]. 150 µg enzyme was dissolved in 100 µl of cold distilled water. The substrate working solution was prepared by diluting 20 µl of the substrate to 100 µl by assay buffer (50 mM Tris-HCl, pH 7.5). The enzyme working solution was prepared by diluting 20 µl of the stock solution to 100 µl with the assay buffer. The assay was done by incubating 10 µl enzyme with 65 µl buffer. The reaction was started by the addition of 25 µl substrate solution, and change of absorbance was monitored at 405 nm for four minutes.

3.8.8: Plasma kallikrein assay

A solution (10 mM) of the substrate Bz-Pro-Phe-Arg-pNA was prepared by dissolving 1.5 mg in 20 µl DMSO and then diluting it in 500 µl distilled water [102]. A freshly prepared substrate solution was used before the assay. The enzyme was supplied as an aqueous solution (50 µg/96.2 µl). Enzyme working solution was prepared by diluting 8 µl stock solution to 100 µl with the assay buffer (50 mM Tris-HCl, 2mM $CaCl_2$, 150 mM NaCl, pH 7.8). For the assay 10 µl enzyme were incubated with 70 µl buffer, and 20 µl substrate was added to start the reaction. Change of absorbance was measured at 405 nm for four minutes.

3.8.9: 20S Proteasome assay

560 µg of the substrate Z-Gly-Gly-Leu-AMC, were dissolved in 1ml DMSO, to assay the chymotrypsin like activity of 20S proteasome [103, 104]. 25 µg enzyme was dissolved in 100 µl of assay buffer (20 mM Tris, pH 7.5), to prepare a stock solution. The enzyme working solution was prepared by diluting 7 µl of the stock solution to 100 µl with the assay buffer. For the assay 10 µl of the enzyme working solution were incubated with 85 µl buffer, and 5 µl of substrate were added to start the reaction. The change of fluorescence of the hydrolyzed 7-amido-4-methyl-coumarin (AMC) group was measured at λ_{ex}= 360 nm and λ_{em}= 480 nm, for 10 minutes.

3.8.10: Snake venom metalloproteinase and serine proteinase assay

The caseinolytic activity of SVMP and SVSP was measured by fluorescence substrate, FTC casein [105, 106]. It was prepared as reported previously [107]. 200 mg casein was dissolved in 20 ml buffer (50 mM sodium carbonate, 150 mM NaCl, pH 9.5). After cooling, the mixture was incubated with 8 mg FITC for 8 hours. The reaction mixture was dialyzed, at 4˚C in dark, against 50 mM Tris, pH 8.5, to remove un reacted FITC, for 24 hours and then against 100 mM Tris pH=7.5. 2 ml aliquots of the substrate were prepared and stored at -20˚C.

5µl of FTC-casein were diluted to 100 µl with buffer to prepare a working solution. Reaction mixture containing 5 µl enzyme (1 µg/µl) and 5 µl of the peptide fraction was incubated at room temperature for 15 minutes, followed by the addition of 5 µl of working solution of FTC-casein, 35 µl assay buffer and incubation at 37˚C for 20 minutes. A positive control was prepared by replacing the inhibitor with the assay buffer (50 mM Tris-HCl, pH 7.4), and to prepare a negative control, buffer was added in place of the enzyme and the inhibitor (peptide fraction). Proteolysis was terminated by adding 120 µl 5% TCA and mixing extensively. The reaction mixture was

allowed to stand for 1/2 h at room temperature, and the TCA-insoluble protein was sediment by centrifugation at 13,000 rpm for 10 minutes. A 90 µl aliquot of the supernatant was diluted with 90 µl of the 0.5 M Tris buffer, pH 8.5, with vigorous mixing to ensure the entire sample was at the assigned pH. Fluorescence was measured at λ_{ex} = 490 nm and λ_{em} at 522 nm. Purified MP-III 60 KDa (*B. moojeni*), and a serine proteinase (*B. alternatus*), were used for this assay (kindly provided by Prof. R.K. Arni, UNESP, Brazil)

3.2.9: Tryptic digestion and mass spectrometric identification of larger peptides

Aliquots of the fractions containing peptides of a molecular mass of 6–7 kDa were dried and subsequently dissolved in 6 M urea. To reduce the disulfide bridges, 1.3 µl 100 mM dithiothreitol dissolved in digestion buffer (100 mM $NaHCO_3$, pH 8.3) was added and the mixture was incubated at 60°C for 10 min. Free cysteine residues were blocked with 1.3 µl iodoacetamide (300 mM dissolved in digestion buffer, incubation for 30 min in the dark). 425 µl digestion buffer and 5µl trypsin solution (sequencing grade modified trypsin; Promega, Madison, USA) at a concentration of 0.25 µg/µl dissolved in re suspension buffer) were added. The mixture was incubated at 37°C for 16 h and afterwards the reaction was stopped by adding formic acid to a final pH of 3.0.

Identification was performed on an Agilent 1100 LC/MSD-trap XCT series system. The electrospray ionization system was the Chip Cube system using a Large capacity Chip (Agilent Technologies, Waldbronn, Germany). Sample loading (5 – 20 µl/sample) onto the enrichment column was performed at a flow rate of 4 µl/min with the mix of the following two mobile phases at a ratio 98:2 (mobile phase A: 0.2% formic acid in H_2O; mobile phase B: 100% ACN). LC gradient was delivered with a flow rate of 400 nl/min. Tryptic peptides were eluted using a linear gradient of 2–40% B in 40 min. For MS experiments, the following mode and tuning parameters were used: scan range: 30–2000 m/z; polarity: positive; capacity voltage: 1900 V; flow and temperature of the drying gas were 4 l/min and 325 °C, respectively. The MS/MS experiments were carried out in auto MS/MS mode using a 4 Da window for precursor ion selection, an absolute threshold of 10,000 after 3 MS/MS spectra. The precursor ion was excluded from fragmentation for one min. The generic files for database searching were generated by Data Analysis software version 3.4; for precursor ion selection a threshold of 5 S/N was applied and the absolute number of compounds was restricted to 1000 per run. Protein

identification was performed with Mascot online search (www.matrixscience.com) [108]. MS/MS datasets were used to search the spectra against the subset "other lobe-finned fish and tetrapod clade" of the Swiss-Prot database [109]. The experiments were carried out in cooperation with the research group of Prof. H. Schlüter, UKE, Hamburg.

3.2.10: Matrix-assisted desorption/ionization time-of-flight mass spectrometry

MALDI-TOF and MALDI-TOF-TOF analyses were performed on an ultrafleXtreme instrument (Bruker Daltonics, Bremen, Germany). Samples were dried after reversed phase chromatography, dissolved in 30% ACN, 0.1% TFA in H_2O and 0.75 µl of the solution was spotted on a MALDI target plate (MTP AnchorChip 384, Bruker Daltonics). After drying a 0.75 µl MALDI matrix (0.7 mg/ml Cyano-4-hydroxycinnamic acid (Bruker Daltonics) dissolved in 85% ACN, 1 mM $NH_4H_2PO_4$ and 0.1% TFA dissolved in H_2O) were spotted on the sample plate.

Data acquisition was performed in positive ion mode using the flexControl software 3.3. The parameters were set as follows: ion source 1: 25 kV, ion source 2: 23.6 kV, lens: 7.5 kV. MS data were collected automatically using autoXecute. Parameters were set as follows: laser power: 47%; laser shots: 1000; movement, random walk with 100 shots per raster spot. Peaks were selected for LIFT measurement if they met the following criteria: signal to noise > 8, peak intensity > 300.

MS spectra were processed in flexAnalysis (version 3.3, Bruker Daltonics). Further data analysis was performed using BioTools (version3.2, Bruker Daltonics) and Mascot Inhouse Search. Mascot [108] version 2.1.03 was used to search the spectra against the subset "other lobe-finned fish and tetrapod clade"of the Swissprot database. The precursor ion mass tolerance was set to 1 Da, the fragment ion mass tolerance was 0.5 Da.

3.2.11: Electrospray ionization time-of-flight mass spectrometry

ESI analysis was performed on an ESI-TOF-MS system (Agilent Technologies 6224). The samples were dissolved in a 1:1 solution of 0.1% TFA in ACN and 0.1% TFA in water. 1µl of the sample was injected at a flow rate of 0.2ml/min and an internal standard (ESI-TOF reference mix, Agilent Technologies) was used for calibration. Data acquisition was carried out using the Agilent Mass Hunter software (version B.03.01) in positive ESI mode using a gas temperature of 325°C, a gas flow of 10 L/min, a capillary voltage of -4000 V and the fragmentor voltage was set

to 230 V. Data were acquired in a range of m/z 110 to m/z 3200. These experiments were carried out by the technical staff, department of mass spectrometry, institute of organic chemistry, University of Hamburg.

3.2.12: ESI-QTOF mass spectrometry for peptide sequencing

For protein identification using nano electrospray mass spectrometry, experiments were carried out using an electrospray quadrupole time-of-flight mass spectrometer (Q-TOF-2 electrospray mass spectrometer, Waters, Eschborn, Germany) in the positive ion mode. Raw data were acquired and analyzed using the software MassLynx 4.1 (Micromass, Manchester, United Kingdom). Parameters not specified have been the default parameters of the software. The capillary tip voltage was set to 0.70 kV, the cone voltage to 35 V. For CID experiments, ions were selected within a precursor mass window of ± 1 Da in the quadrupole analyzer and fragmented in the collision cell using Argon as collision gas (Ar) and collision energies of 27 to 35 eV. For peptide identification, peptide tandem mass spectrometry (MS/MS) spectra were deconvoluted by MaxEnt 3 and manually sequenced, supported by PepSeq application for *de novo* sequencing (both part of the MassLynx software package). The sequence information of a few peptides was obtained by using the PEAKS Online software, version 5.2 [110]. These experiments were also carried out at the research group of Prof. H. Schlüter, UKE, Hamburg, by Sönke Harder.

3.2.13: ESI-FTICR mass spectrometry for peptide sequencing

High-resolution mass spectra were acquired using a Finnigan LTQ Fourier transform ion cyclotron resonance (FTICR ULTRA) mass spectrometer (Thermo Fisher, Waltham, USA) equipped with a 7 tesla superconducting magnet. Spectra were acquired at a resolution of 100,000 and the mass error was below 3 ppm at all times. Mass and resolution calibration was performed according to the manufacturer's recommendations. For CID experiments precursor ions were isolated in the linear ion trap using a mass window of 1.5–2 u and were transferred into the FTICR cell after fragmentation. Collision energies were adjusted in order to detect low intensities of the precursor ion (ca. 20% relative abundance). Electrospray ionization (ESI) of the samples was carried out using a TriVersa Nanomate (Advion BioSystems). An electrospray voltage of 1.5 kV, a pressure of 0.3 psi and a transfer capillary temperature of 200 °C were applied. Samples were diluted in 0.1% formic acid with a 60% methanol part. For data

processing Qual Browser 2.0.7 (Thermo Fisher) was used and the peptide sequencing was performed manually. These experiments were carried out by Violette Frochaux, Department of Chemistry, Humboldt University, Berlin.

3.2.16: Crystallization experiment: soaking of a native StmPr1 crystal with a peptidic fraction from *Agkistrodon bilineatus* venom

In an internal collaboration with Dr. Amr Negm, a crystal complex of StmPr1 was prepared with a peptide fraction from the venom of *Agkistrodon billineatus*, according to the crystallization procedure mentioned in his thesis [97]. The experimental conditions are briefly described here. Native StmPr1 crystals were grown by hanging drop vapour diffusion method, using 1.8 ammonium sulphate and 100 mM Tris-HCl buffer at pH 8.0, by incubating Linbro Plates at 20˚C for three weeks. The crystals were soaked with the peptidic fraction from *Agkistrodon bilineatus* venom one day before data collection. The data were collected by exposing a single crystal at the synchrotron Consortium-Beamline X13 DESY, Hamburg. The three dimensional model of the complex was built by using the programme Coot [111] and Refmac5 [112]. These experiments were mainly carried out by Dr. Amr Negm.

3.2.17: Molecular modelling

In order to predict the mode of interaction of Kunitz type serine protease inhibitors, isolated in this work, with Trypsin and kallikrein, rigid body docking was performed. Cytotoxin-1, showing inhibitory activity towards chymotrypsin and 20S proteasome, was also docked with chymotrypsin. Structural models of serine protease inhibitor 1, tigerin-1, tigerin-3 and cytotoxin-1 were generated by using the server SWISS-MODEL [113-115].

ClusPro [116-119], a fully automated online server was used to model these complexes. To build a Trypsin-Inhibitor complex, PDB file (PDB code: 3D65) was used. Chymotrypsin-Cytotoxin-1 complex was built by using the PDB file (PDB code: 1MTN). To build the catalytic complex of Kallikrein-Kunitz/BPTI, PDB file (PDB code: 2ANY) was used. In case of each complex generated by the program, the 10 top-ranked complexes from ClusPro were further analyzed, based on the prior knowledge of active site interactions. PDB sum server was used to study the interactions across the protein-protein interface.

The models of the complexes of the human testis angiotensin converting enzyme and selected bradykinin potentiating peptides, isolated in this work, were built using the flexidock module of the program SYBYL-X, version 1.3. The crystal structure of human tACE in complex with lisinopril (PDB code: 1O86) was used for docking studies. The enzyme was prepared by removing the ligand and water molecules and the energy was minimized. The structures of the bradykinin potentiating peptides, used as ligands, were also prepared by the program SYBYL-X and selecting Gasteiger-Hückel, as the charge model. The ligand was prepositioned in the cavity based on the knowledge obtained from the crystal structure. The biding site was defined around a region of 3 Å and each flexidock simulation was performed with 24,000 generations. The protein-ligand interactions were studied using the PDB sum server.

4: Results and Discussion

The work flow proposed and followed through this work is presented in Fig. 10. First a SEC separation of the crude venom was performed. The fractions were pooled according to the peaks present in the corresponding chromatogram.

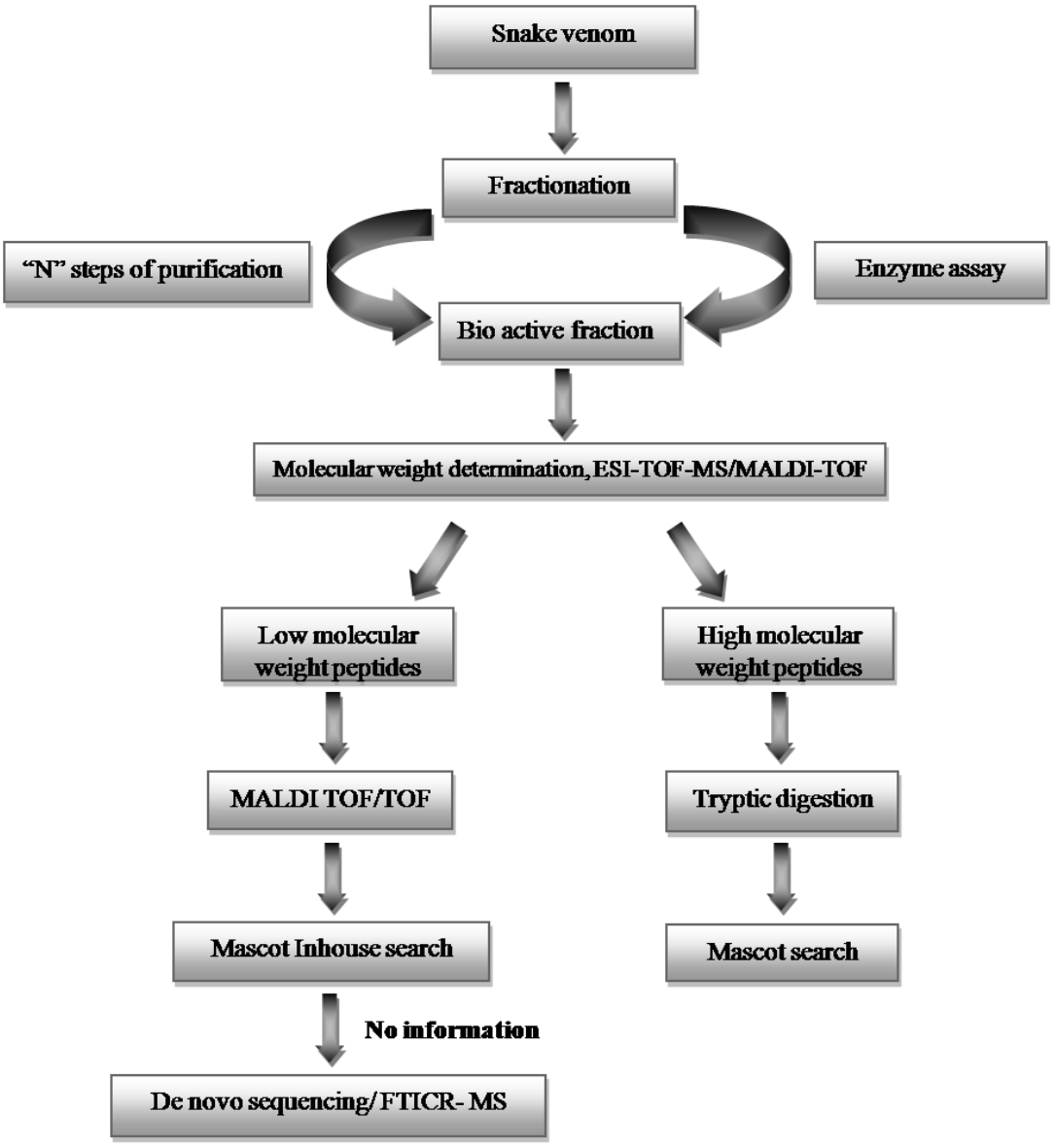

Fig. 10: A flow diagram showing the procedures to isolate and identify bioactive peptides from crude venoms.

The pooled fractions containing peptides with molecular masses below 10 kDa were screened for inhibitory activity towards a set of selected enzymes.

The enzymes were chosen so as to give insights into the possible function of the peptides present in the venom. A set of enzymes; thrombin, factor Xa, kallikrein and plasmin, were chosen from the hemostatis system, which might be affected by the injection of the venom into its prey. Trypsin and chymotrypsin were selected, to serve as a probe to identify the serine protease inhibitors, and also to identify Kunitz type inhibitors. Angiotensin converting enzyme, playing a crucial role in the cardiovascular system, was selected to identify the peptides affecting the blood pressure regulatory system of the prey. StmPr1 is a subtilisin like protease, which is produced as an extracellular protease by the bacteria *Stenotrophomonas maltophilia*, causing disease in humans. This enzyme was included in the work as a part of an internal collaboration in order to identify promising inhibitors of this enzyme within the snake venom, supporting future drug design.

The objective to test the inhibitory activity towards SVSP and SVMP was to look for potential inhibitors that might be responsible for preserving the venom gland from auto digestion, by these enzymes.

The pooled fractions showing inhibitory activity were further purified by liquid chromatography and the active fractions were further characterized by mass spectrometry. The peptides, isolated from the venoms of the four snakes, were classified into protein/peptide families using three indexes/properties: molecular mass, enzyme inhibitory activity and amino acid sequence.

4.1: Fractionation of the *Vipera ammodytes meridionalis* venom by size exclusion chromatography and purification of peptides by liquid chromatography

The first five fractions contained proteins with molecular masses > 10 000 Da (Fig. 11 B). Fractions 6-11 contained peptides with molecular masses below 10 kDa, which are boxed in Fig. 11A. Fractions 6-12 were screened against the selected enzymes and fractions showing inhibitory activity were subjected to further purification. Peak 6 showed inhibitory activity towards trypsin and peaks 8-11 showed inhibitory activity towards ACE.

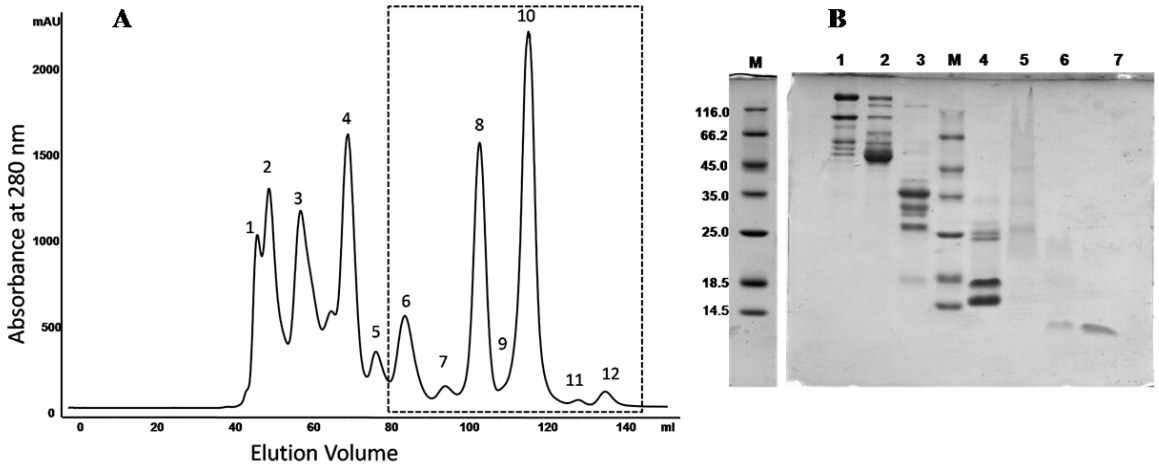

Fig. 11: (A) SEC of *Vipera a. meridionalis* venom on Superdex-75 column at pH 5; (B) SDS-PAGE of fractions 1-7 from SEC separation of *V.a. meridionalis*. Fractions 1-5 contain proteins with molecular mass above 10 kDa. Fractions 6-7 contain peptides with lower molecular mass.

Peak 6 was further fractionated by liquid chromatography on a Mono-S 5 x 50 column at pH 5.0 (Fig. 12A). The first major peak, labelled by an arrow, exhibited inhibitory activity towards trypsin.

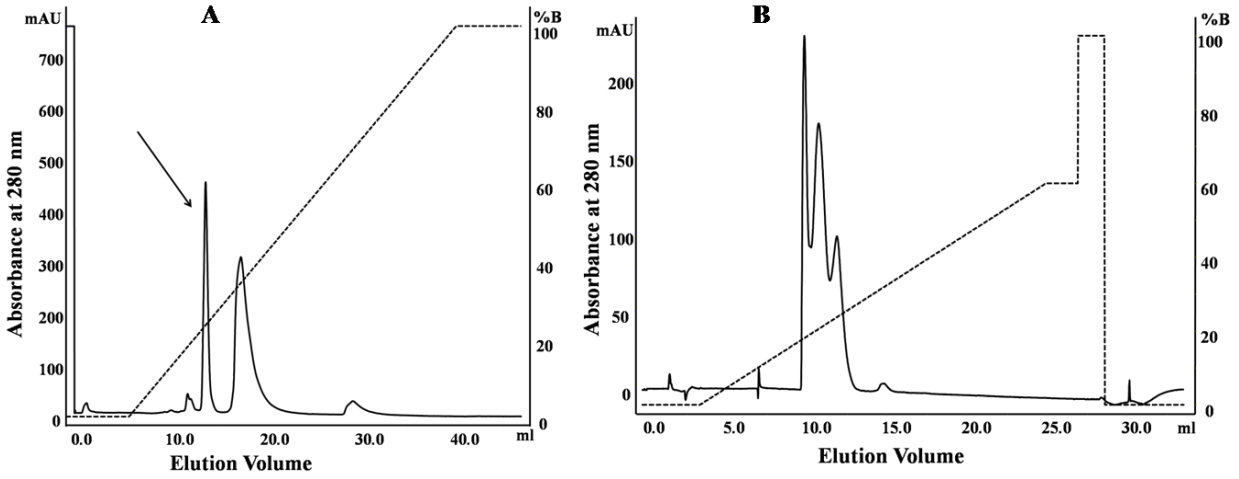

Fig. 12: (A) Fractionation of peak 6 shown in Fig. 11, by FPLC on a Mono-S column at pH 5; (B) Chromatography of the first main fraction shown in Fig. 12 A on a 15 RPC 4.6X100 column

Three peaks were observed after a chromatography of this fraction on a 15 RPC 4.6 x 100 columns (Fig. 12B). Inhibitor activity towards trypsin and kallikrein was found in fractions of all

these peaks. Electrospray-time of flight mass spectrometry (ESI-TOF-MS) of the second peak showed the presence of two components with masses 6859 and 7383 Da (Fig. 13). The same procedure was applied to the other fractions, demonstrating the presence of peptides with masses 6841 and 7401 Da.

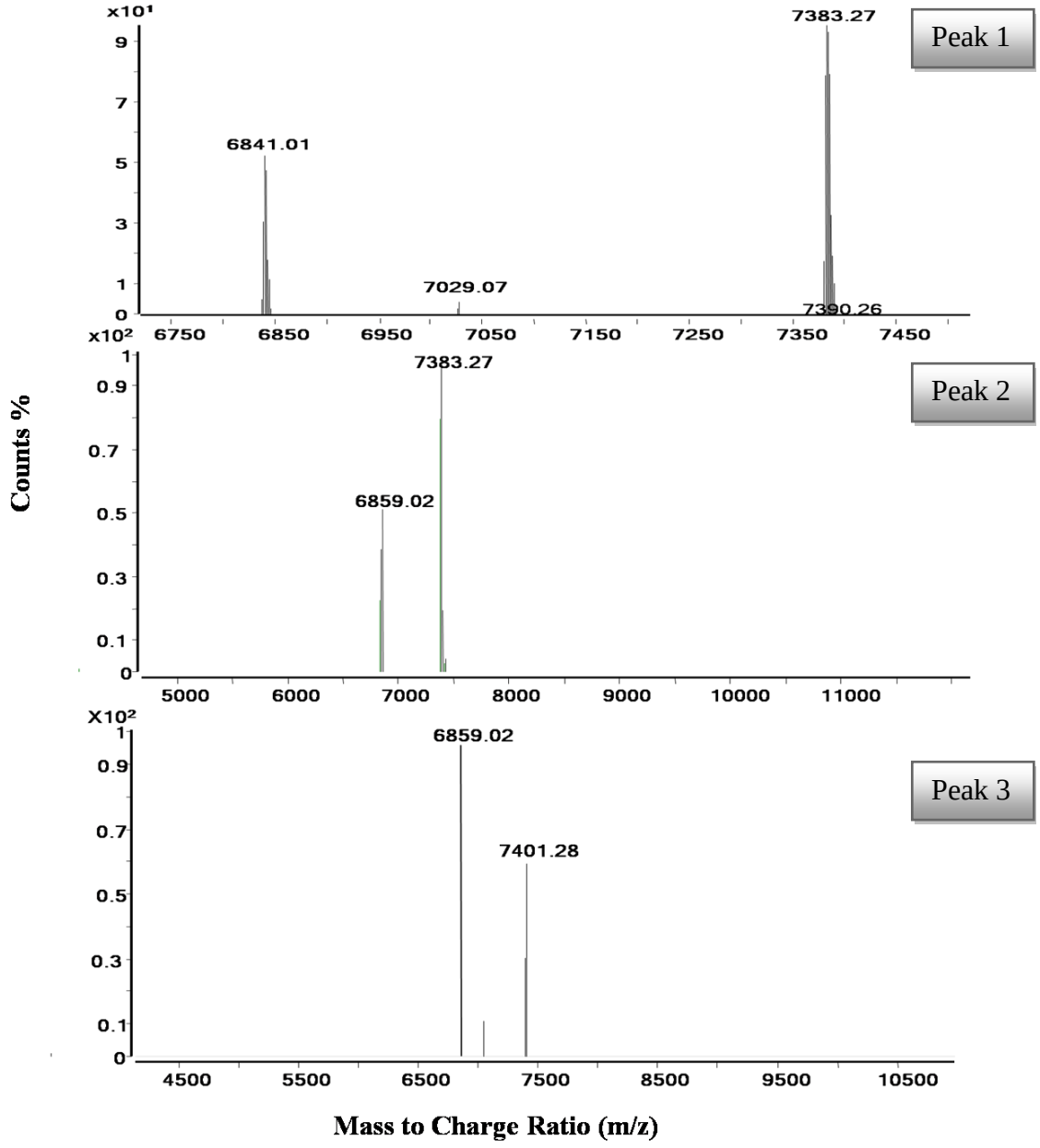

Fig. 13: ESI- TOF-MS analysis (deconvoluted peaks) of the three peaks in Fig. 12 B.

Peak 8 was further fractionated on a C18 column (PerfectSil 300 ODS-C18 5µm), Fig. 14. All of these fractions were lyophilized resuspended in water and tested for inhibitory activity towards ACE. All the fractions showed inhibitory activity towards ACE. ESI-TOF analysis showed the presence of peptides in the mass range 890-159 $(M+H)^+$. The ESI-MS spectra of these fractions are shown in Fig. 15. The ESI spectrum of these peptides, for example peak 1, Fig. 15, shows a doubly charged peak, at, 572.8 $(M+H)^{+2}$, a singly charged peak at 1144 $(M+H)^+$, a singly charged peak at 932 $(M+H)^+$, which fits to the loss of a PP residue (212 Da) from the mass of 1144 $(M+H)^+$. A singly charged peak of mass 213 $(M+H)^+$, corresponding to a PP residue can also be seen in the spectrum.

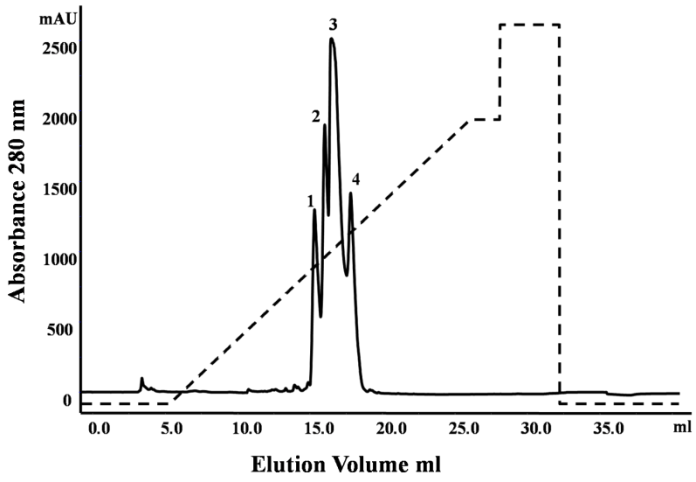

Fig. 14: Purification of peak 8 from the chromatogram (Fig. 11 A) on a C18 column by FPLC.

The pool of fractions in the valley between peak 8 and 10 in the chromatogram (Fig. 11), labeled as 9, was fractionated on a C8 column as shown in Fig. 16. Five main peaks appeared as a result of this fractionation. All of these fractions showed inhibition of ACE, with the lowest inhibitory activity in peak 3. The ESI-TOF-MS of these fraction showed masses in the range between 444 $(M+H)^+$-1159 $(M+H)^+$. The ESI-TOF-MS spectrum of Peak 2 shows a single peptide with a mass of 809 $(M+H)^+$ Da, and that of peak 3 shows 444 Da $(M+H)^{+,}$ with highest intensity, and the peptide 809 $(M+H)^+$ at low intensity. So a small inhibitory activity of this fraction can be concluded due to the mixing of peptide 809 $(M+H)^+$ in peak 3.

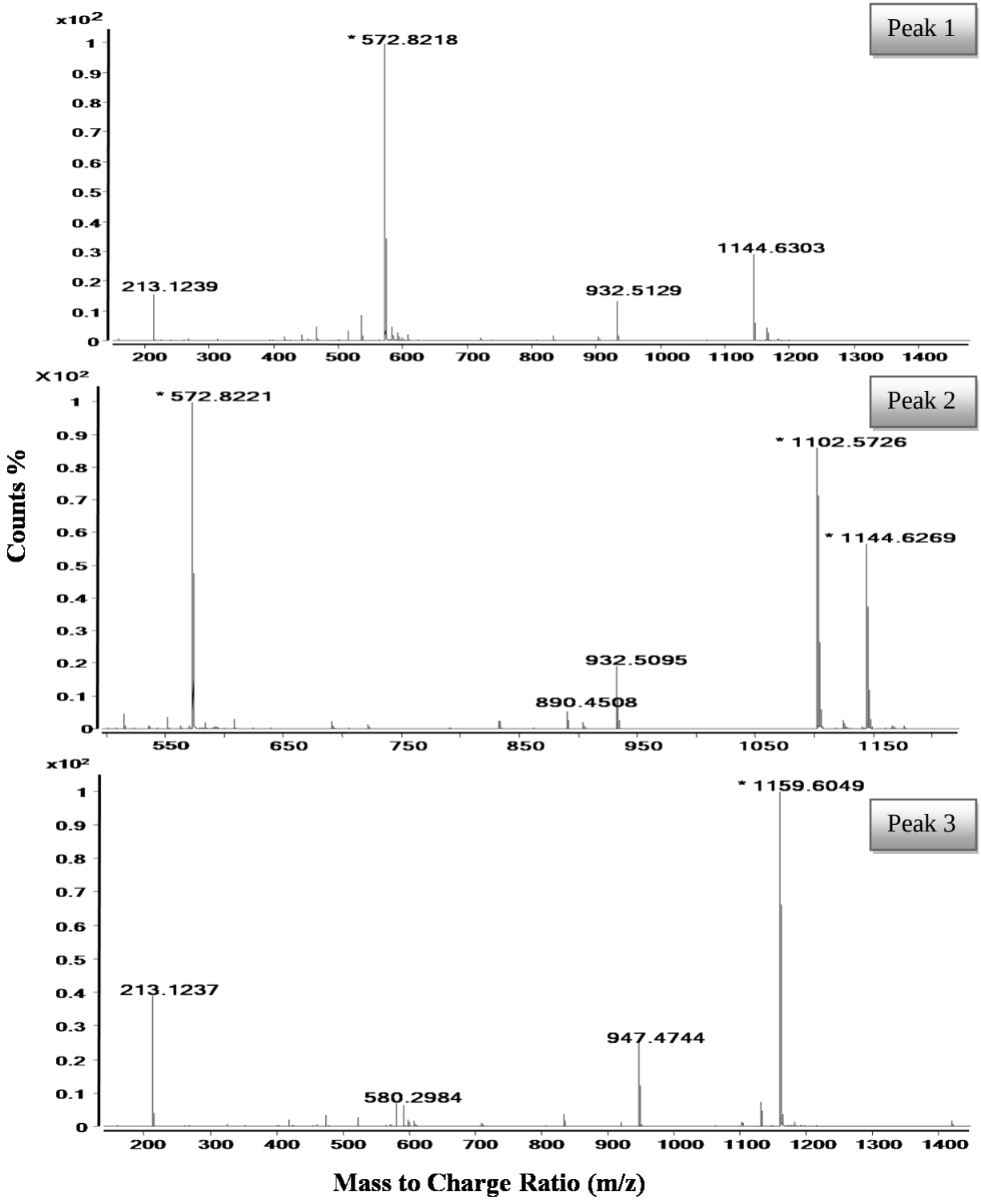

Fig. 15: ESI-TOF-MS spectra of selected peaks from the chromatogram shown in Fig. 14.

The peaks 4 and 5 contain the peptides with a mass of 1102 $(M+H)^+$, and 1159 $(M+H)^+$, as observed in the previous fractions (Fig. 14) responsible for the inhibition of ACE.

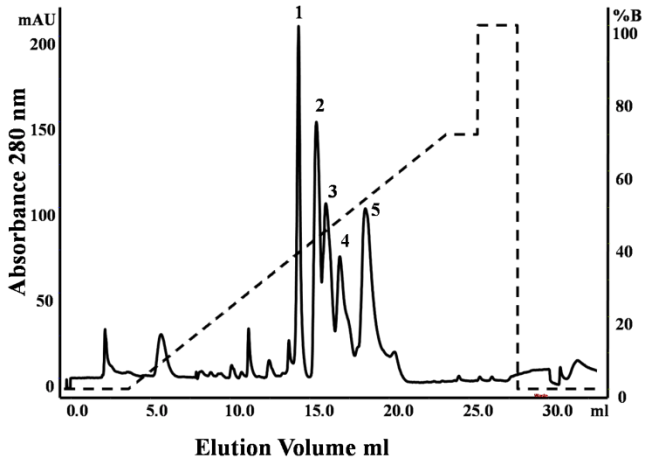

Fig. 16: Purification of peak 9 (Fig. 11), on a C8 column by FPLC.

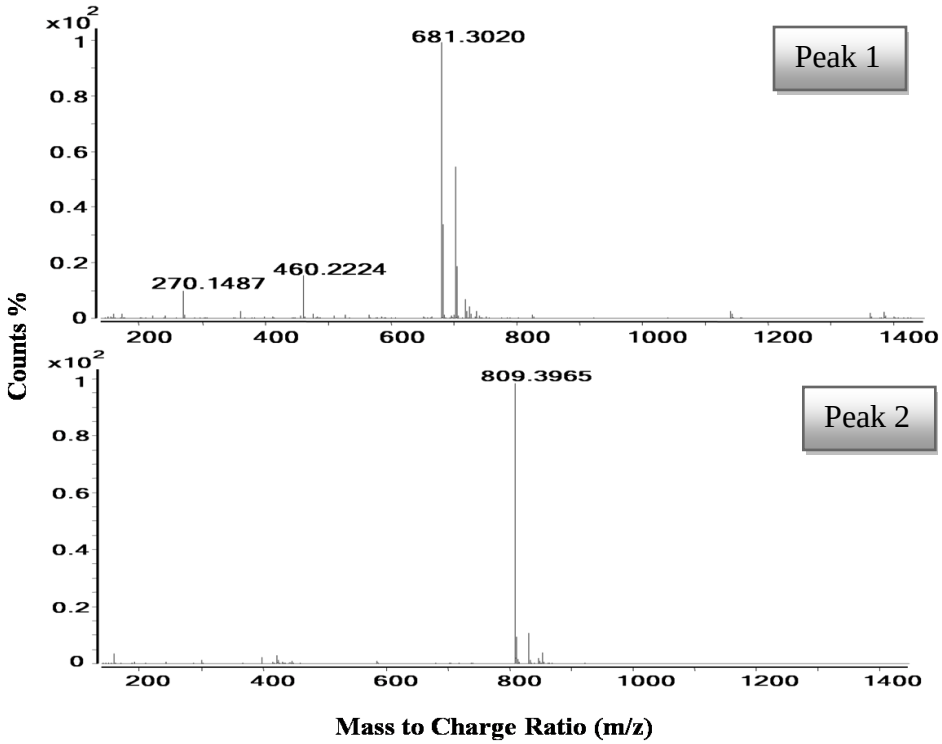

Fig. 17: ESI-TOF-MS spectrum of peaks 1 and 2 from the chromatogram shown in Fig. 16.

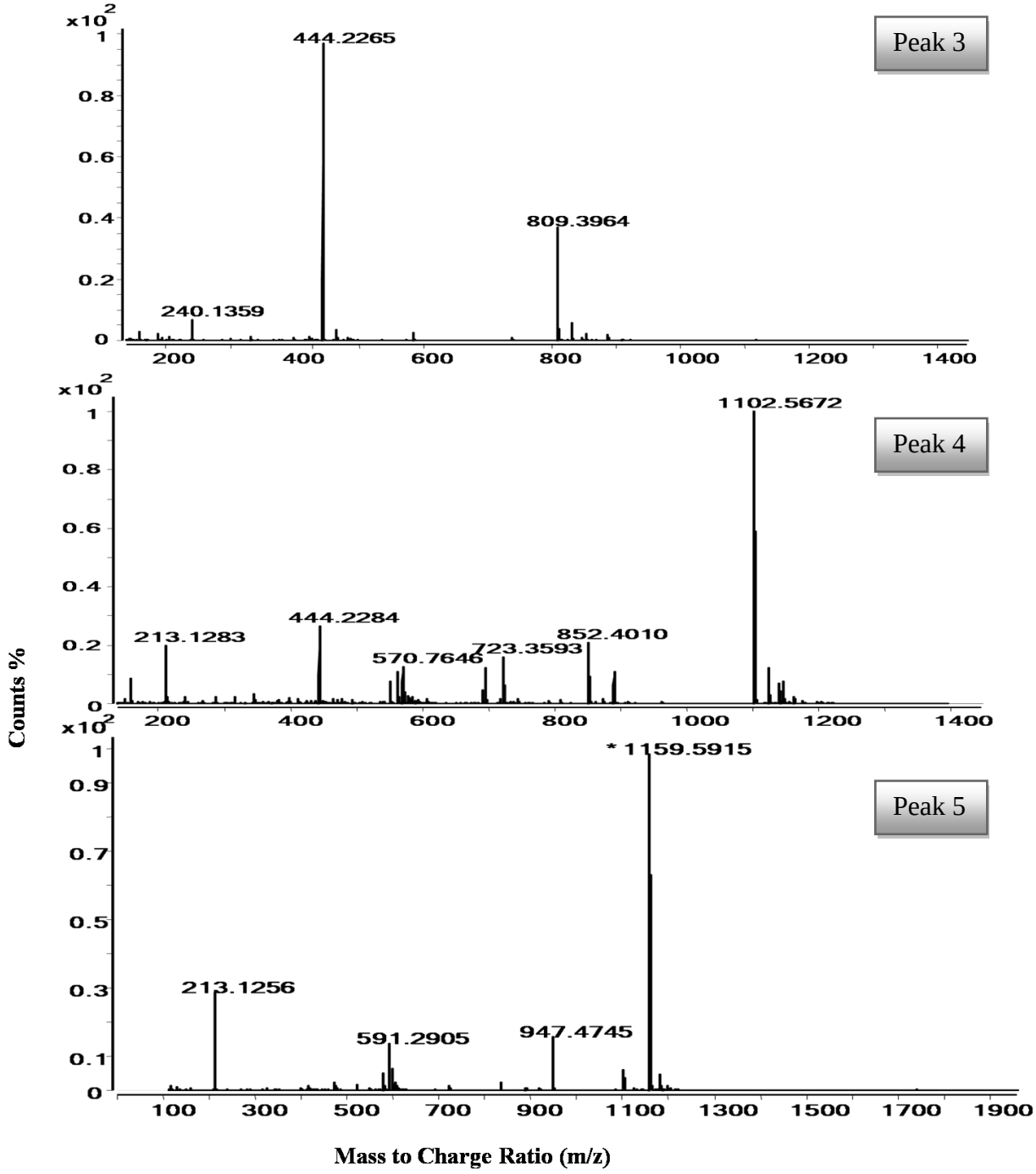

Fig. 18- ESI-TOF-MS spectra of peaks 3, 4 and 5 of the chromatogram shown in Fig. 16.

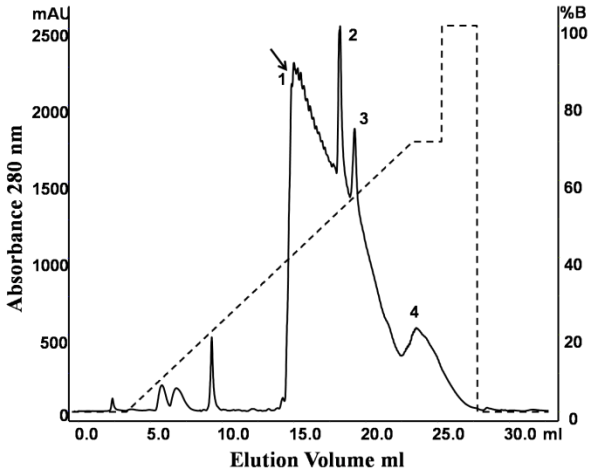

Fig. 19: Fraction of peak 10 of Fig. 11, on a C8 column by FPLC

Peak 10 of the size exclusion chromatogram, Fig. 11, was fractionated on a C8 column, by FPLC. The fractions eluting between 5-10 ml and between 14-25 ml were collected and subjected to ESI-TOF-MS analysis. All fractions were also tested for inhibition of ACE. Fractions eluting in peaks 3 and 4 showed inhibition of ACE. The ESI-TOF-MS spectra of the four peaks showed masses in the range 444 $(M+H)^+$-1445.7 $(M+H)^+$**,** illustrated in Fig. 20 and 21.

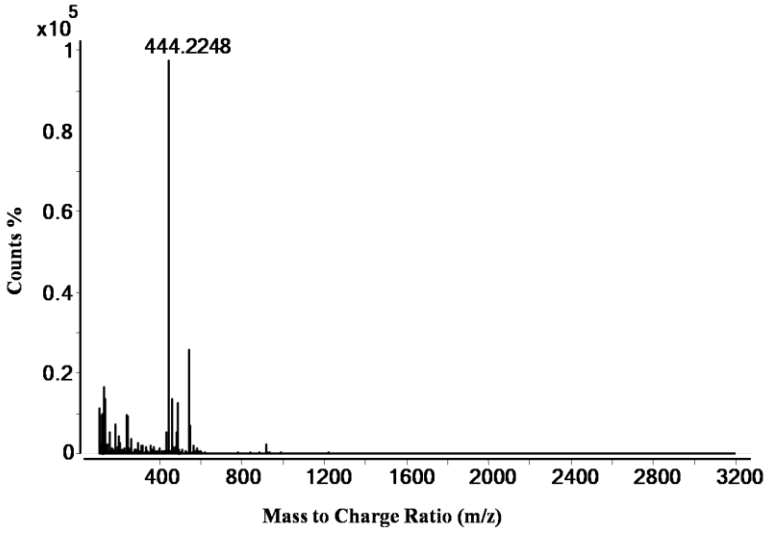

Fig. 20: ESI-TOF-MS spectrum of the peak 1 from the chromatogram shown in Fig. 19.

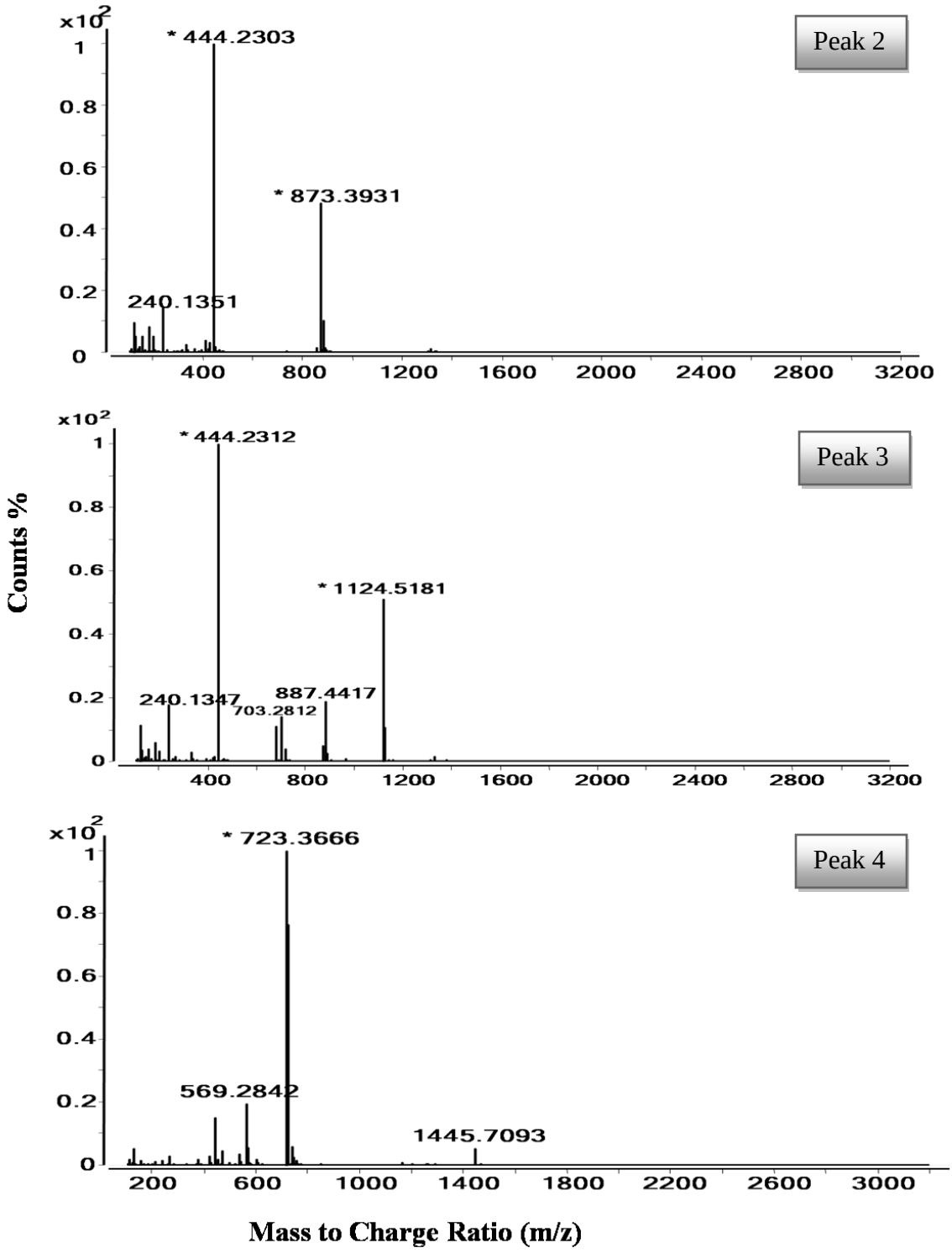

Fig. 21- ESI-TOF-MS spectrum of peaks 2, 3 and 4 from the chromatogram shown in Fig. 19.

The ESI-spectrum, Fig. 20, of peak 1 from the chromatogram shown in Fig. 19 shows a mass of 444 Da $(M+H)^+$. The formula ($C_{22}H_{29}N_5O_5$) was generated, by selecting this peak, using the "Generate Formulas" option in the software Agilent Mass Hunter Qualitative Analysis (version B.03.01). The variables in the method editor of "Generate Formulas" were fixed as, charge carrier to "Hydrogen ion", the MS ion electron state to "even electron" and the isotope model was fixed to "peptides". The formula fits to the tri peptide ZKW, previously reported as a metalloproteinase inhibitor in the venom of the snake *Trimeresurus mucrosquamatus* [105]. This fraction was then sent to Violette Frochaux, department of Chemistry, Humboldt University, Berlin, for de novo sequencing. To identify other similar N-terminally blocked tri peptides in the mass spectrum, a table was prepared with approximate molecular weights, fixing pyroglutamate at the N-terminal, tryptophan at the C-terminal and varying the amino acid in the middle, summarized in table 2.

Table 2: Possible sequences of N-terminally blocked tripeptides

Amino Acid	Molecular weight	Molecular weight -18	Z+X+W	Sequence
Ala: 89.00	89	71	386	ZAW
Arg: 174.00	174	156	471	ZRW
Asn: 132.00	132	114	429	ZNW
Asp: 133.00	133	115	430	ZDW
Cys: 121.00	121	103	418	ZCW
Gln: 146	146	128	443	ZQW
Glu: 147	147	129	444	ZEW
Gly: 75.00	75	57	372	ZGW
His: 155	155	137	452	ZHW
Ile: 131.00	131	113	428	ZIW
Leu: 131.00	131	113	428	ZLW
Lys: 146.00	146	128	443	ZKW
Met: 149.000	149	131	446	ZMW
Phe: 165.000	165	147	462	ZFW
Pro: 115.000	115	97	412	ZPW
Ser: 105.000	105	87	402	ZSW
Thr: 119.000	119	101	416	ZTW
Trp: 204.000	204	186	501	ZWW
Tyr: 181.000	181	163	478	ZYW
Val: 117.000	117	99	414	ZVW

Peak 11 of the size exclusion chromatogram (Fig. 11) was fractionated on a C8 column as shown in Fig. 22. All peaks marked were screened for inhibitory activity towards ACE. Peak 1 showed inhibition of ACE.

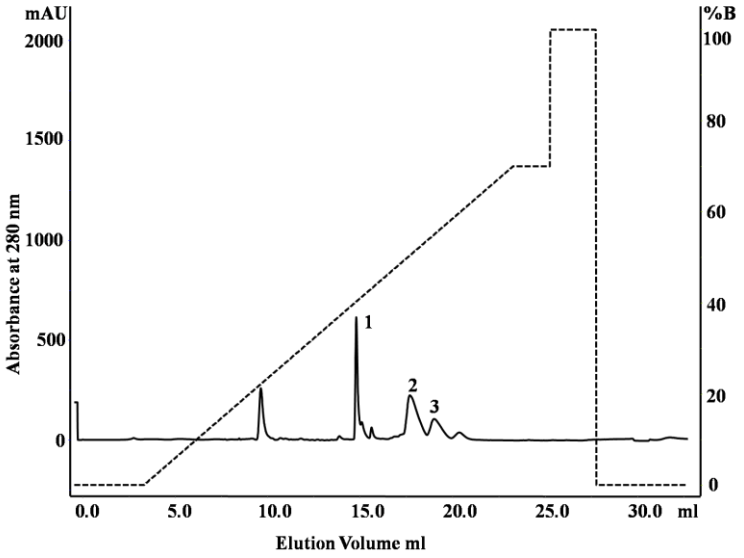

Fig. 22: Purification of peak 11 from the chromatogram (Fig. 11) on a C8 column by FPLC

The fractions eluting in the marked peaks were subjected to ESI-TOF-MS analysis and showed masses in the range 413 Da-1276 Da $(M+H)^+$. The ESI-TOF-MS spectrum of peak 1 is shown in Fig. 23

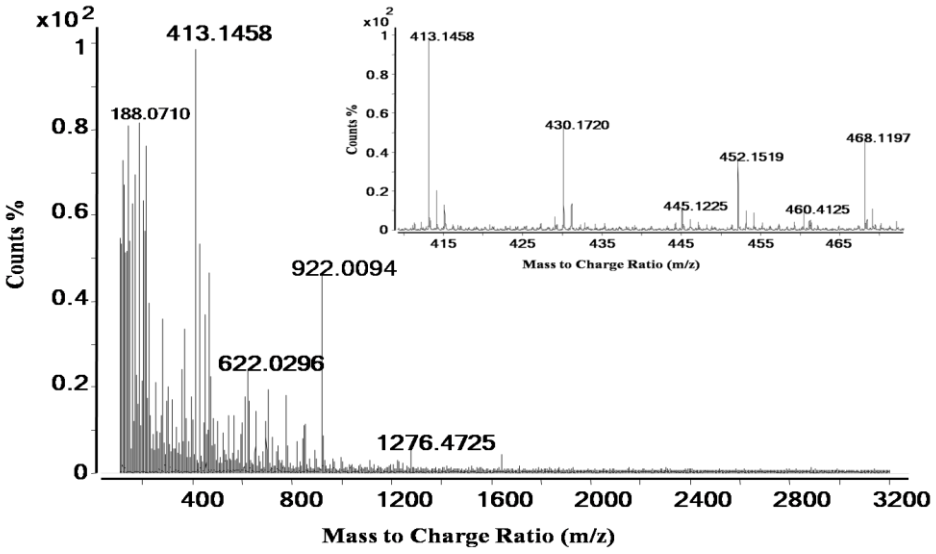

Fig. 23: ESI-TOF-MS spectrum of peak 1 from the chromatogram shown in Fig. 22.

The mass 922 Da $(M+H)^+$, is that of an internal standard. The inset shows the zoom of the spectrum in the range between 400-470 Da and gave an indication about the presence of the tripeptides based on the calculations summarized in table 2. The ESI-MS spectra of peaks 2 and 3 are shown in Fig. 24

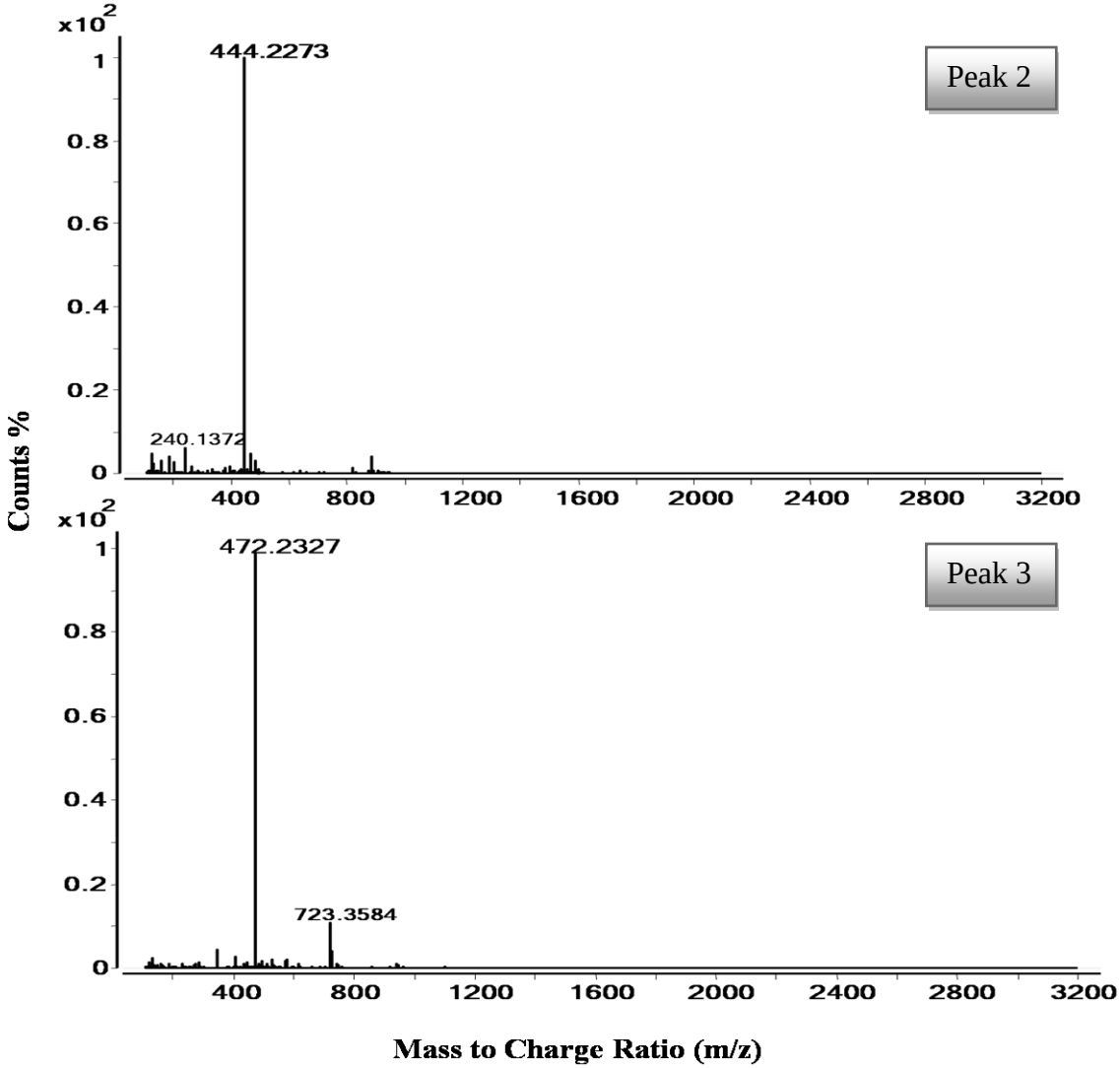

Fig. 24: ESI-TOF-MS spectra of peaks 2 and 3 from the chromatogram shown in Fig. 22.

The ESI-TOF-MS spectra (Fig. 24) also showed mass match to N-terminally blocked tripeptides. The inhibitory activity of the tripeptides towards snake venom metalloproteinase was tested with a synthetic tripeptide ZQW (obtained from China Peptide Company), at a concentration of 100

µM. It showed complete inhibition of the SVMP at this concentration. All of these samples were given for protein identification and de novo sequencing.

4.2: Kunitz-type, ACE and metalloproteinase inhibitors in the *Vipera ammodytes meridionalis* venom

Four signals of a Kunitz type peptide inhibitor (Venom basic protease inhibitor I) were identified in the venom of *Vipera a. meridionalis* (Table 3). The inhibitor has been identified using a tryptic digest analysis by LC/ESI ion trap MS and subsequent data base search. The tryptic peptides that were identified are shown in bold red colour (Table 3). Deconvoluted masses of the intact molecules were M = 6841, 6859.02, 7383.27 and 7401.28 Da as shown in Fig. 13. They belong to the 66 amino acid propeptide (M = 7401), the mature inhibitor (M = 6859) [120] and two associated signals of both species with a mass shift of -18 Da which might hint to a pyroglutamate at the N-terminus [mass shift of -18 Da, Glu > pyro-Glu (N-term Q)] often reported in snake venom peptides. Further mass differences in both blocked and unblocked species, point to an amino acid exchange in the *Vipera a. meridionalis* venom peptide compared to its counterpart in the *Vipera a. ammodytes* venom, where this inhibitor has been described, or to post-translational modifications such as amidation.

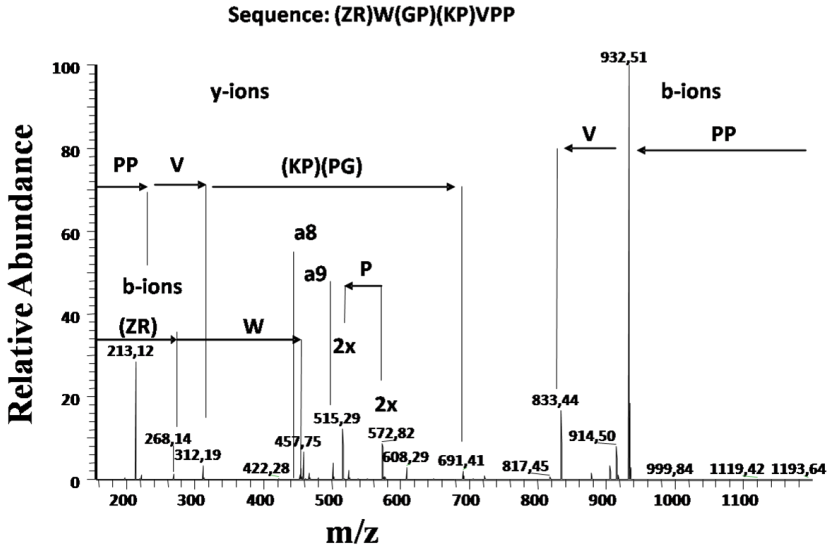

Fig. 25: FTICR MS/MS spectrum of the doubly charged ion peak [M +2 H]$^{+2}$ at m/z 572.82. The peptide was manually sequenced de novo. The figure shows b and y ion series and also other internal fragments.

Table 3: Peptide composition of the *Vipera ammodytes meridionalis* venom.

Fraction No. (SEC)	Observed m/z	Sequence determined	Inhibitory activity	Homology with peptide from	Peptide family	Mode of measurement
6	6859.02	QDHPK**FCYLPADPGR**CKA HIPR**FYYDSASNKCNKFIY GGCPGNANNFKTWDECR QTCGASA**	Trypsin, Kallikrein	P00991: *Vipera ammodytes*	Kunitz /BPTI	Tryptic digestion, LC/ion trap
8	890.60 $(M+H)^+$	ZPGPVSPQV	ACE	P01021.4: *Gloydius blomhoffi*	BPP	Q-TOF, manual sequencing
8	1102.5685 $(M+H)^+$	ZNWPGPKVPP	ACE	B0VXV8: *Sistrurus c. edwardsii*	NP	MALDI-TOF/TOF
8	562.90 $(M+2H)^{+2}$	PNVTPGCGSVPP	ACE	A8S6B3.1: *Austrelaps superbus*	NP	Q-TOF, sequence determined by PEAKS Online software
8	572.82 $(M+2H)^{+2}$	ZRWGPKPVPP	ACE	P0C7S7.1: *Protobothrops mucrosquamatus*	BPP	FTICR-MS
8	466.80 $(M+2H)^{+2}$					
8	1166.50 $(M+H)^+$					
8	1172.50 $(M+H)^+$					
9	681.3019 $(M+H)^+$		ACE		BPP	
9	809.3965 $(M+H)^+$	ZNWPGPK	ACE	B0VXV8: *Sistrurus c. edwardsii*	BPP	MALDI-TOF/TOF
9	570.7646 $(M+2H)^{+2}$					
9	1159.5913 $(M+H)^+$		ACE		BPP	
10	444.2247 $(M+H)^+$	ZKW		A8YPR6: *Echis ocellatus*	MPI	FTICR-MS
10	723.3574 $(M+H)^+$	ZRWPGP	ACE	Q7T1M3.1: *Bothrops jararacussu*, B0VXV8: *Sistrurus c. edwardsii*	BPP	FTICR-MS
10	1445.7045 $(M+H)^+$		ACE		BPP	
11	430.1721 $(M+H)^+$	ZNW			MPI	Q-TOF, manual sequencing
11	472.2307 $(M+H)^+$	ZRW			MPI	FTICR-MS
11	1276.4733 $(M+H^+)$		ACE		BPP	

Abreviations used: ACE: angiotensin-converting enzyme; BPP: Bradykinin-potentiating peptide; NP: natriuretic peptide; CNP: C-type natriuretic peptide; MPI: metalloproteinase inhibitor; Z means pyroglutamyl residue; SEC: size-exclusion chromatography.

Four doubly charged ions of *m*/*z* 467–591 $[M +2 H]^{+2}$ and 12 ions of *m*/*z* 430–1445 $[M + H]^{+}$ were identified by employing different mass spectrometric techniques, as given in table 3. A representative MS/MS spectrum obtained from the doubly charged ion peak $[M +2 H]^{+2}$ at m/z 572.82 is shown in Fig. 25. The sequence was determined manually by the analysis of b and y ion series and other fragments. The fragmentation pattern showed an ion at m/z 213.12, assigned to y_2 ion, which eventuates from the cleavage of C-terminal Pro-Pro, characteristic of BPP peptides [121]. The sequence determination by FTICR-MS/MS of the peptide with molecular weight 723 Da $(M+H)^{+}$ is shown in Fig. 26.

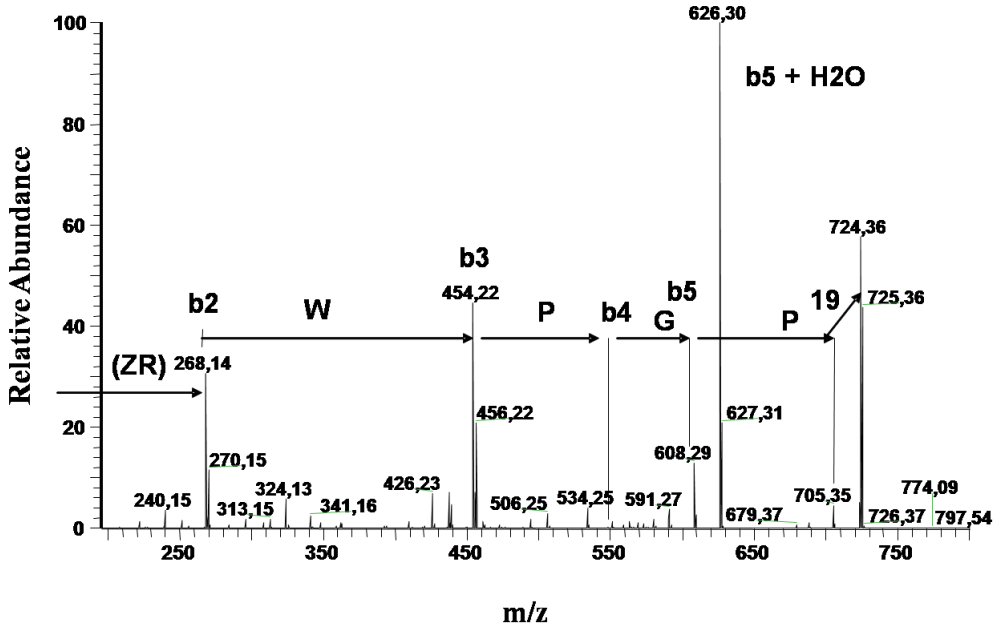

Fig. 26: FTICR-MS/MS spectrum of the peptide with a mass of 723 Da $(M+H)^{+}$

Three metalloproteinase inhibitors were identified and sequenced (Table 3). The peptide with a sequence ZRW has been identified for the first time. The other two peptides ZKW and ZNW have been reported previously in the venom of *Trimeresurus mucrosquamatus* [105]. The sequences ZRW and ZKW were determined by FTICR-MS. FTICR-MS/MS spectrum of ZRW is shown in Fig. 27, and that of ZKW is shown in Fig. 28.

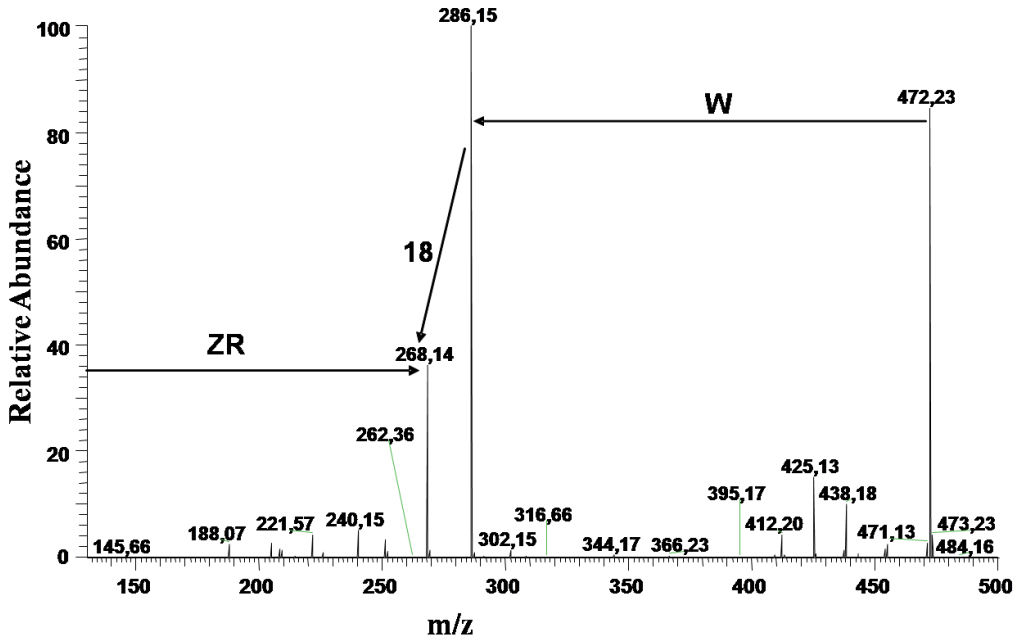

Fig. 27: FTICR- MS/MS spectrum of the tripeptide, with a molecular mass of 472 Da $(M+H)^+$.

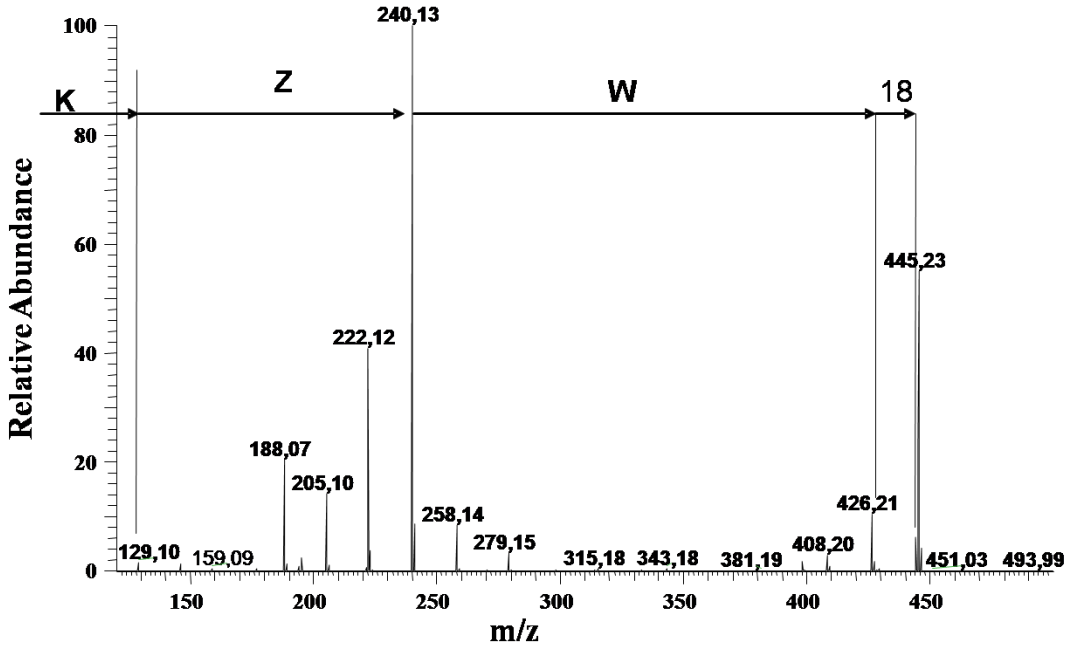

Fig. 28: FTICR-MS/MS spectrum of the tripeptide, with a molecular mass of 444 Da $(M+H)^+$.

Molecular masses between 680–1444 Da are typical for snake venom ACE inhibitors (Table 3). The sequences of six BPPs were determined as ZPGPVSPQV, ZNWPGPKVPP, PNVTPGCGSVPP, ZRWGPKPVPP, ZNWPGPK and ZRWPGP where Z is a pyroglutamyl residue. Four of these peptides show homology with BPPs and/or with natriuretic peptides from the Crotalinae venoms (*Gloydius blomhoffii*, *Bothrops jararaca*, *Sistrurus catenatus* and *Protobothrops mucrosquamatus*). Moreover, one of the identified *Vipera a. meridionalis* peptides showed homology with a natriuretic peptide from the venoms of Elapidae snakes (*Austrelaps superbus*). This indicates a homology between pharmacologically important components of the venom peptidomes of snakes from the two families: Viperidae and Elapidae. Interestingly, the Viper BPPs show an amino acid substitution close to the C-terminal portion of the molecule, when compared to the *Bothrops* peptides. The latter display an isoleucine followed by a double proline, while the former have the isoleucine substituted by valine. Such feature has also been identified in *Vipera berus* BPP [122], and might represent a common motif in this genus. The effects of these substitutions on the inhibition of ACE are yet to be investigated.

Structures of the other *Vipera a. meridionalis* venom peptides were not determined due to the low quantities of the isolated material. Search in the database (UniProt and Swiss Prot) showed that they are probably new peptides.

4.3: Fractionation of the *Bothrops jararacussu* venom by size exclusion chromatography and purification of peptides by liquid chromatography

The elution profile shown in Fig. 29A, demonstrates the presence of proteins with molecular masses > 10 kDa in the first three peaks. Several peaks were observed in the region of low molecular mass peptides (peaks 4–10). The fractions from peaks 4-9, were further separated by reverse phase chromatography and the peptides subjected to ESI-TOF-MS or MALDI-TOF-MS analysis.

The peaks 4-10 were screened to test inhibitory activity towards the selected enzymes. Peaks 4-9 showed inhibitory activity towards ACE. Peaks 4-10 were further purified by PLRP column at pH 9. All the chromatograms are shown in Fig. 30 and 31.

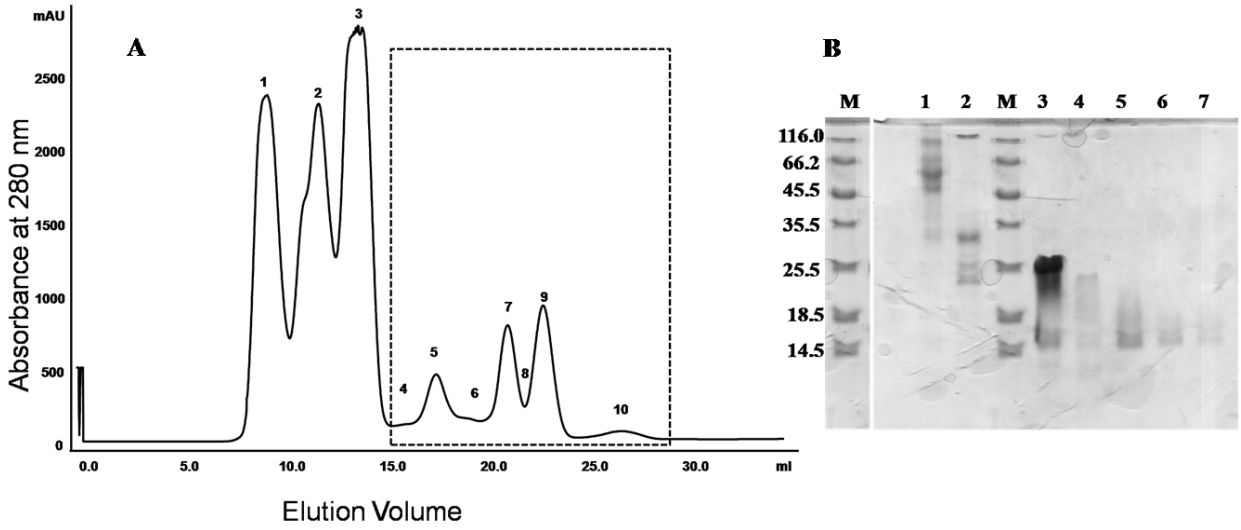

Fig. 29: (A) SEC of *Bothrops jararacussu* on a Superdex-75 column by FPLC at pH 5.0; (B) SDS-PAGE of fractions 1-7 from SEC separation of *Bothrops jararacussu.*

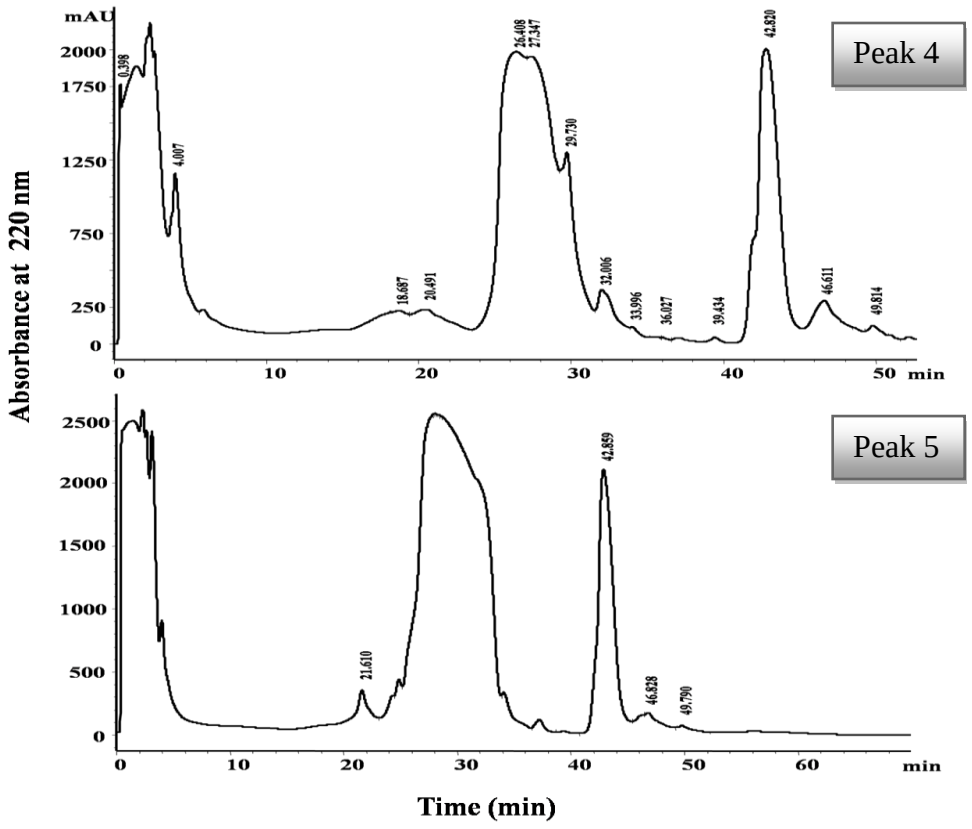

Fig. 30: Purification of peaks 4 and 5 of SEC, Fig. 29, on a PLRP column by HPLC at pH 9.0

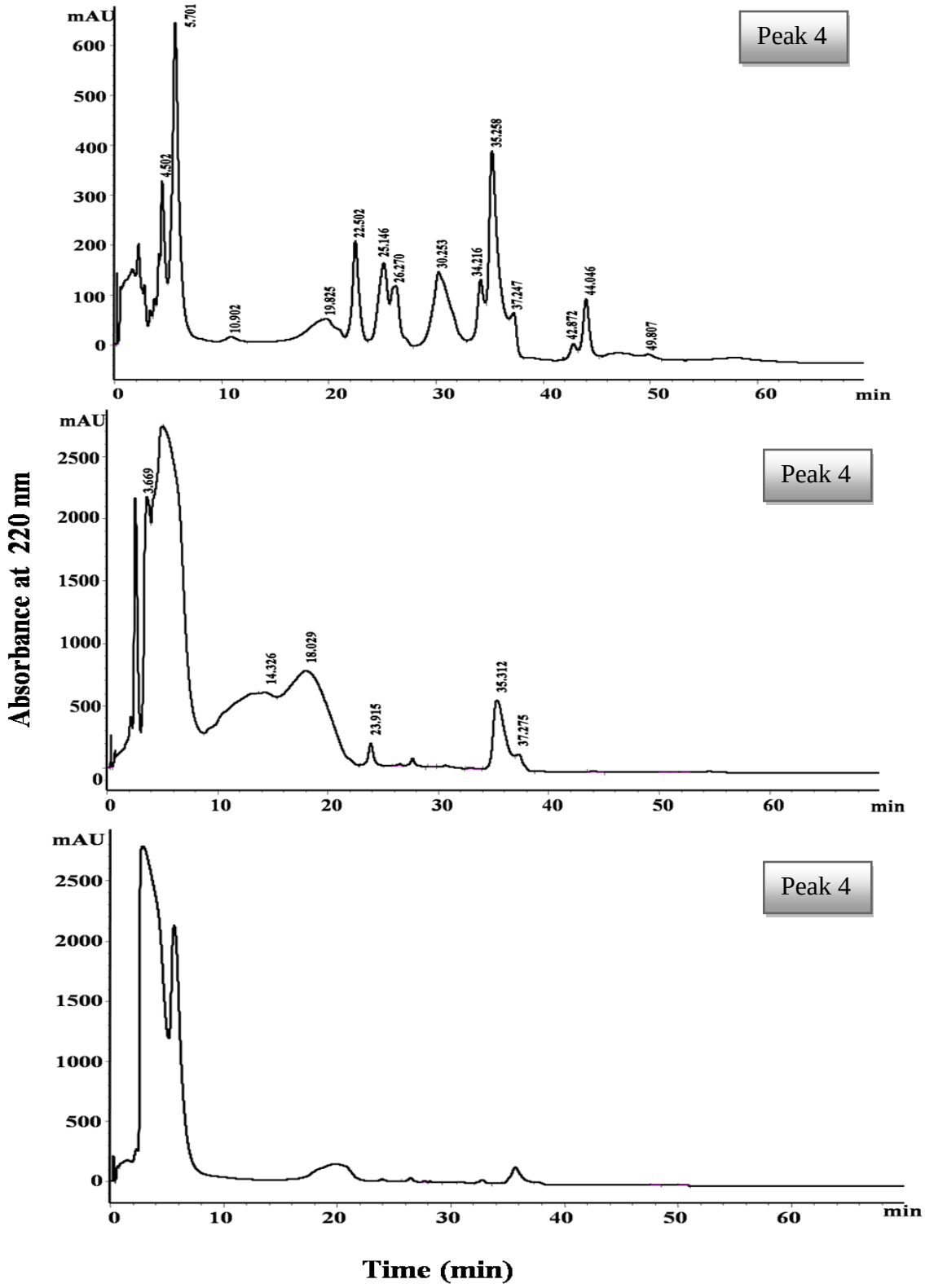

Fig. 31: Purification of peaks 6 and 7 and 8 of SEC, Fig. 29, on a PLRP column by HPLC at pH 9.

The fractions were collected, lyophilized and re suspended in water, and analyzed by MALDI-TOF mass spectrometry. The fractions were tested for inhibitory activity towards ACE. The fractions showing inhibitory activity were further purified on a Chromolith C18 column, and analyzed by MALDI-TOF-TOF mass spectrometry. Selected MALDI-TOF spectra of the purified fractions are shown in Fig. 32 and 33.

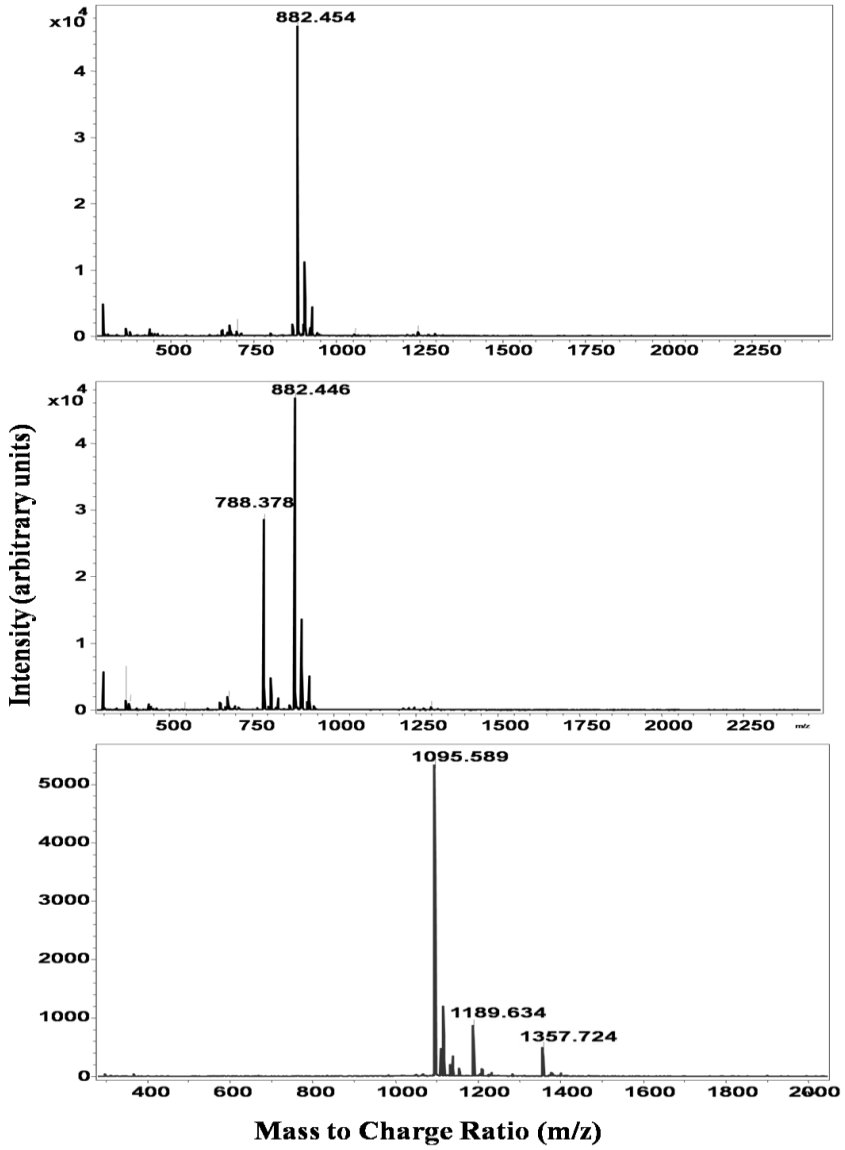

Fig. 32: Selected MALDI-TOF-MS spectra of purified low molecular weight peptide fractions from *Bothrops jararacussu* venom.

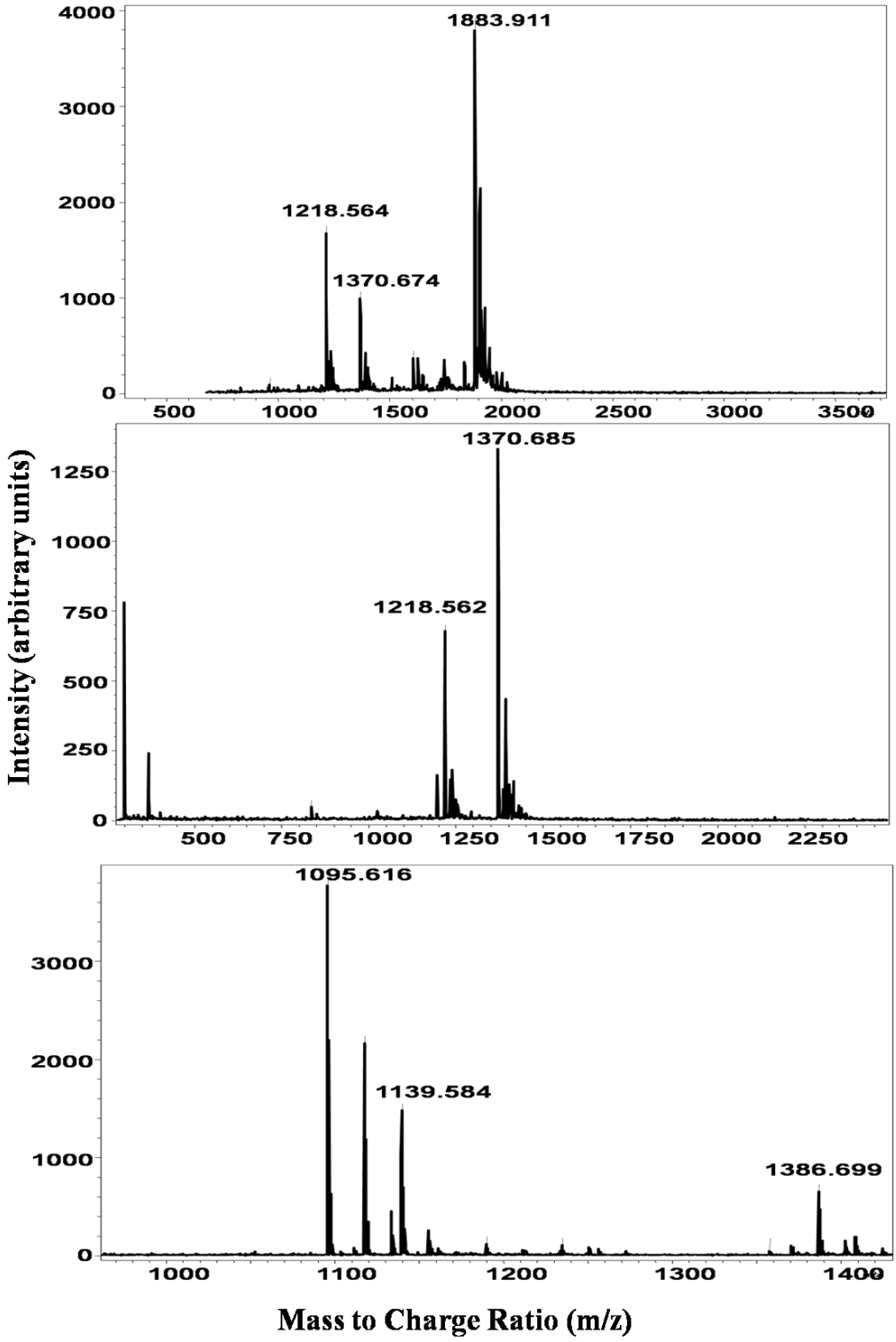

Fig. 33: Selected MALDI-TOF-MS spectra of purified low molecular weight peptide fractions from *Bothrops jararacussu* venom.

The sequence information of the peptides showing inhibition towards ACE was obtained by MALDI-TOF-TOF mass spectrometry and by analyzing the data with BioTools and Mascot Inhouse search. The sequence annotation pictures of the MALDI-TOF-TOF spectra were prepared with the Bruker software ProteinScape, version 3.0. Selected MS/MS spectra with sequence annotation are shown in the Fig. 34-37.

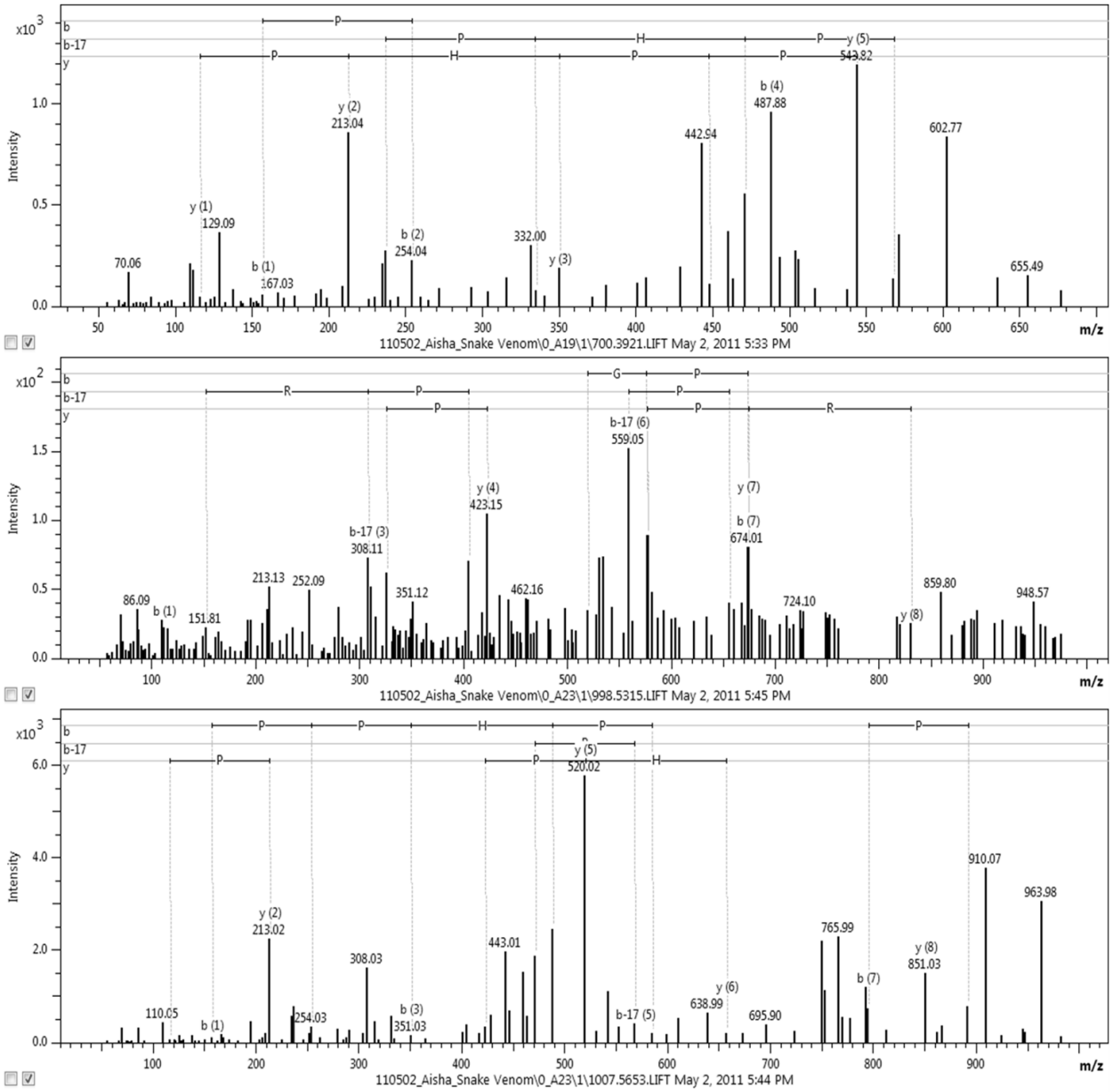

Fig. 34: Selected MALDI-TOF-TOF-MS spectra of purified *Bothrops jararacussu* venom peptides.

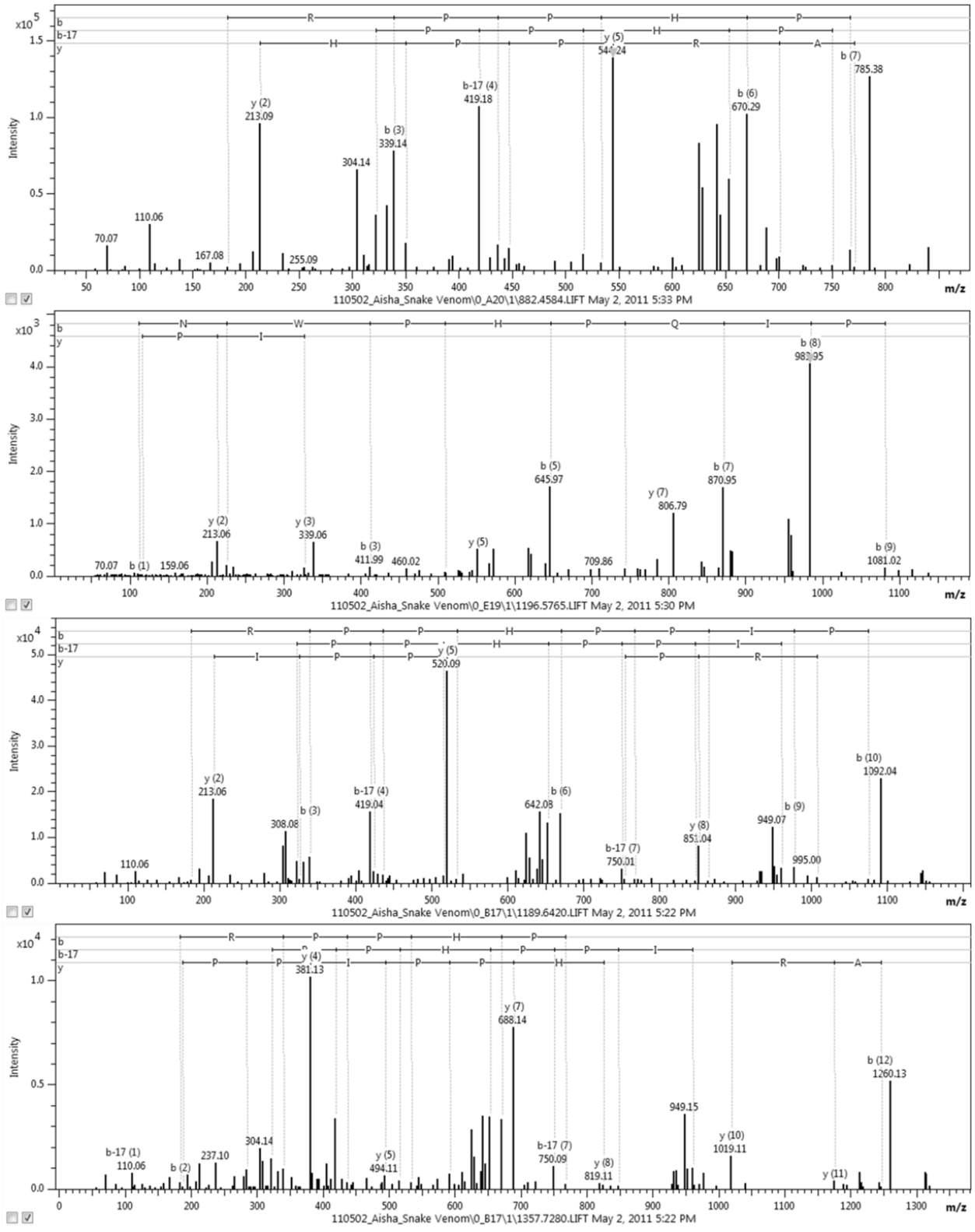

Fig. 35: Selected MALDI-TOF-TOF-MS spectra of purified *Bothrops jararacussu* venom peptides

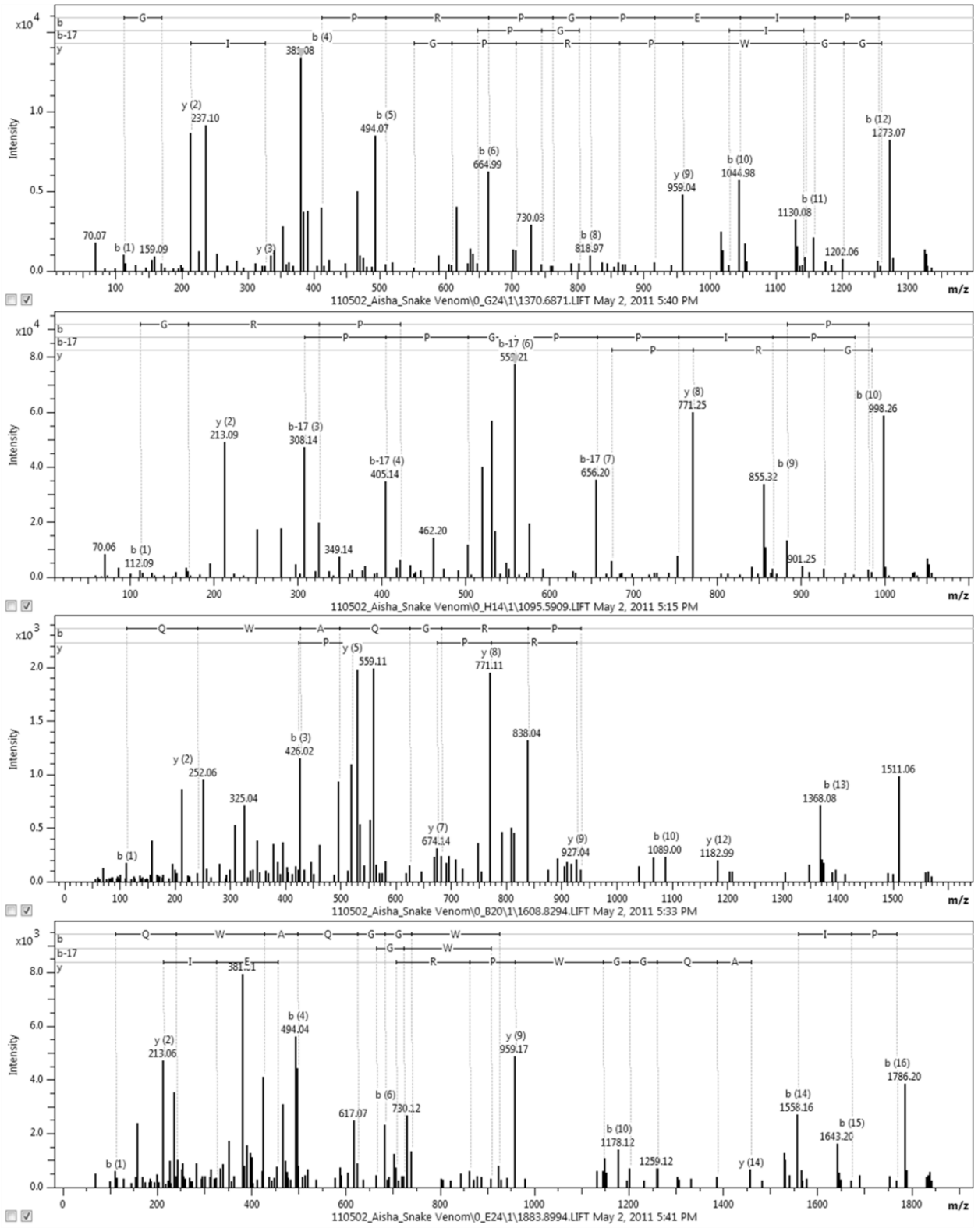

Fig. 36: Selected MALDI-TOF-TOF-MS spectra of purified *Bothrops jararacussu* venom peptides.

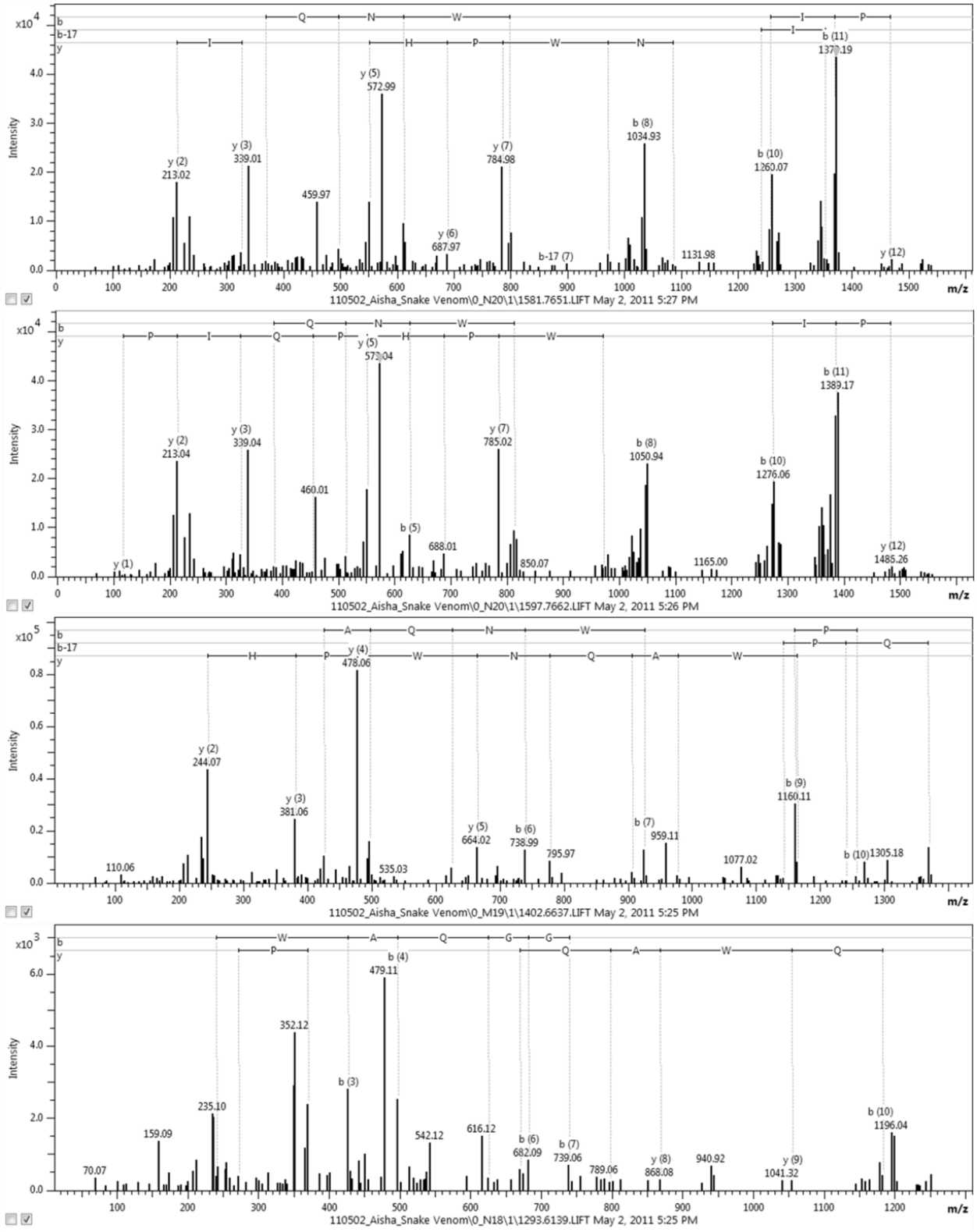

Fig. 37: Selected MALDI-TOF-TOF-MS spectra of purified *Bothrops jararacussu* venom peptides.

4.4: ACE inhibitors in the *Bothrops jararacussu* venom

Table 4: Peptide composition of the *Bothrops jararacussu* venom

Fraction No.	Molecular mass $(M + H)^+$	Sequence determined	Inhibitory activity towards	Homology with peptide from	Peptide family
4	700.3920	RPPHPP	ACE	Q9PW56: *Bothrops jararaca*	BPP and CNP
4	788.4041	ZGRPPGPP	ACE	Q7T1M3: *Bothrops jararacussu*	BPP and CNP
4	882.4584	ZARPPHPP	ACE	Q7T1M3: *Bothrops jararacussu*	BPP and CNP
4	934.5085	SKAPAAPHR		Q9PW56: *Bothrops jararaca*	BPP
4	984.5524	GRPPGPPIPP	ACE	Q7T1M3: *Bothrops jararacussu*	BPP and CNP
4	998.5315	ZGRPPGPPIP	ACE	Q7T1M3: *Bothrops jararacussu*	BPP and CNP
4	999.4832	DLRPDGKQA		A8YPR6: *Echis ocellatus*	SVMPI
4	1007.5560	RPPHPPIPP	ACE	P85167: *Bothrops jararaca*	BPP
				Q7T1M3: *Bothrops jararacussu*	BPP and CNP
4	1078.5571	SGSKAPAAPHR		Q9PW56: *Bothrops jararaca*	BPP
4	1095.5871	ZGRPPGPPIPP	ACE	Q7T1M3: *Bothrops jararacussu*	BPP and CNP
4	1189.6420	ZARPPHPPIPP	ACE	Q7T1M3: *Bothrops jararacussu*	BPP and CNP
4	1139.5407	SQGLPPGPPIP/Phospho (S)		P01021: *Agkistrodon h. blomhoffi*	BPP and CNP
4	1357.7280	ZARPPHPPIPPAP	ACE	Q7T1M3: *Bothrops jararacussu*	BPP and CNP
4	1370.6819	ZGGWPRPGPEIPP	ACE	Q7T1M3: *Bothrops jararacussu*	BPP and CNP
4	1608.8294	ZQWAQGRPPGPPIPP	ACE	Q7T1M3: *Bothrops jararacussu*	BPP and CNP
5	755.4457	ZPPTTKT		P68417: *Naja haje annulifera*	Short neurotoxin
5	791.4226	ZTIGRAY		Q7T1T4: *Bothrops jararacussu*	Zinc metalloproteinase (Fragment)
5	856.4091	ZQWAQGR		Q7T1M3: *Bothrops jararacussu*	BPP and CNP
5	873.4671	ZQKFSPR		Q7T1T4: *Bothrops jararacussu*	Zinc metalloproteinase (Fragment)
5	889.3941	QNWPHPQ		Q7T1M3: *Bothrops jararacussu*	BPP and CNP
5	959.5414	PRPGPEIPP		Q7T1M3: *Bothrops jararacussu*	BPP and CNP
5	1050.5130	ZQWAQGRPP		Q7T1M3: *Bothrops jararacussu*	BPP and CNP
5	1196.5765	ZNWPHPQIPP	ACE	Q7T1M3: *Bothrops jararacussu*	BPP and CNP
5	1386.6845	QGGWPRPGPEIPP	ACE	Q7T1M3: *Bothrops jararacussu*	BPP and CNP
5	1402.6857	QQWPRDPAPIPP	ACE	P86721: *Bothrops atrox*	BPP
5	1883.8993	ZQWAQGGWPRPGPEIPP	ACE	Q7T1M3: *Bothrops jararacussu*	BPP and CNP
6	934.4392	ZGGWPRPGP	ACE	Q7T1M3: *Bothrops jararacussu*	BPP and CNP
6	1384.6777	ZQWPRDPAPIPP	ACE	P86721: *Bothrops atrox*	BPP
6	1709.7891	ZQWAQNWPHPQIPP	ACE	Q7T1M3: *Bothrops jararacussu*	BPP and CNP
				Q6LEM5: *Bothrops jararaca*	BPP and CNP
				Q9PW56: *Bothrops jararaca*	BPP and CNP
				P68515: *Bothrops insularis*	BPP and CNP
7	1581.7651	ZWAQNWPHPQIPP	ACE	Q7T1M3: *Bothrops jararacussu*	BPP and CNP
7	1597.7662	QWAQNWPHPQIPP	ACE	Q7T1M3: *Bothrops jararacussu*	BPP and CNP
7	1597.7662	ZWSQNWPHPQIPP	ACE	B0VXV8: *S. c. edwardsii*	BPP and CNP
7	1613.7647	QWSQNWPHPQIPP	ACE	B0VXV8: *S. c. edwardsii*	
8	1402.6637	ZQWAQNWPHPQ		Q7T1M3: *Bothrops jararacussu*	BPP and CNP
8	1418.4953	QQWAQNWPHPQ		Q7T1M3: *Bothrops jararacussu*	BPP and CNP
				Q6LEM5: *Bothrops jararaca*	BPP and CNP
				P68515: *Bothrops insularis*	BPP and CNP
				Q9PW56: *Bothrops jararaca*	BPP and CNP
9	1293.6139	ZQWAQGGWPRP		Q7T1M3: *Bothrops jararacussu*	BPP and CNP

All the peptides were characterized by MALDI-TOF/TOF. Abbreviations used: ACE: angiotensin-converting enzyme; BPP: bradykinin-potentiating peptide; NP: natriuretic peptide; CNP: C-type natriuretic peptide; MPI: metalloproteinase inhibitor; Z means pyroglutamyl residue; SEC: size-exclusion chromatography.

37 peptides of the peptide fraction of the *Bothrops jararacussu* venom were identified (Table 4). The amino acid sequences of all peptides were determined by MALDI-TOF-TOF. The identified peptides have molecular masses in the range m/z 700–1883. 32 of them belong to the BPP family of peptide inhibitors involved in the hypotensive effects of the snake venom. The other four are

small fragments of snake venom metalloproteinase and of a short neurotoxin (Table 4). In one of the BPPs, with a molecular mass of 1138 Da, having the sequence SQGLPPGPPIP, the b-ion series of the MS/MS spectra indicated the phosphorylation of a serine residue. However, this result needs further validation. Some of the peptides have previously been reported: ZGRPPGPPIPP, ZNWPHPQIPP, ZARPPHPPIPP, ZARPPHPPIPPAP and ZGGWPRPGPEIPP, where Z means pyroglutamyl residue [121, 123-125]. Variability in the C-terminal parts of BPPs was observed. Thus, ZARPPHPP is a modified form of a peptide found in the *B. jararacussu* venom [121], lacking the C-terminal I-P-P. The peptide ZARPPHPPIPP is another form of ZARPPHPPIPPAP of the *B. jararacussu* peptidome [121]. The peptides QNWPHPQ and ZGGWPRPGP, identified in the present work, are modified forms of peptides identified before in *B. insularis* and *B. newiedi* venoms [124], lacking the C-terminal I-P-P and E-I-P-P segments, respectively. The structure ZQWAQNWPHPQ is homologous to that of other peptide identified in this work, containing a C-terminal extension of I-P-P (Table 4). ZQWAQNWPHPQIPP is an isoform of a peptide, shown in table 4 and having additional N-terminal Q but lacking a C-terminal I-P-P (Table 4).

4.5: Fractionation of the *Naja mossambica mossambica* venom by size exclusion chromatography and purification of peptides by liquid chromatography

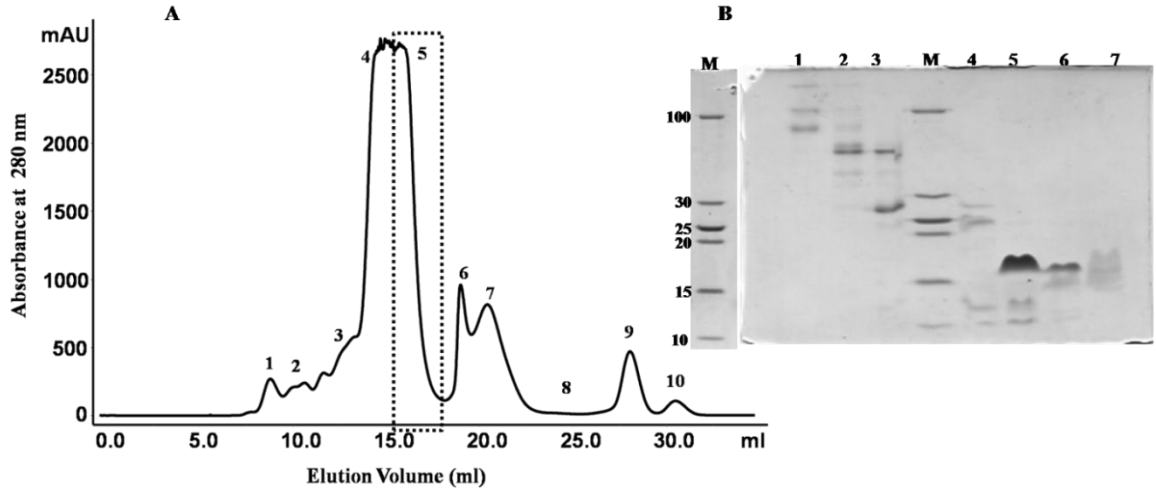

Fig. 38: (A) SEC of *Naja mossambica mossambica* venom on Superdex-75 column at pH5; (B) SDS-PAGE of fractions 1-7 from SEC separation of the venom.

Crude venom of *Naja mossambica mossambica* was fractionated by SEC on a Superdex-75 column at pH 5.0, (Fig. 38 A). Peaks 4-10 contain peptides below 10 KDa, as seen in SDS-PAGE (Fig. 38 B). The inhibitory activity of fractions 4-10 was tested with the selected enzymes. Peak 5 showed inhibitory activity towards subtilisin, chymotrypsin and Trypsin. The fractions in the valley marked as 8, and peak 10 showed inhibitory activity towards ACE. Peak 5 was further purified on a resource S column at pH 5.5, by FPLC (Fig. 39).

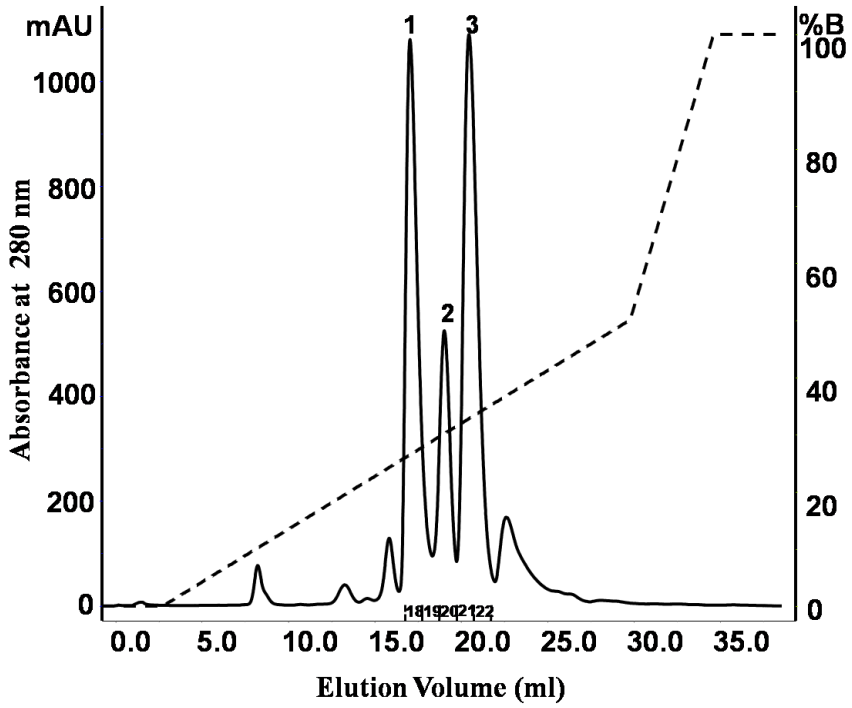

Fig. 39: Purification of peak 5 eluting from SEC (Fig. 38 A) on a Resource-S column.

Three major peaks were observed. The fractions were not pooled. All of the fractions were desalted by Superdex-Peptide (10x300) column, and lyophilized. The fractions were tested for inhibitory activity towards chymotrypsin and bacterial subtilisin, Stmpr1. Peak 1 (fraction 18) showed inhibitory activity towards both the enzyme. This fraction also inhibited proteasome 20S. The peaks 1-3, were further analyzed by MALDI-TOF mass spectrometry. A peptide with a molecular mass of 6726 Da was observed in peak 2, and a mass of 6837 Da was observed in peak 3 (Fig. 40). The peaks at m/z 13453 $(M+H)^+$ and 13675 $(M+H)^+$ are the dimmers of the masses 6727 $(M+H)^+$, and 6838 $(M+H)^+$ respectively. Since the MALDI-TOF mass spectrum of

peak 1 (fraction 18) showed a broad band, therefore it was analyzed by ESI-TOF-MS to obtain the exact molecular mass of the peptide.

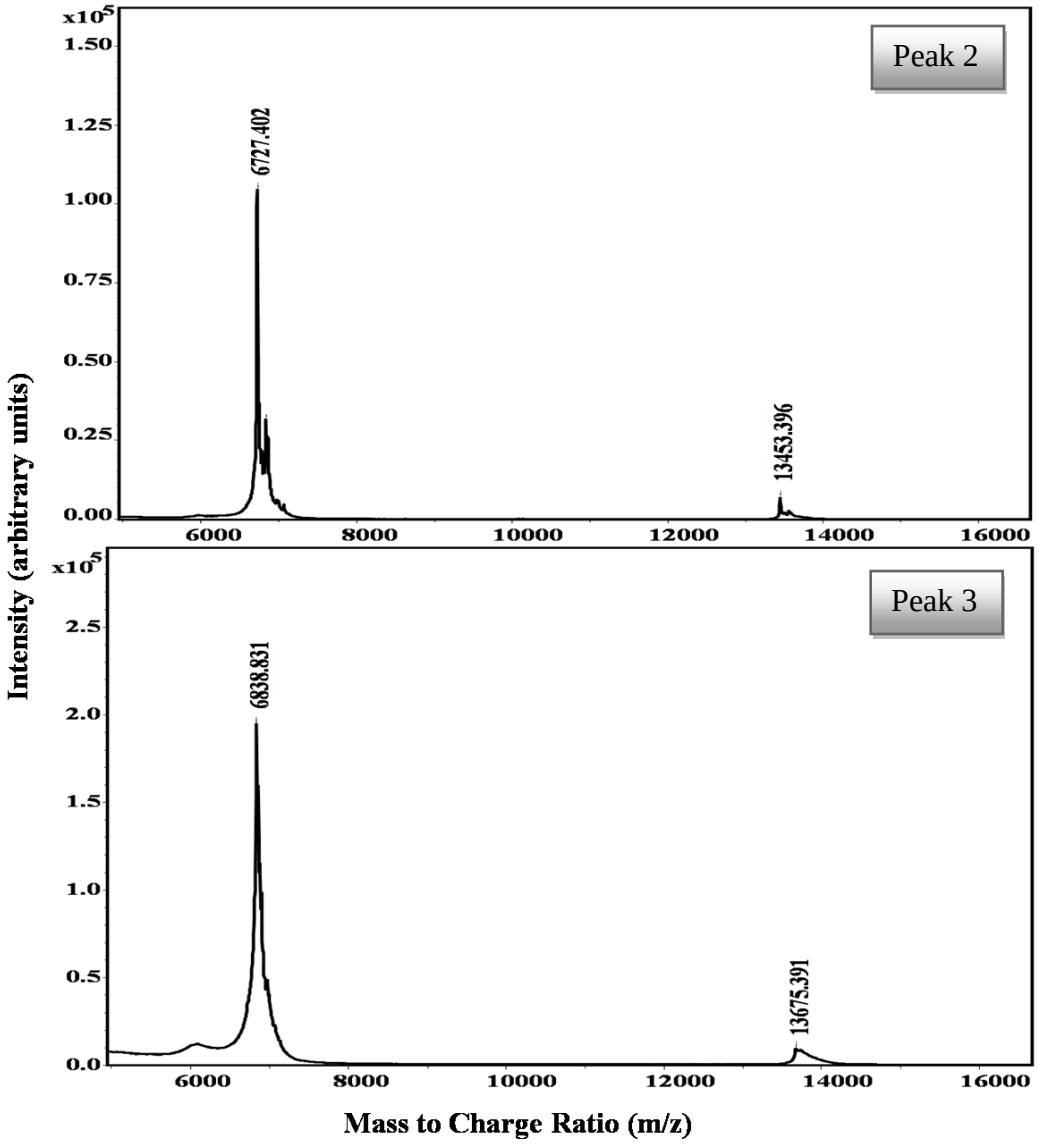

Fig. 40: MALDI-TOF-MS spectra of peak 2 and 3 from the chromatogram (Fig. 39).

The ESI-MS spectrum (Fig. 41) showed the presence of six signals which correspond to the multiply charged ions at m/z 2274.1, 1705.8, 1364.8, 1137.5, 975.2, and 853.4. From these multiply charged peaks the mass of the peptide was accurately determined as 6819.28 Da.

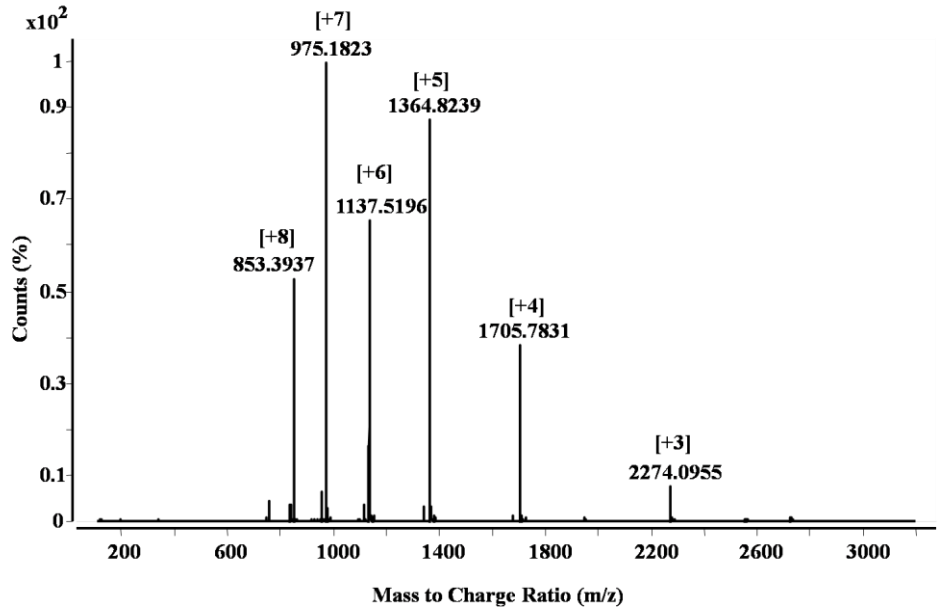

Fig. 41: ESI-TOF-MS spectrum of peak 1 (fraction 18) of the chromatogram shown in Fig. 39.

The SDS page of peak 6 from the chromatogram in Fig. 38 also showed a band in the low molecular mass region, so it was also subjected to purification by reverse phase chromatography on a C-8 column, Fig. 42.

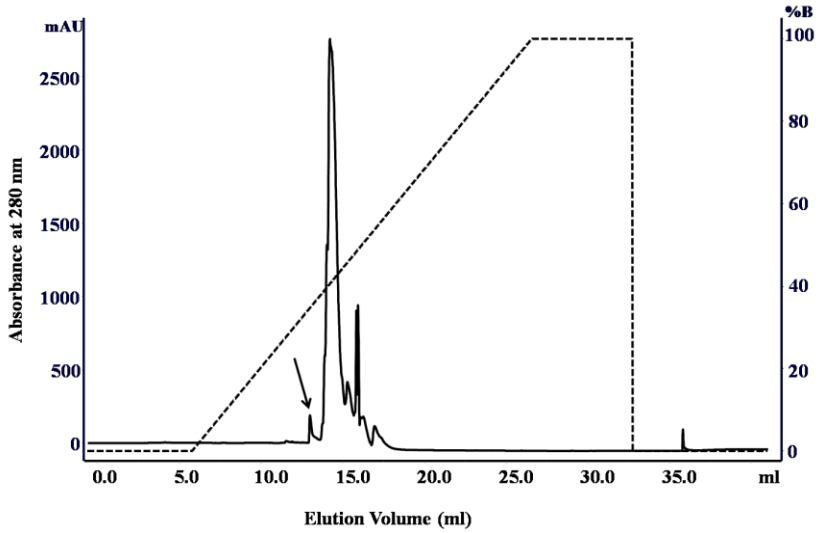

Fig. 42: Purification of peak 6 (Fig. 38) on a C-8 column by FPLC.

The fractions were not pooled and the molecular mass of all the fractions was determined by ESI-TOF-MS spectrometry. The peak marked by an arrow in Fig. 42, showed the presence of peptides with molecular masses below 10 kDa (Fig. 43). The peptides were identified by tryptic digestion.

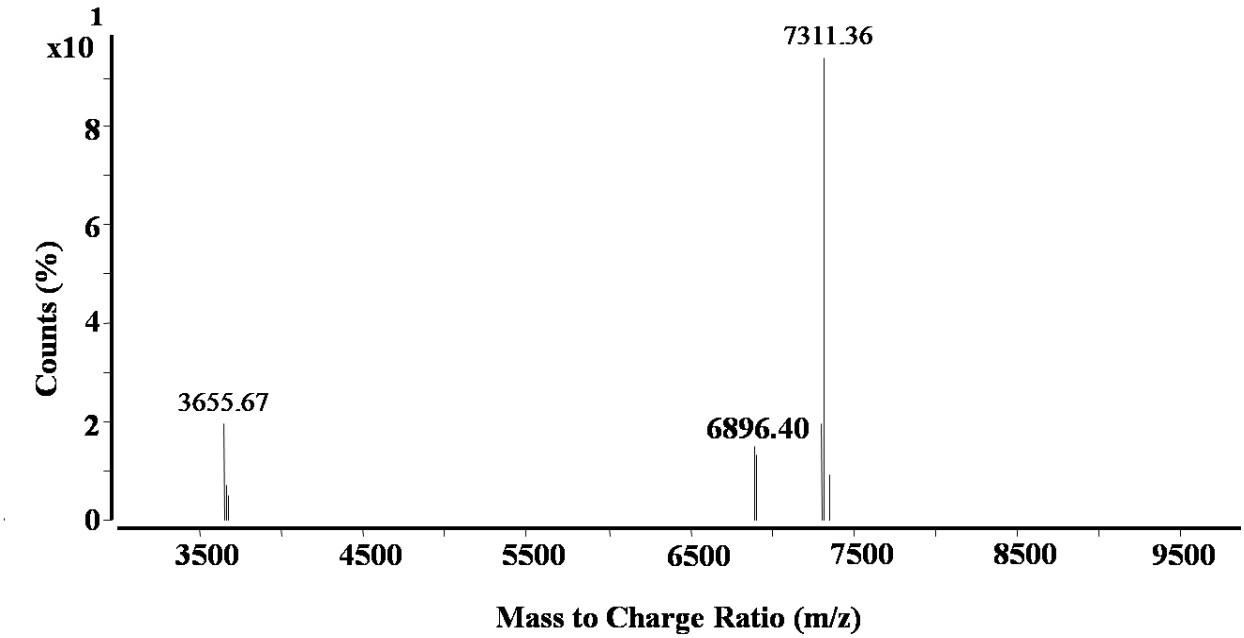

Fig. 43: ESI-TOF-MS spectrum (deconvoluted) of the peak marked by an arrow from the chromatogram (Fig. 42).

The fractions in valley marked as peak 8, from the size exclusion chromatogram shown in Fig. 38A, showing inhibition of ACE, were pooled and subjected to further purification on a C-18 column by FPLC, as shown in Fig. 44. The chromatogram shows two main peaks. The fraction in the peak marked by an arrow in the chromatogram (Fig. 44) inhibited ACE. This fraction was further analyzed by MALDI-TOF-MS and MALDI-TOF-TOF mass spectrometric analysis.

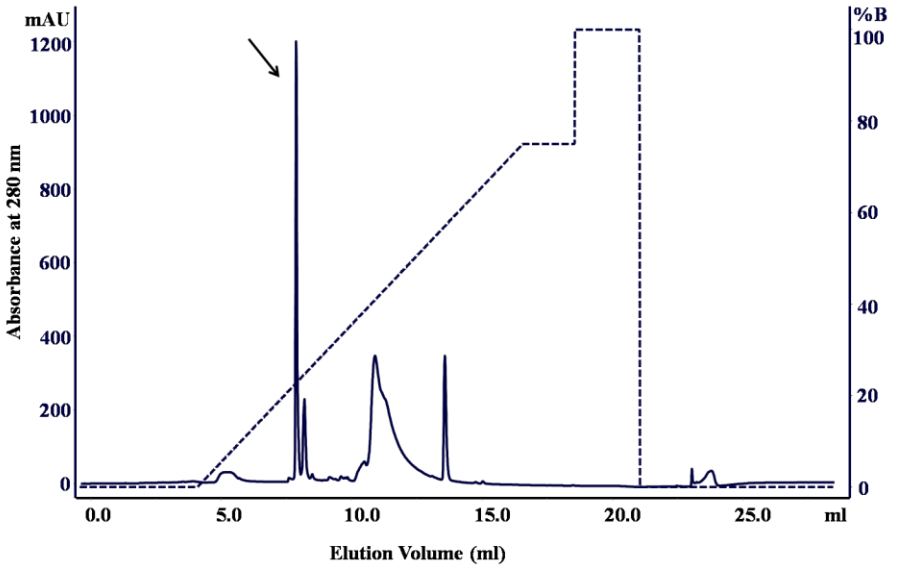

Fig. 44: Purification of peak 8 from the chromatogram (Fig. 38) on a C-18 column by FPLC.

The MALDI-TOF spectrum showed masses in the range 379 $(M+H)^+$-1243 $(M+H)^+$, as shown in Fig. 45 below.

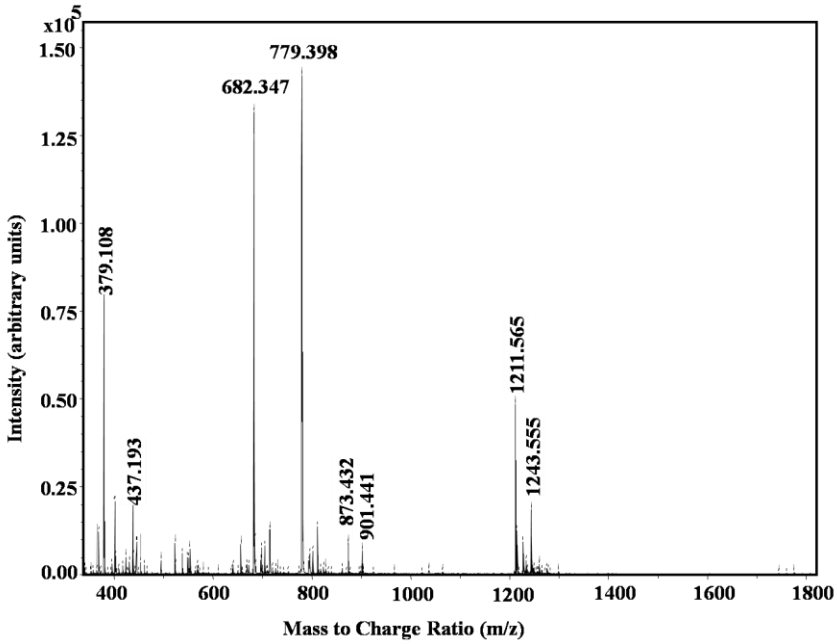

Fig. 45: MALDI-TOF-MS spectrum of the first peak from the chromatogram (Fig. 44).

Peak 10 from the SEC (Fig. 38) was also purified on a C18-column under the same condition as that of peak 8. The resulting chromatogram is shown in Fig. 46.

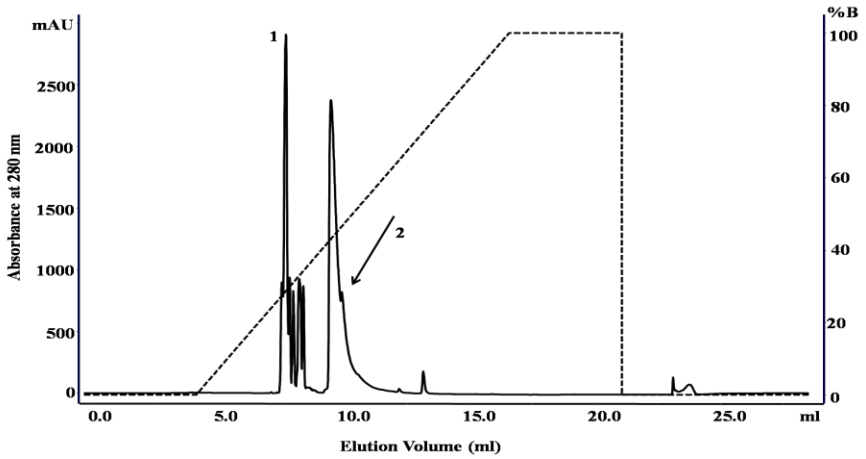

Fig. 46: Purification of peak 10 from SEC (Fig. 38) on a C-18 column by FPLC.

The MALDI-TOF-MS spectrum of peak 1 marked illustrates the presences of molecules with masses in the range 437 $(M+H)^+$-1345 $(M+H)^+$, shown in the Fig. 47.

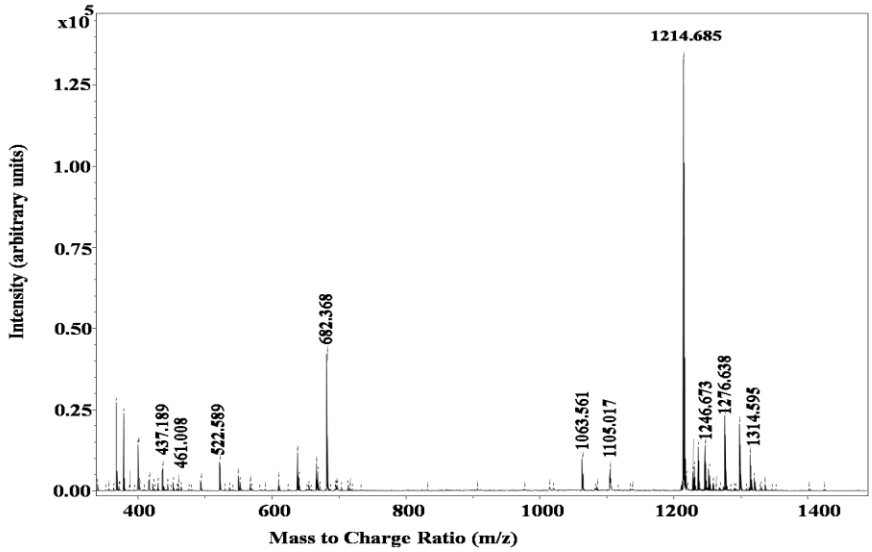

Fig. 47: MALDI-TOF-MS spectrum of peak 1 from the chromatogram shown in Fig. 46.

The MALDI-TOF-MS spectrum of the peak 2 marked in the chromatogram (Fig. 46) showed same molecular masses as in peak 1, but at a lower intensity. The sequence annotation pictures of MALDI-TOF-TOF spectra of the bradykinin potentiating peptides purified from peaks 8 and 10 from the size exclusion chromatogram (Fig. 39) are shown in the Fig. 48 and 49. The sequence annotation pictures were prepared with Bruker software ProteinScape, version 3.0.

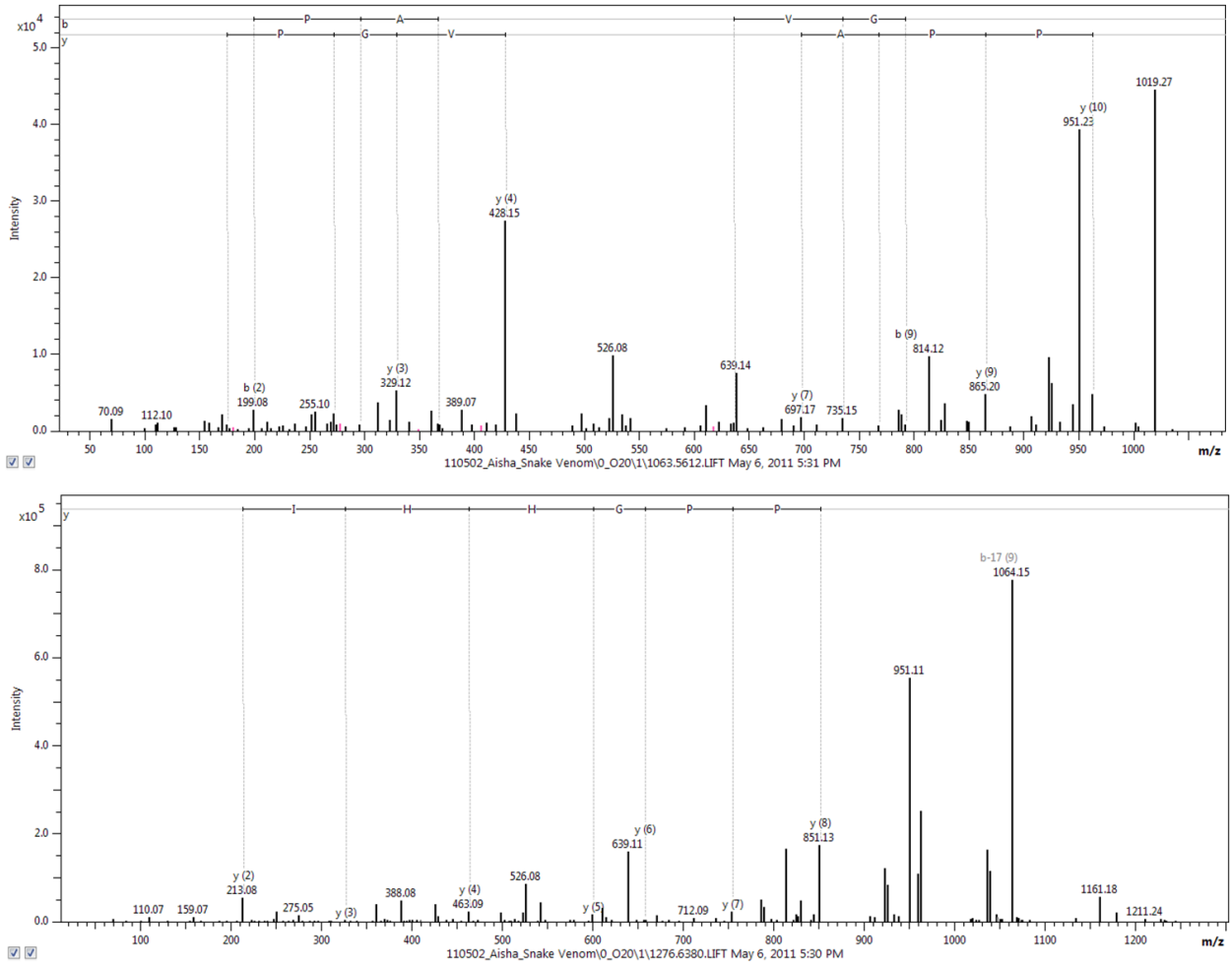

Fig. 48: MALDI-TOF-TOF mass spectra of the peptides purified from peak 8 and 10 from SEC (Fig. 38), of *Naja mossambica mossambica venom.*

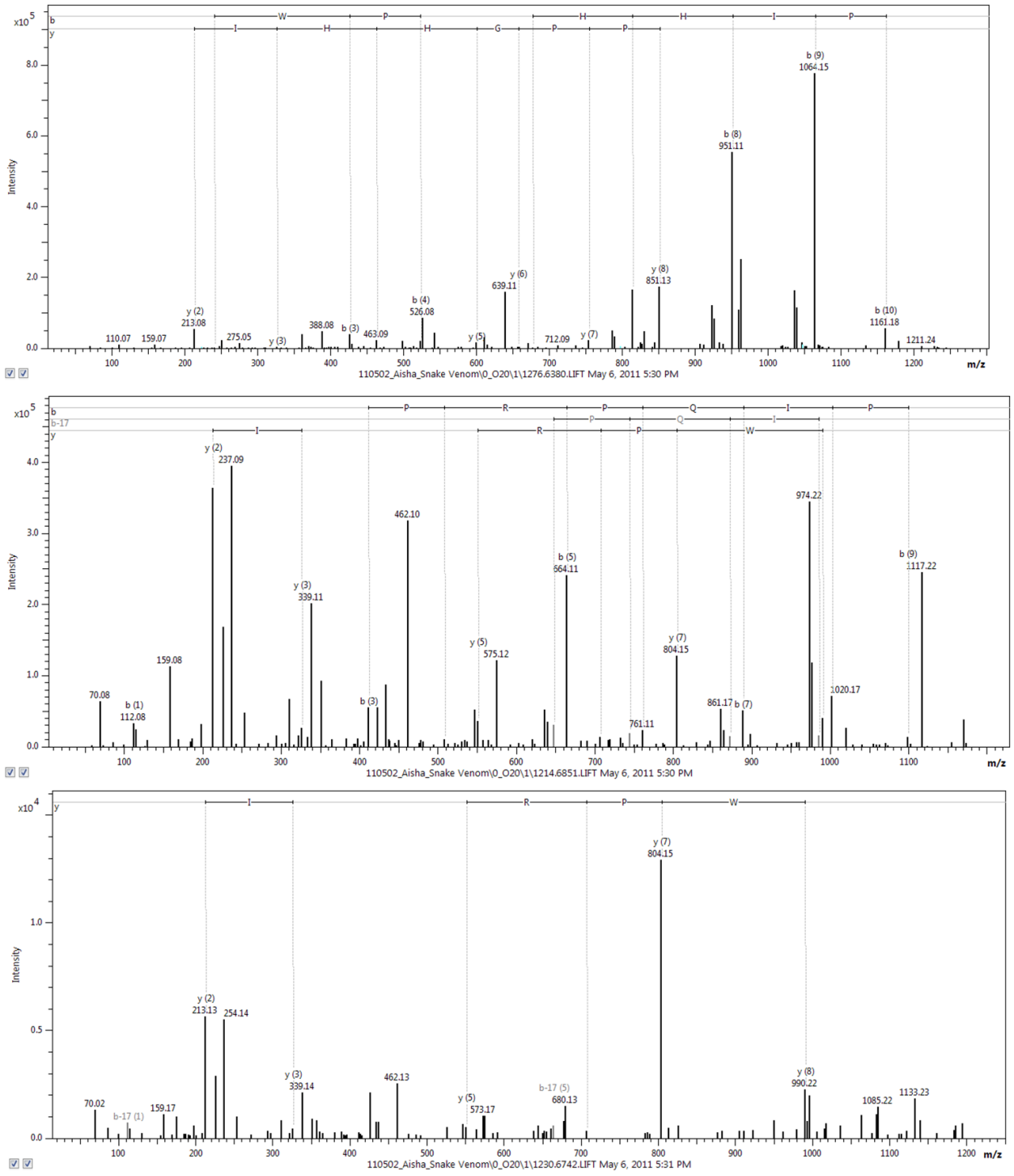

Fig. 49: MALDI-TOF-TOF mass spectra of the peptides purified from peak 8 and 10 from SEC (Fig. 38), of *Naja mossambica mossambica venom.*

4.6: Cytotoxins, ACE inhibitors and a bradykinin inhibitor peptide in the *Naja mossambica mossambica* venom

Three cytotoxins (Tabel 5), cytotoxin-1, cytotoxin-3 and cytotoxin-4 were identified in this study. Fraction 18 in peak 1, Fig. 39, contained cytotoxin-1, peak 2 cytotoxin-4 and peak 3 was a mixture of cytotxin 1 and 3. Cytotoxin-3 was also identified in peak 6 (Fig. 38) as shown in the ESI-spectrum (Fig. 43). The cytotoxins were identified by the analysis of tryptic digest, by LC/ESI ion trap MS and subsequent database search. The fragments of the cytotoxins that were identified by tryptic digestions, are shown in bold red color (Table 5). Theses cytotoxins are 60 amino acid polypeptides. Sequence alignment of the three cytotoxins is shown in Fig. 50. The different amino acid residues in the three cytotoxins are colored red, and the cysteine residues are highlighted in yellow color.

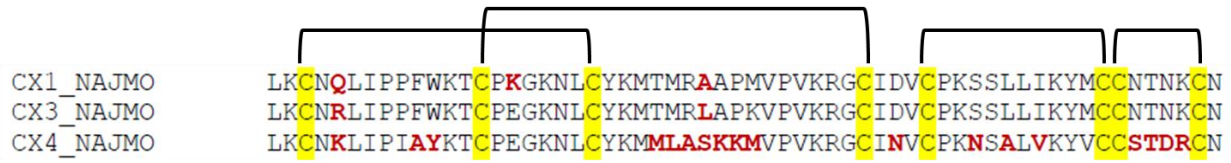

Fig. 50: Sequence alignment of cytotoxin-1, cytotoxin-3 and cytotoxin-4. The sequences were aligned using ClustalW2 [126]. The cysteine residues are shaded yellow and the disulfide linkages are outlined.

Cytoxin-1 and 3 show 93 % sequence identity with each other. The three cytotoxins have a different amino acid at position 5, and 28. At position 16 there is a lysine in cytotoxin-1, while in the other two glutamic acid is present at this position. Cytotoxin-4 shows 68% sequence identity to the other two cytotoxins, and have differences in amino acids in all the three loop regions as compared to cytotoxin-1 and 3. Cytotoxin-1 and cytotoxin-3 have proline at position 30 and therefore can be classified as P-type cytotoxins, while cytotoxin-4 has serine 28 and hence it can be classified as S-type cytotoxin [127]. The differences in amino acid residues among the three cytotoxins could be responsible for imparting functional specificities to these polypeptides.

Interestingly it was found that fraction 18 in peak 1, Fig. 39, inhibited a bacterial subtilisin and chymotrypsin. The MALDI-TOF MS spectrum and the ESI-TOF MS spectrum showed that a single component was present in this peak and the results of tryptic digestion showed that this

component is a cytotoxin-1. Although peak 3 (Fig. 39), also contains cytotoxin-1, but it did not inhibit any of the tested enzymes. The chromatogram (Fig. 39) also shows that peak 1 is eluting earlier at a lower salt concentration as compared to peak 3. This difference in the elution behavior and inhibitory activity of cytotoxin-1 can be accounted for by the presence of the cytotoxin-1 in two different aggregation states. From the ESI-TOF-MS spectrum (Fig. 41) the molecular mass of the cytotoxin-1 in fraction 18 (Fig. 39) was calculated to be 6819.3 Da. The mass shift of -7 Da indicates the formation of three disulphide bridges (indicating that it is folded into a tertiary structure) which compensates for a shift of -6 Da, and a further difference of mass could be due to an amino acid exchange compared to the cytotoxin-1, originally described in *Naja mossambica* venom [128]. The observed mass of cytotoxin-3 was 6896.4 Da, having a mass shift of 2 Da. The observed mass of cytotoxin-4 was 6726 Da with a mass shift of 11 Da. The mass shift in these two cytotoxin, as compared to the reported masses [128], could be due the exchange of an amino acid or modification of an amino acids in these polypeptides.

The fraction 18 in peak 1 (Fig. 39) was further tested for the inhibition of chymotryptic activity of 20S proteasome, and was found to strongly inhibit chymotryptic like activity of this enzyme. 20S proteasome is a 700 kD multicatalytic complex constituting the proteolytic core of 26S proteasome complex. This protein consists of three main active sites: chymotrypsin like, trypsin like and peptidyl-glutamyl peptide hydrolyzing (PGPH) like [103][and references there in]. Proteasomes are present in the nucleus and cytoplasm of the cell and the main function of this complex is to degrade the unwanted or damaged proteins. The cells use ubiquitin-proteasome systems to maintain the concentration of specific proteins and to remove misfolded proteins [129, 130]. The ubiquitin-proteasome pathway thus plays a key role in many cellular processes such as regulation of cell cycle progression, division, development and differentiation, apoptosis, cell trafficking, and modulation of the immune and inflammatory responses [131].

Studies have shown that cytotoxins can bind to the cell membrane, and form pores [132]. The internalization of CT3 from *Naja kaouthia* in promyelocytic leukameia HL60 cells was shown by confocal spectral imaging technique. In this study it was concluded that the internalization and lysosome-targeted action of CT3 plays an important role in CT-mediated cytotoxicity [133]. Another study also described the intracellular penetration of the cytotoxin by using immunofluorescence [134].

Keeping in view the possibility that snake venom cytotoxin can enter the cell, it is proposed that after envenomation, cytotoxin-1 might be involved in the inhibition of the 20S proteasome, leading to the dysregulation of cellular homeostasis, and thereby contributing to cytoxicity of cells of the prey. However further investigations are required in this regard.

Table 5: Peptide composition of *Naja mossambica mossambica* venom

Fraction No. (SEC)	Observed m/z	Sequence determined	Inhibitory activity	Homology with peptide from	Peptide family
5	6819.3 Da	**LKCNQLIPPFWK**TCPKGKNL CYKMTMR**AAPMVPVKR**GCI DVCPK**SSLLIK**YMCCNTNKC N	Bacterial subtilisin (Stmpr1), chymotrypsin and proteasome 20S	P01467: *Naja mossambica*	Snake three finger toxin (CTX M1)
5, 6	6896.4 Da	LK**CNRLIPPFWK**TCPEGKNL CYKMTMRLAPK**VPVKRGCID VCPKSSLLIK**YMCCNTNKCN		P01470: *Naja mossambica*	Snake three finger toxin (CTX M3)
5	6726 Da	LK**CNKLIPIAYKTCPEGKNL CYKMMLASKKMVPVKRGCI NVCPKNSALVKYVCCSTDR**C N		P01452: *Naja mossambica*	Snake three finger toxin (CTX M4)
8	873.4511 $(M+H)^{+1}$	ZQKFSPR		P85314: ***Bothrops moojeni***	Zinc metalloproteinase
8	901.4614 $(M+H)^{+1}$	ZQRFSPR		Q072L5: ***Bothrops asper***	Zinc metalloproteinase/ disintegrin
8	779.3983 $(M+H)^{+1}$	ZLWPRP	ACE	P0C7R6: ***Agkistrodon piscivorus piscivorus***	BPP
10	1214.6581 $(M+H)^{+1}$	ZLWPRPQIPP	ACE	P0C7S6: *Crotalus atrox*	BPP
10	1276.6380 $(M+H)^{+1}$	ZQWPPGHHIPP	ACE	P0C7J9: *Crotalus adamanteus*	BPP
10	1063.5611 $(M+H)^{+1}$	TPPAGPDVGPR		Q27J49 **:** *Lachesis muta muta*	Bradykinin inhibitor peptide
10	1230.6743 $(M+H)^{+1}$	QLWPRPQIPP	ACE	P0C7S6: *Crotalus atrox*	BPP
10	1277.6380	ZEWPPGHHIPP	ACE	Q27J49: *Lachesis muta muta*	BPP

High molecular weight peptides were identified by tryptic digestion and analyzed by LC/ion trap MS. The low molecular weight peptides were measured by MALDI-TOF/TOF mass spectrometry.

Eight singly charged ions of m/z 873-1277 $(M+H)^+$ were identified (Tabel 5). The sequences of all the peptides were determined by MALDI-TOF/TOF mass spectrometry. Five of them belong to the BPP family, manifesting hypotensive effects of envenomation. One is a bradykinin inhibitor peptide, previously isolated and identified from *Lachesis muta muta* and *Agkistrodon bilineatus* venom. The other two are small fragments of snake venom metalloproteinase. The peptide ZLWPRPQIPP is the modified form of QLWPRPQIPP, which was isolated from *Crotalus atrox,* with N-terminal Q modified to pyroglutamate. ZEWPPGHHIPP and ZQWPPGHHIPP are homologous to each other, having a variation in single amino acid at C-terminal. ZLWPRP is another form of ZLWPRPQIPP lacking the C-terminal QIPP.

4.7: Fractionation of the *Notechis ater niger* venom by size exclusion chromatography and purification of selected peptides by liquid chromatography

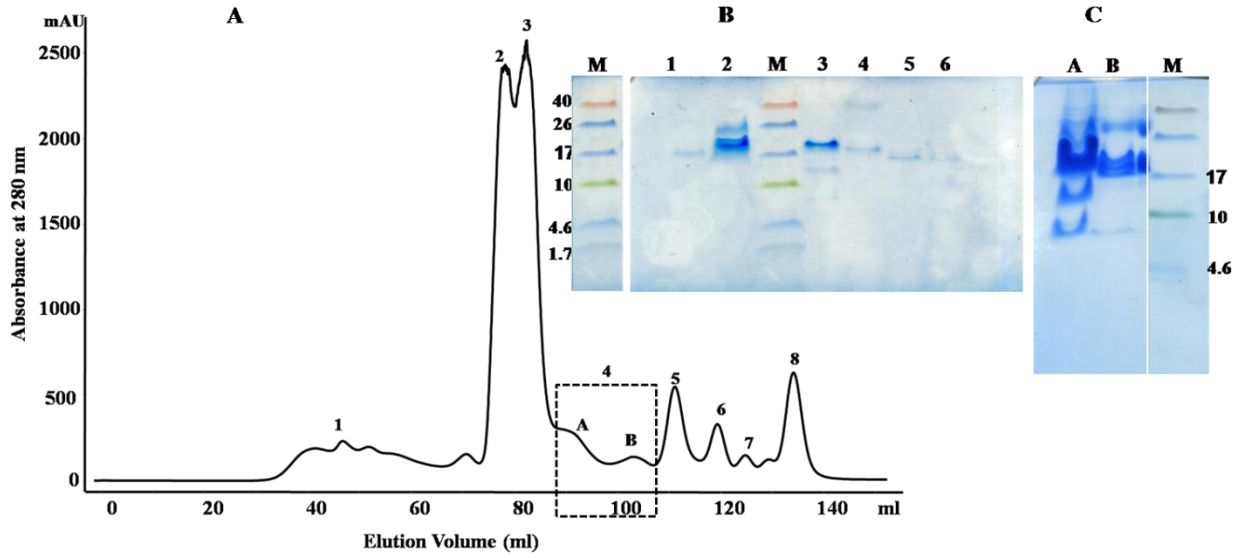

Fig. 51: (A) Fractionation of crude venom of *Notechis ater niger* applying a Superdex-75 column by FPLC at pH 5; (B) SDS-PAGE of fractions 1-6 from the size exclusion chromatographic separation of the crude venom; (C) SDS-PAGE of the concentrated fractions marked as A and B in peak 4, show bands smaller than 10 kDa.

The crude venom of *Notechis ater niger* was fractionated with a Superdex-75 column at pH 5. Fractions 2-8 were screened against a set of selected enzymes. Inhibitory activity towards trypsin, kallikrein, plasmin and angiotensin converting enzyme was found in peak 4. The

fractions in peak 4 were pooled and fractionated on SOURCE 5RPC. The chromatogram is shown in Fig. 52.

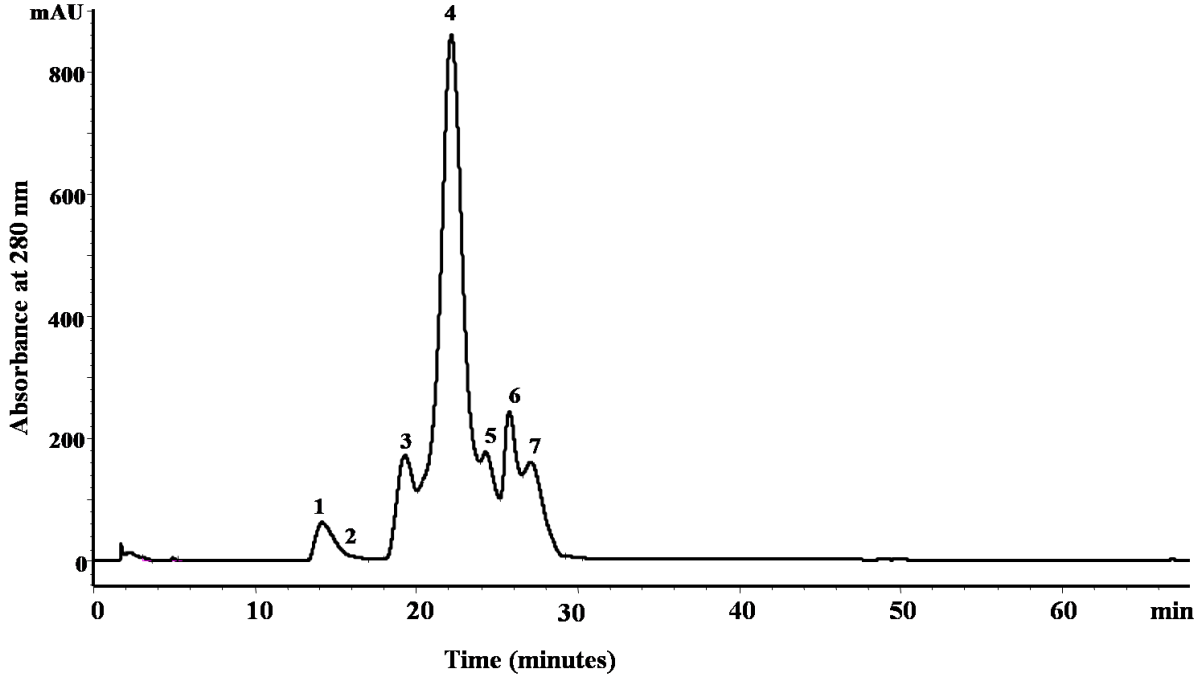

Fig. 52: Purification of peak 4 (Fig. 51) with a SOURCE 5RPC column by HPLC.

Fractions were collected between 10-30 minutes and were not pooled. All the fractions were subjected to MALDI-TOF-MS analysis. The samples were prepared using DHB matrix. The fractions were also tested for the inhibition of ACE, trypsin, kallikrein and plasmin. Peak 3 and 5 showed inhibitory activity towards trypsin. Kallikrein and plasmin inhibitory activity was found in peak 5. The inhibition of plasmin was weaker as observed for trypsin and kallikrein. Fraction in peak 6 showed weak inhibition of ACE. Selected MALDI-TOF-MS spectra are shown in Fig. 53 and Fig. 54.

In order to isolate BPPs the pooled fractions in the peak 4 (Fig. 51) were filtered through 3 kDa cutoff Amicon membrane. The filtrate was lyophilized and loaded on a C-18 column. The chromatogram is shown in Fig. 55A. Small peaks with very low intensity were observed.

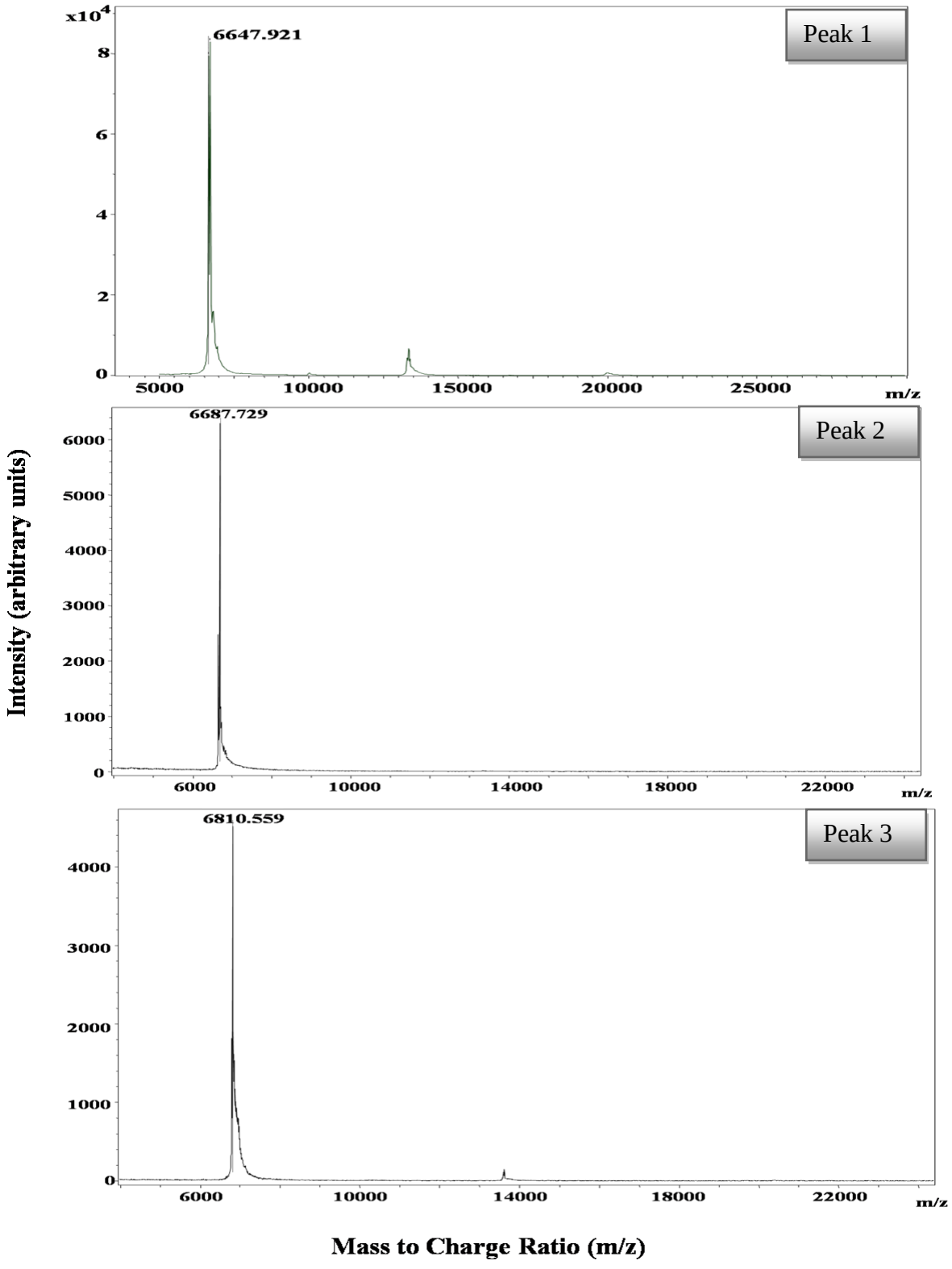

Fig. 53: MALDI-TOF-MS spectra fractions in peaks 1, 2 and 3 from chromatogram shown in Fig. 52.

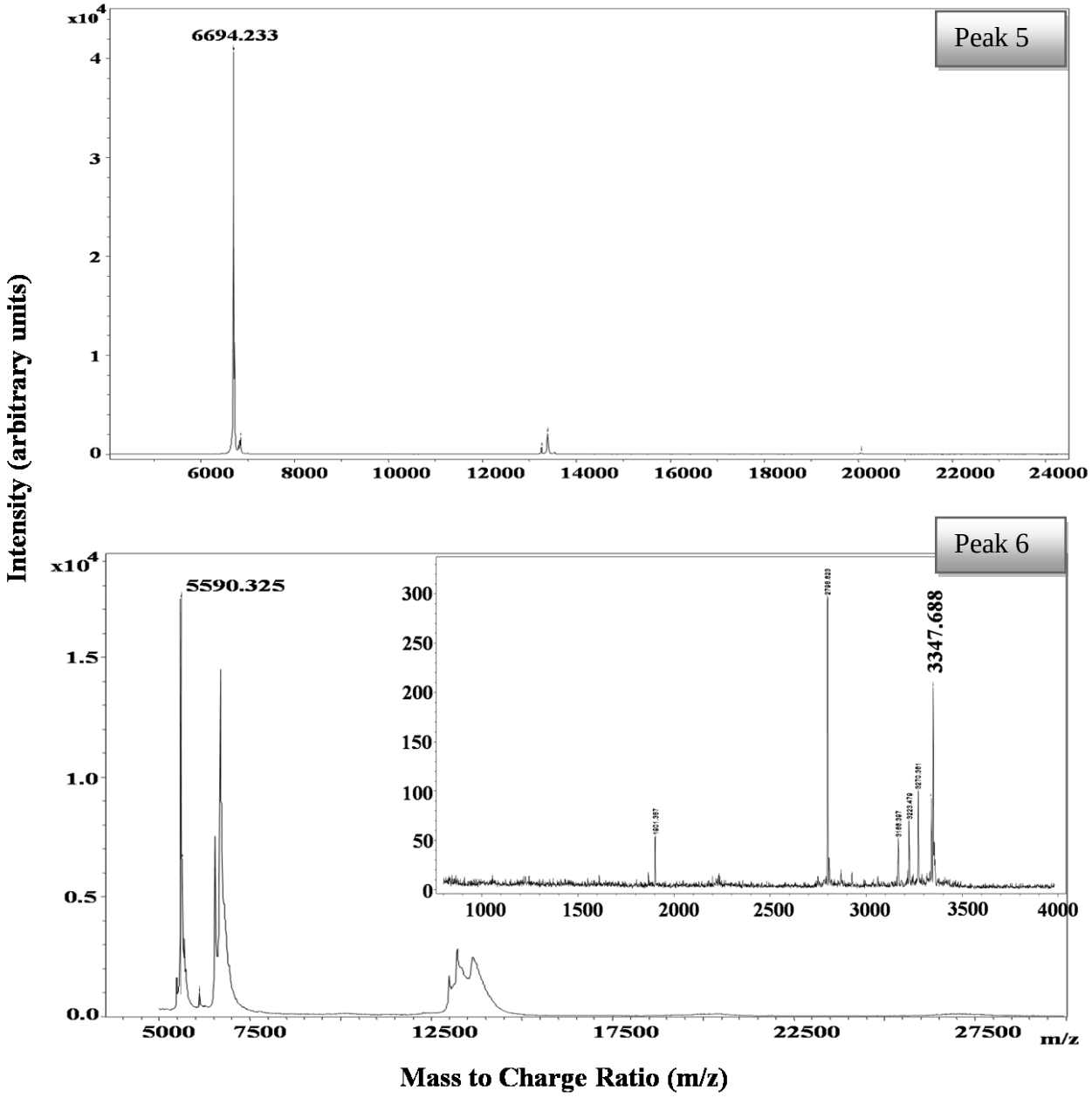

Fig. 54: MALDI-TOF-MS spectra of peak 5 and 6 from the chromatogram shown in Fig. 52. Inset of the spectrum (Peak 6) shows spectrum in the low range 500-4000 m/z.

Fractions were collected between 10-15 minutes. Fractions in peak 1 and 2 showed high inhibition of ACE. These two fractions were subjected to MALDI-TOF/TOF analysis and also given for de novo sequencing by ESI-QTOF. The MALDI-TOF spectra of the two fractions are shown in Fig. 55 (B and C).

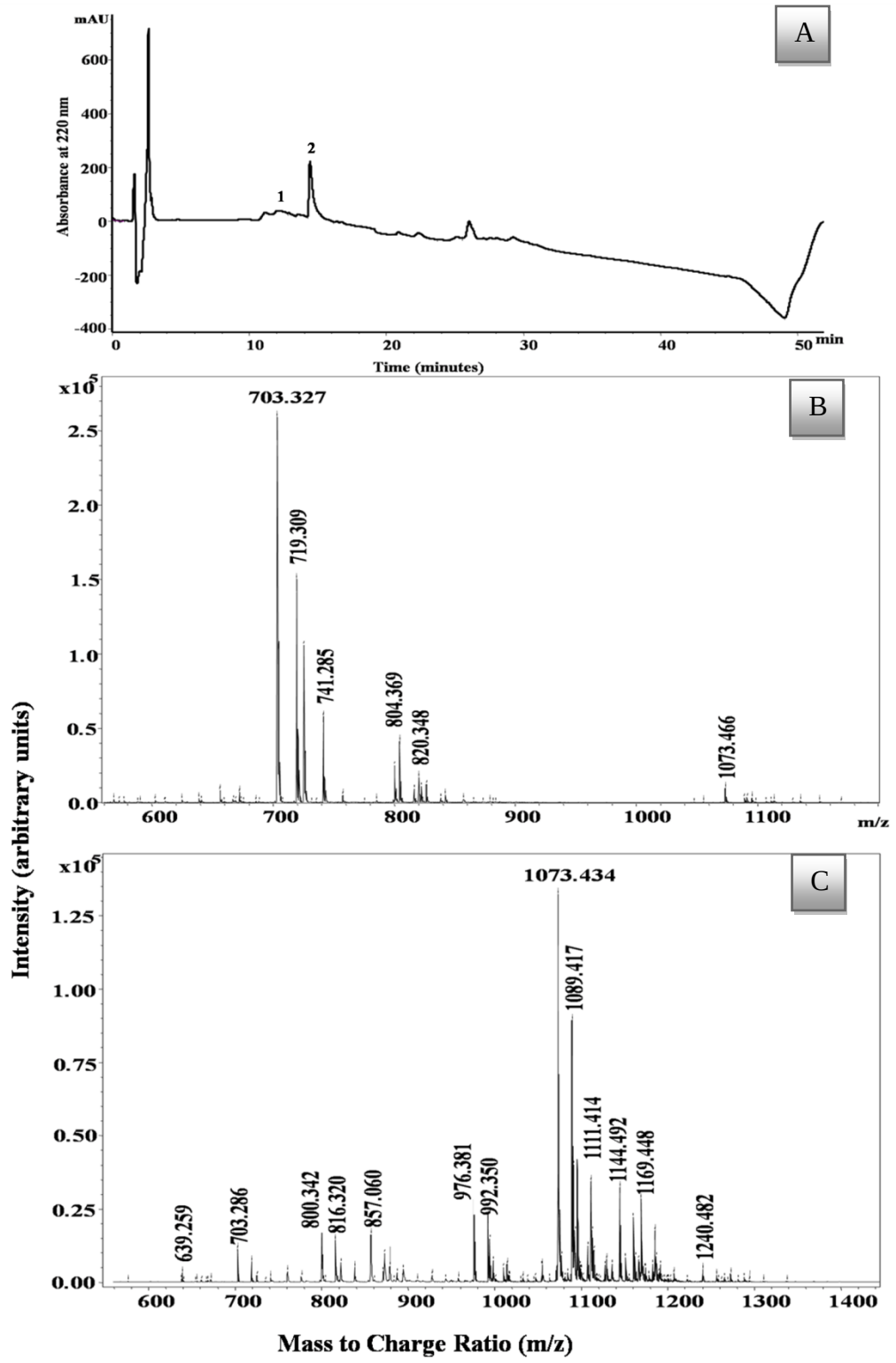

Fig. 55: (A) Purification of filtrate of peak 4 (Fig. 51A) passed through 3kDa membrane on a chromolith C-18 column by HPLC; (B) and (C) MALDI-TOF-MS spectra of peak 1 and 2 from the chromatogram shown in Fig. 55A.

4.8: Neurotoxin, natriuretic and Kunitz type peptides in *Notechis ater niger* venom

The peptides purified from the venom of *Notechis ater niger* are shown in Table 6. All the peptides were isolated from the peak 4 of size exclusion chromatogram (Fig. 51). The peptides identified by tryptic digestion are shown in bold red.

Table 6: Peptide composition of the *Notechis ater niger* venom

Observed m/z $(M+H)^+$	Sequence determined	Inhibitory activity	Homology with peptide from	Peptide family	Mode of measurement
6647.92 Da	MTCCNQQSSQPK**TTTTCA ESSCYKK**TWRDHRGTITE R**GCGCPNVKPGVQINCC KTDECNN**		A8HDK0: ***Notechis scutatus scutatus***	Snake three finger toxin (SNTX-1)	Tryptic digestion, LC/ion trap
6687.73Da	MTCCNQQSSQPK**TTTTCA ESSCYKK**TWR**DHRGTIIE R**GCGCPNVKPGIQLVCCET NECNN		A8S6A4: ***Austrelaps superbus***	Snake three finger toxin (SNTX-1)	Tryptic digestion, LC/ion trap
6810.56 Da	K**DRPHFCHLPHDTGPCN RNTQAFYYNPVYHTCLK FIYGGCQGNSNNFKTIDE CKR**TCAA	Trypins	B5KL32: ***Notechis scutatus scutatus***	Kunitz/BPTI (Tigerin-3)	Tryptic digestion, LC/ion trap
6694.23 Da	KDHPEFCELPADSGPCR**GI LHAFYYHPVHRTCLEFIY GGCYGNANNFKTIDECK R**TCAA	Trypsin, kallikrein, plasmin	Q6ITB3**:** ***Notechis scutatus scutatus***	Kunitz/BPTI (Tigerin-3)	Tryptic digestion, LC/ion trap
3347.69 Da	SGSEVAK**IGDGCFGLPLD R**IGSASGMGCRSVPKP	ACE	Q3SAE8: ***Notechis scutatus scutatus***	NP	Tryptic digestion, LC/ion trap
1154.56 Da	QNPPKPISGES		Q3SAX8: ***Oxyuranus scutellatus scutellatus***	NP	MALDI-TOF/TOF
764 $(M+H)^{+2}$ Da				Glycopeptidr	Q-TOF
681 Da				Glycopeptide	Q-TOF

Two short neurotoxins with molecular mass 6647.9 $(M+H)^{+1}$ and 6687.3 $(M+H)^{+1}$ (Table 6) were purified by reverse phase chromatography. These neurotoxins have been previously reported at transcript level in the venom of other Australian elapid snakes *Notechis scutatus scutatus* and *Austrelaps superbus* [135]. These neurotoxins are 60 amino acid polypeptides and show high homology to each other. The sequence alignment of the two neurotoxins created in ClustalW2 is shown below.

```
A8HDK0          MTCCNQQSSQPKTTTTCAESSCYKKTWRDHRGTITERGCGCPNVKPGVQINCCKTDECNN 60
A8S6A4          MTCCNQQSSQPKTTTTCAESSCYKKTWRDHRGTIIERGCGCPNVKPGIQLVCCETNECNN 60
```

Cysteines are highlighted in yellow color. A difference in the amino acids, colored grey, is observed near the C-terminal. A mass shift of 29 Da was observed in the neurotoxin having a molecular mass of 6687.3 $(M+H)^{+1}$ (Peak 2, Fig. 52), as compared to its counterpart reported in *Austrelaps superbus*. This could be possibly due to the substitution of an amino acid in this peptide.

Two Kunitz/BPTI peptides tigerin-1 and tigerin-3 (Table 6) were also purified by reverse phase chromatography. They are 59 amino acid polypeptides and have also been previously reported at transcript level in the venom gland of *Notechis scutatus scutatus* [136]. Tigerin-1 shows inhibitory activity towards trypsin, kallikrein and also weakly inhibits plasmin. While tigerin-3 inhibits only trypsin. The sequence analysis of the two Kunitz inhibitor shows that the reactive bond site residues are different in both peptides, Fig. 56. The P1 residue is considered to be the most critical site to define the specificity and extent of inhibitory interaction of serine proteases by the Kunitz type inhibitors [137, 138]. Tigerin-1 has a positively charged residue arginine at P1 position while tigerin-3 has an asparagine, a neutral amino acid at this site. Other amino acids at the primary binding loop (P3P2P1P1′P2′P3′P4′) can also interact with the enzyme [139] . The sequence of this loop is PCRGILH in case of tigerin-1 and TGPCNRNTQ in tigerin-3. Thus there are significant differences in the amino acid residues at the primary binding loop. Previous studies have shown that at least one of the residues at P2′ or P4′ should have a basic residue histidine, to form a complex with kallikrein [120][and references therein]. Tigerin-1 has a histidine at P4′ position, and protease inhibitor-1 has histidine at postion P2′ isolated from *vipera ammodytes meridionalis* (Table 3), thus preferring complex formation with kallikrein, while tigerin-3 has glutamine at this position and shows no inhibition of kallikrein. Therefore it can be concluded

that the different amino acid residues present at the primary binding loop of tigerin-1 and tigerin-3, are responsible for their specificity towards different serine proteases. Further search in the UniProt data base indicates that the sequence motif NRN at P1P1´P2´ position is found only in *Notechis scutatus scutatus* venom Kunitz inhibitor, a closely related species to *Notechis ater niger*. A mass shift of 11 Da in tigerin-1, and 12 Da in tigerin-3, could also be due to an amino exchange residue in these polypeptides as compared to their analogues reported in *Notechis scutatus scutatus*.

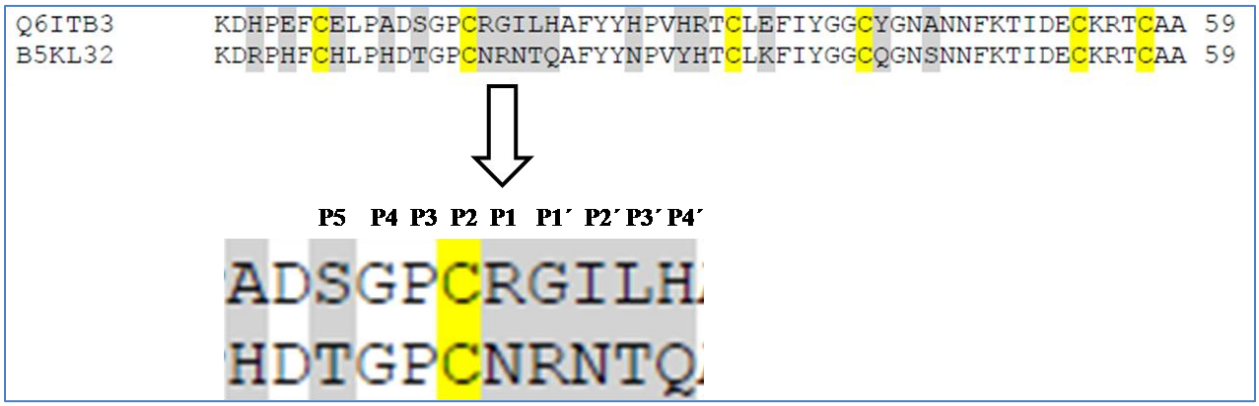

Fig. 56: Sequence alignment of the Kunitz inhibitors, tigerin-1 and tigerin-3 shows variation in the reactive bond residues. Cysteines are shaded yellow and different amino acids are shaded grey.

A natriuretic peptide NsNP-a, inhibiting ACE was identified in peak 6 (Fig. 52), by the analysis of the tryptic digest. Low molecular weight peptides were also seen (Fig. 55), mass range 600-1600 Da $(M+H)^+$. Strong inhibition of ACE was observed in these fractions. The molecular mass range suggests that they are probably novel BPPs. The MALDI-TOF/TOF analysis and subsequent data base search by Inhouse Mascot search did not give any sequences. The ESI-QTOF analysis of these peptide fractions provided information about the presence of glycopeptides. Signals were observed for the glycan moieties Hexose, N-acetylhexoseamine and N-acetylneuraminic (Fig. 57). It was not possible to determine the peptide sequence of the glycopeptides because the CID technique mainly fragments the carbohydrate moiety. The material was insufficient to perform different mass spectrometric experiment as electron transfer dissociation, which would provide the sequence information of the peptide by fragmenting the amino acids and preserves the glycosylation on the peptide backbone [140]. Further to determine nature carbohydrate moieties and configuration of the glycosidic linkage between them, other

experiments like GC-MS or LS-MS in combination with NMR analysis are necessary [141]. Thus more sample is required to perform these experiments. There is one report about the isolation of glycopeptides from the venom of *Dendroaspis angusticeps* [142]. In this study it was described that these glycopeptides have a high proportion of proline residue and molecular masses ranging from 1.3- 2.4 kDa.

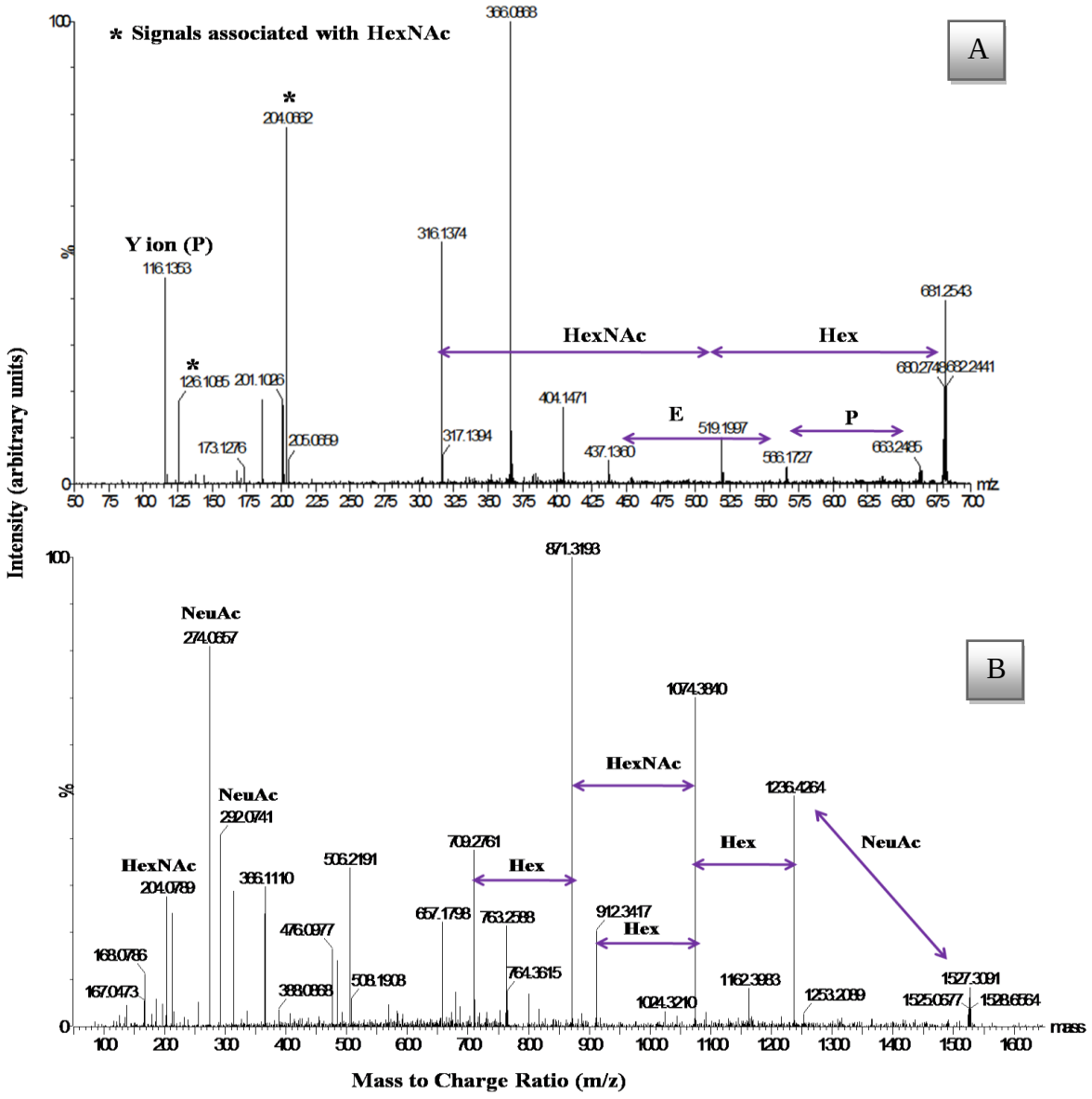

Fig. 57: ESI-QTOF MS/MS spectrum of the glycopeptides; (A) 681 Da $(M+H)^{+}$; (B) 764 Da $(M+H)^{+2}$. Spectrum A shows signals for Hex and HexNAc moiety and spectrum B shows additional signals for NeuAc.

4.9: Fractionation of the *Agkistrodon bilineatus* venom by size exclusion chromatography.

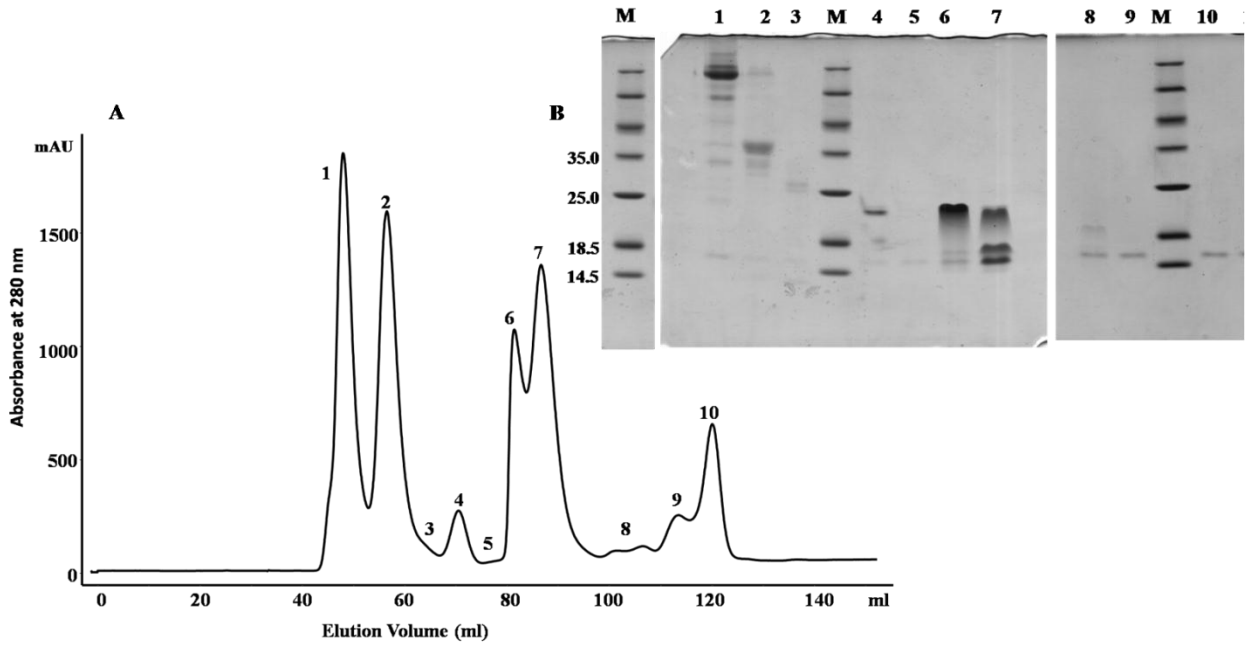

Fig. 58: (A) Fractionation of the crude venom of *Agkistrodon bilineatus* venom on Superdex-75 column by FPLC; (B) SDS-PAGE of the fraction 1-10 from the SEC separation.

The *Agkistrodon bilineatus* venom was also included among the initial experiments to identify potential inhibitors of the selected enzymes. The size exclusion chromatogram of the fractionation of crude venom is shown in Fig. 58A. Fractions in peak 8 strongly inhibited a bacterial subtilisin StmPr1 (a protease produced by *Stenotrophonomonas maltophilia*). This fraction was filtered through 3 k Da Amicon membrane. Inhibitory activity was tested both with filtrate and retentate. The filtrate inhibited Stmpr1. The ESI-TOF-MS analysis of the filtrate showed that no peptide above 1100 Da is present in this fraction (Fig. 59). Attempts were made to purify this inhibiting peptide with a C-18 column, but it was not successful.

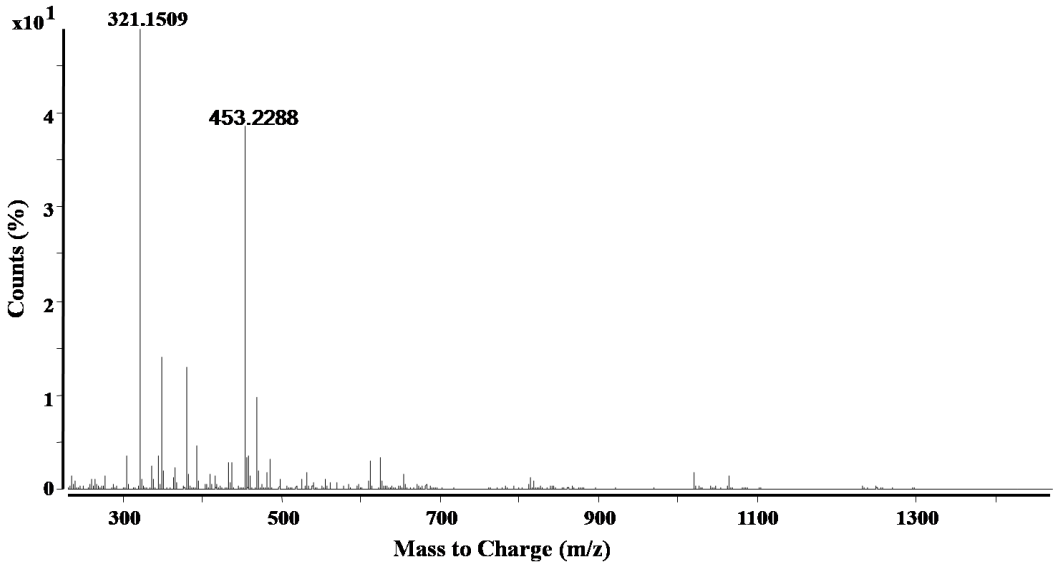

Fig. 59: ESI-TOF-MS spectrum of the filtrate (through 3 kDa membrane) of peak 8 from SEC (Fig. 58).

4.9.1: Preparation of crystal complex of a new peptidic inhibitor from *Agkistrodon bilineatus* venom with bacterial subtilisin StmPr1

The entire fraction in peak 8 (Fig. 58A) was concentrated and used for soaking a StmPr1 crystal. The diffraction data were collected at the Consortium-Beam Line X13, DESY, Hamburg. The data collection and refinement statistics are summarized in Table 7.

4.9.2: Structural analysis of the crystal complex

The interpretation of the crystal structure data showed that a tetrapeptide, out the heterogeneous mixture of the venom fraction, is bound at the active site of StmPr1 (Fig. 60). The sequence of the peptide was determined as Ala-Ser-Pro-Ser (now abbreviated as ASPS). The structure is stabilized by 8 hydrogen bonds between the six residues (His^{105}, Gly^{143}, Ser^{176}, Gly^{178}, Asn^{207} and Ser^{289}) of StmPr1 and the main chain atoms of the inhibitor (Fig. 60), in addition to three water molecules which form three hydrogen bonds with the atoms N1, O4, and O7 of the ASPS peptide. In total 11 hydrogen bonds stabilize the inhibitor inside the active site of StmPr1. The hydrogen bonds to the peptide backbone are made primarily with side-chains on the enzyme. The C-terminal serine residue of the inhibitor is bound to the primary specificity pocket of the enzyme through four hydrogen bonds. The StmPr1-ASPS complex model was refined to an R-factor of 14.9%, with good geometry at a resolution of 1.78 Å. All four residues of the peptide inhibitor are well-localized in the putative S1 through S4 sites.

The oxygen atom occupying the ‘‘oxyanion hole’’ region of the enzyme accepts two hydrogen bonds; one from the polypeptide backbone and one from the positively charged amino group of Asn[207].

Table 7: Statistics for the *Agkistrodon bilineatus* snake venom peptide-StmPr1 complex

Parameters	
Space group	$C222_1$
a (Å)	60.56
b (Å)	86.78
c (Å)	132.11
V_M ($Å^3$/ Da)	2.17
Solvent content (%)	43.30%
Completeness of data (%)	97.3 (85.1)
No. of total reflections	132119(15673)
No. of unique reflections	32679(4123)
Average I/sigma intensity	14.8(5.5)
Resolution (Å)	26.28-1.78(1.88-1.78)
Redundancy	4.0(3.8)
*Rmerge (%)	6.1(21.3)
No. of reflections used in refinement	30966
Rcrystal (%)	14.9
No. of reflections used in Rfree	1548
Rfree (%)	18.77
Protein atoms	2734
Amino Acids:	356
Calcium Ions	1
Sulphate Ions	5
Glycerol molecules	2
Water molecules	344
Root mean square deviation	
Bonds (Å)	0.028
Bond angles (°)	2.06
Residues in regions of the Ramachandran plot (%)	
Most favored	90.0
Allowed	10.0
Generally allowed	0
Disallowed	0

The interactions of the peptide inhibitor complex are summarized in table 8. Fig. 61 shows the surface view of StmPr1 with the peptide inhibitor at the active site of StmPr1.

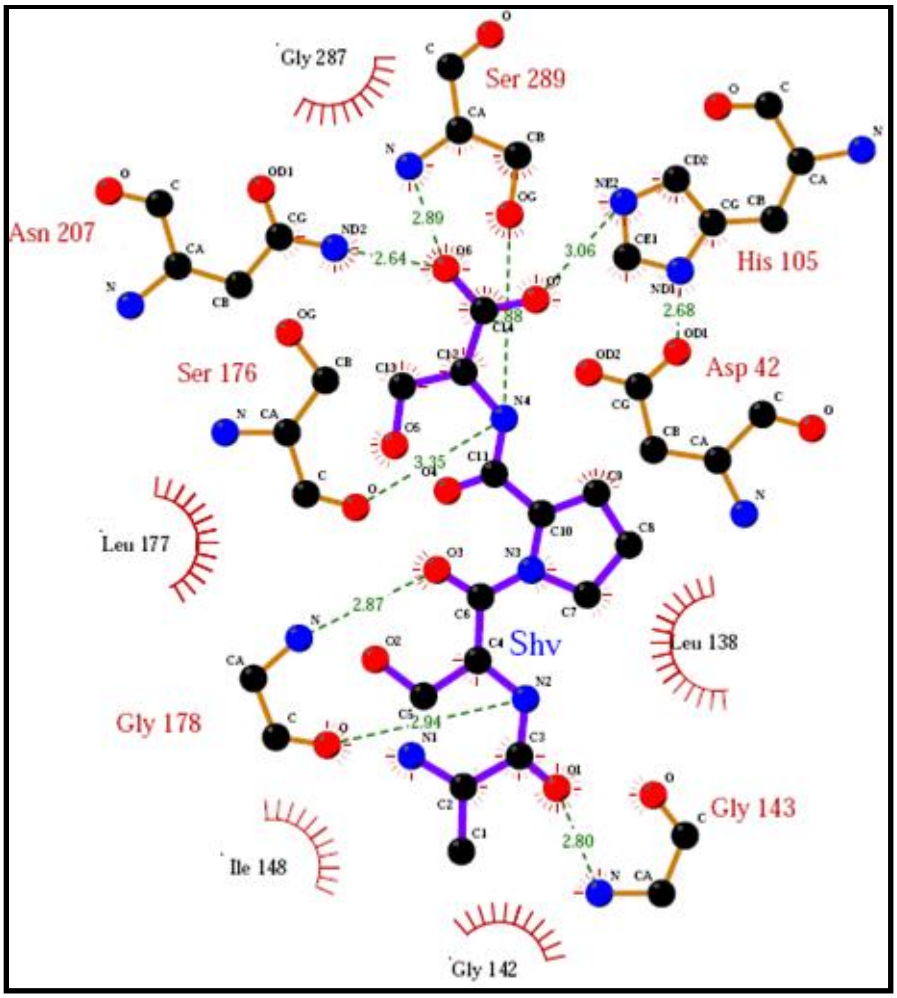

Fig. 60: Ligplot of the StmPr1-*Agkistrodon bilineatus* venom peptide inhibitor complex.

Table 8: Interactions of the *Agkistrodon bilineatus* venom peptide inhibitor complex

Nr.	Residue name	Atom name		Atom name	Distance (Å)	Bond type
1.	Ser-289	OG	ßà	N4	2.88	H-bond
2.	Ser-289	N	ßà	O6	2.89	H-bond
3.	Asn-207	ND2	ßà	O6	2.64	H-bond
4.	His-105	NE2	ßà	O7	3.06	H-bond
5.	Ser-176	O	ßà	N4	3.35	H-bond
6.	Gly-178	O	ßà	N2	2.94	H-bond
7	Gly-178	N	ßà	O3	2.87	H-bond
8	Gly-143	N	ßà	O1	2.80	H-bond

No significant movements of the active site residues of StmPr1 upon complexation with the inhibitor were observed. This observation is in accordance with a preliminary experiment where the snake venom peptide fraction showed stronger inhibition with StmPr1 than with chymotrypsin. Thus, the ASPS peptide seems to exhibit some specificity for StmPr1. The crude snake venom fraction (molecular weight < 11kDa) contains many compounds, however, crystals grew and only one peptide was found in the active site, which is remarkable from a technical point of view. In this case the crystal served as a purification tool, and crystallography allowed the identification of a new inhibitory compound. The results of this experiment have supported the notion that snake venom is a potential source of novel bioactive peptides.

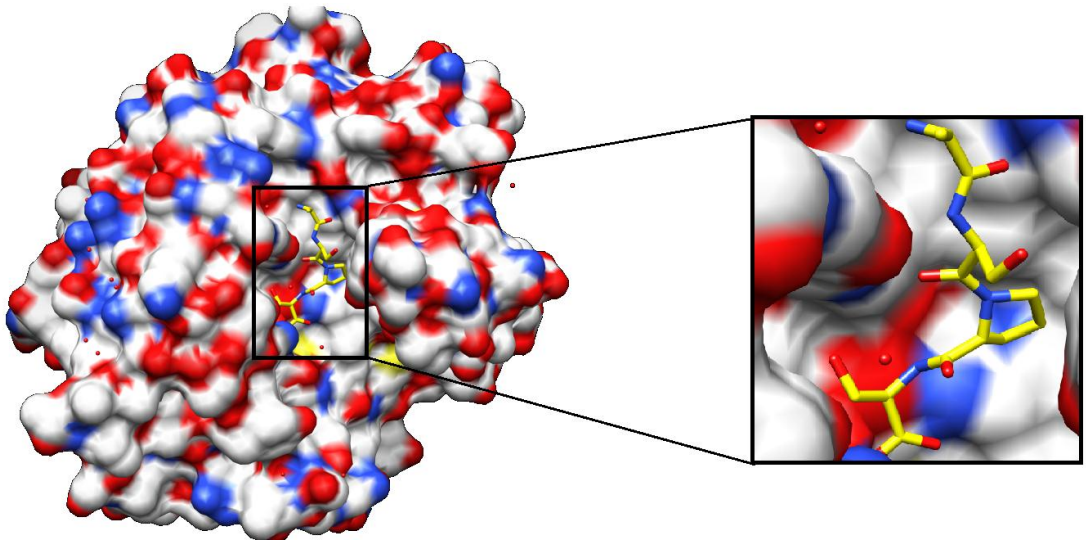

Fig. 61: **Surface view of StmPr1 showing the peptide inhibitor (in sticks) in the binding site of StmPr1**

4.10: Molecular modelling of snake venom Kunitz/BPTI inhibitors with trypsin and kallikrein

The crystal structures the Kunitz inhibitors tigerin-1, tigerin-3 and protease inhibitor-1 were not available therefore their models were generated by using the server SWISS-MODEL. The models show that despite variation in the sequence, the structural conformation of the three peptides is very similar to each other (Fig. 62) and to aprotinin, and on visual inspection the chains overlay.

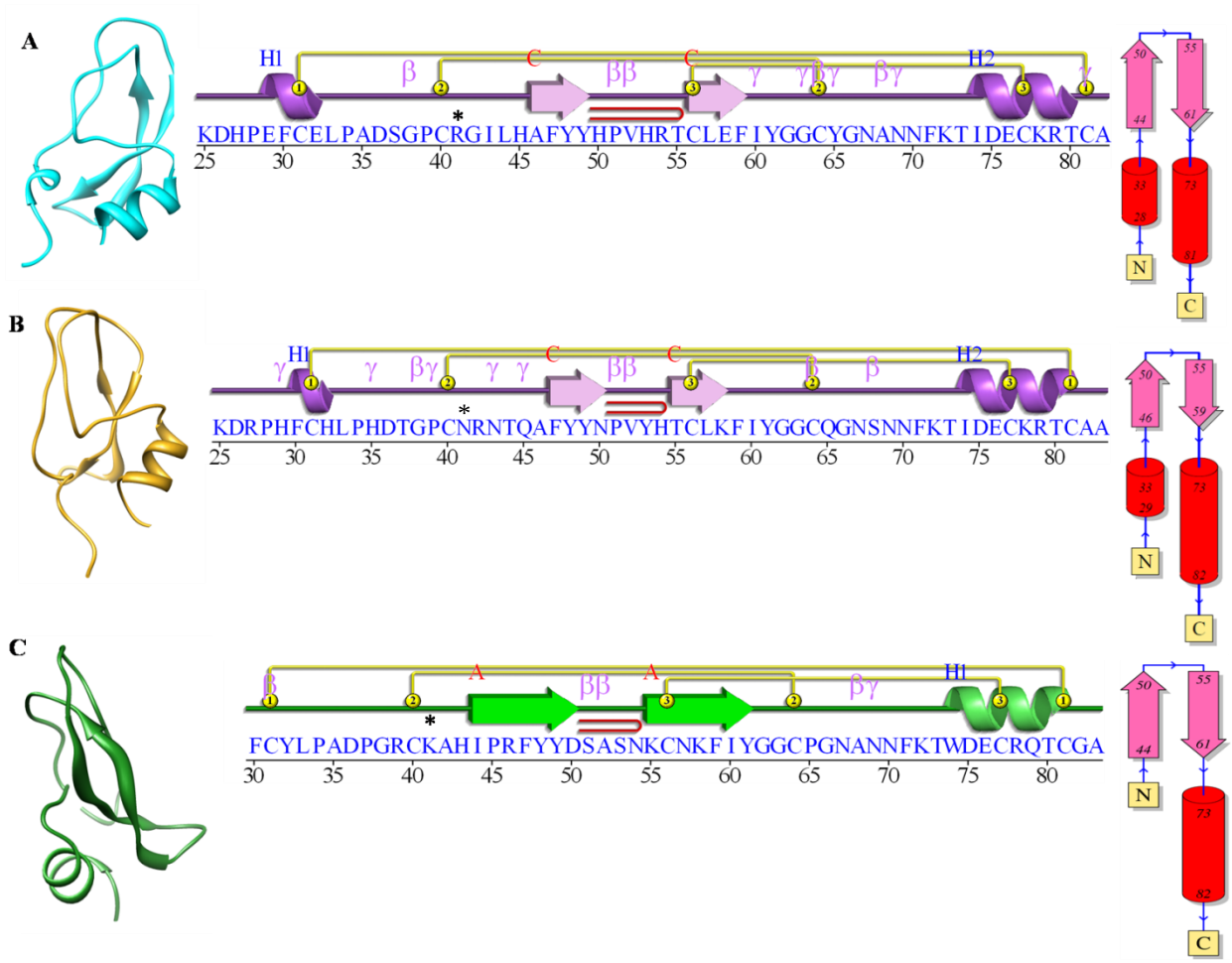

Fig. 62: Molecular models of snake venom Kunitz inhibitors generated by the server SWISS MODEL; (A) Tigerin-1; (B) Tigerin-3; (C) Protease inhibitor-1. Diagram showing structure-sequence relationship is shown besides each peptide and the P1 residue is marked by an *. Topology diagram of each peptide is also shown on extreme right of each peptide model.

The secondary structure of the polypeptides includes two β-strands linked by a short hair pin loop, a 3_{10} helix near the N-terminus and an α-helix near the C-terminus. Three disulfide bonds stabilize the secondary structure. The structure of protease inhibitor-1 does not show 3_{10} helix near N-terminus, which could be due to the reason that for unknown reasons the SWISS-MODEL server truncates the amino acids 25-29 for creating the model of this polypeptide and the neighboring residue at the N-terminal side are not available to take part in the formation of this helix.

In order to predict the binding mode and study the possible interactions at the protein-inhibitor interface of tigerin-1, tigerin-3 and protease inhibitor-1 with bovine pancreatic trypsin and the catalytic domain of plasma kallikrein a rigid body docking was performed using the program

ClusPro. Plasma kallikrein is a trypsin like enzyme. A 3D structure of the expressed catalytic domain of human plasma kallikrein [143] was used in this work to model a complex of tigerin-1 with kallkrein. Fig. 63 shows a comparison of the sequence of trypsin and plasma kallkrein.

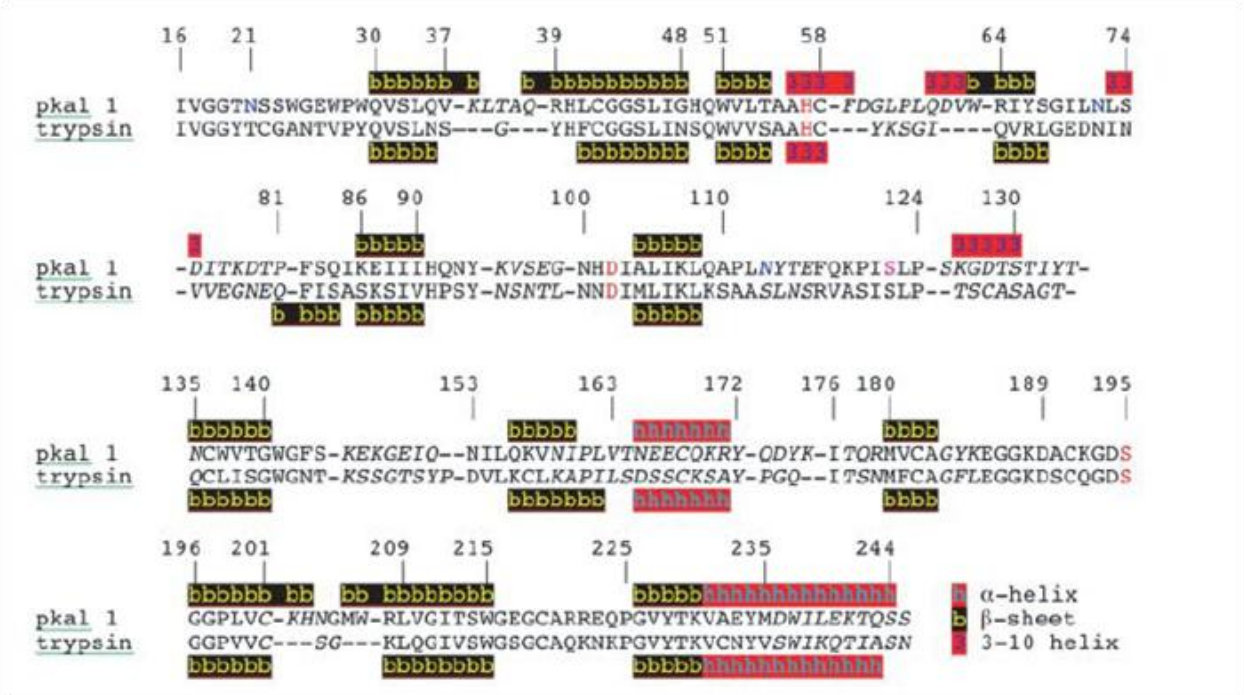

Fig. 63: Sequence alignment of trypsin and plasma kallikrein (*pkal 1*). Active site residues are shown in red [143]

The ClusPro program did not create an acceptable model of the protease inhibitor 1 either with trypsin or kallikrein. Therefore a model of the protease inhibitor-1 in complex with trypsin was built with Coot, by mutating the amino acids of BPTI with that of protease inhibitor-1, using the crystal structure PDB ID: 3OTJ.

4.10.1: Molecular docking of tigerin-1 with trypsin

The interaction of the active site residues of trypsin and tigerin-1 are shown in Fig. 64. The P1 residue Arg^{41}forms string hydrogen bonded salt bridges with Asp^{189}, present at the bottom of S1 pocket. Arg^{41} also forms a hydrogen bond with Ser^{190}. The back bone carbonyl oxygen of Arg^{41} and nitrogen of Gly^{42} (P1′) forms a hydrogen bond with Ser^{195}. Gly^{42} forms a hydrogen bond with His^{57} nitrogen. Hydrogen bond formation between Ser^{37} (P5) and Gln^{192} could result in further stabilization of the complex as the Trypsin residue Gln^{192} is known to add stability to the catalytic complexes [144]. The important interactions of the complex are summarized in table 9.

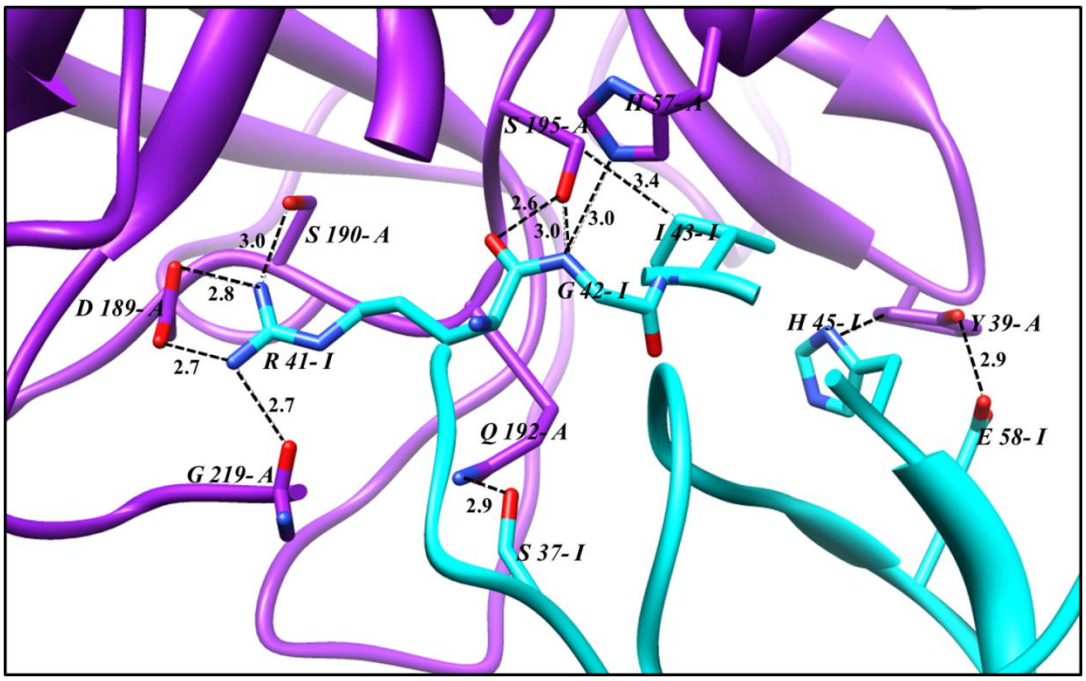

Fig. 64: (A) Tigerin-1 in complex with trypsin; (B) Interactions of tigerin-1 with active site residues and other side chain residues of trypsin. ■ Chain A (trypsin), ■ Chain I (tigerin-1).

Table 9: Key intermolecular interactions of tigerin-1 and trypsin

	<----- A T O M 1 ----->					<----- A T O M 2 ----->					
	Atom no.	Atom name	Res name	Res no.	Chain		Atom no.	Atom name	Res name	Res no.	Chain	Distance
1.	156	N	GLY	42	I	<-->	351	NE2	HIS	57	A	3.0
2.	148	NH1	ARG	41	I	<-->	1538	OD1	ASP	189	A	2.8
3.	151	NH2	ARG	41	I	<-->	1539	OD2	ASP	189	A	2.7
4.	148	NH1	ARG	41	I	<-->	1546	OG	SER	190	A	3.0
5.	116	OG	SER	37	I	<-->	1564	NE2	GLN	192	A	2.9
6.	155	O	ARG	41	I	<-->	1587	OG	SER	195	A	2.6
7.	156	N	GLY	42	I	<-->	1587	OG	SER	195	A	3.0
8.	145	NE	ARG	41	I	<-->	1741	O	GLY	219	A	2.9
9.	151	NH2	ARG	41	I	<-->	1741	O	GLY	219	A	2.7

4.10.2: Molecular docking of tigerin-1 with the catalytic domain of human plasma kallikrein (*pkal 1*).

The main intermolecular interaction between tigerin-1 and *pkal-1* are illustrated in Fig. 65.

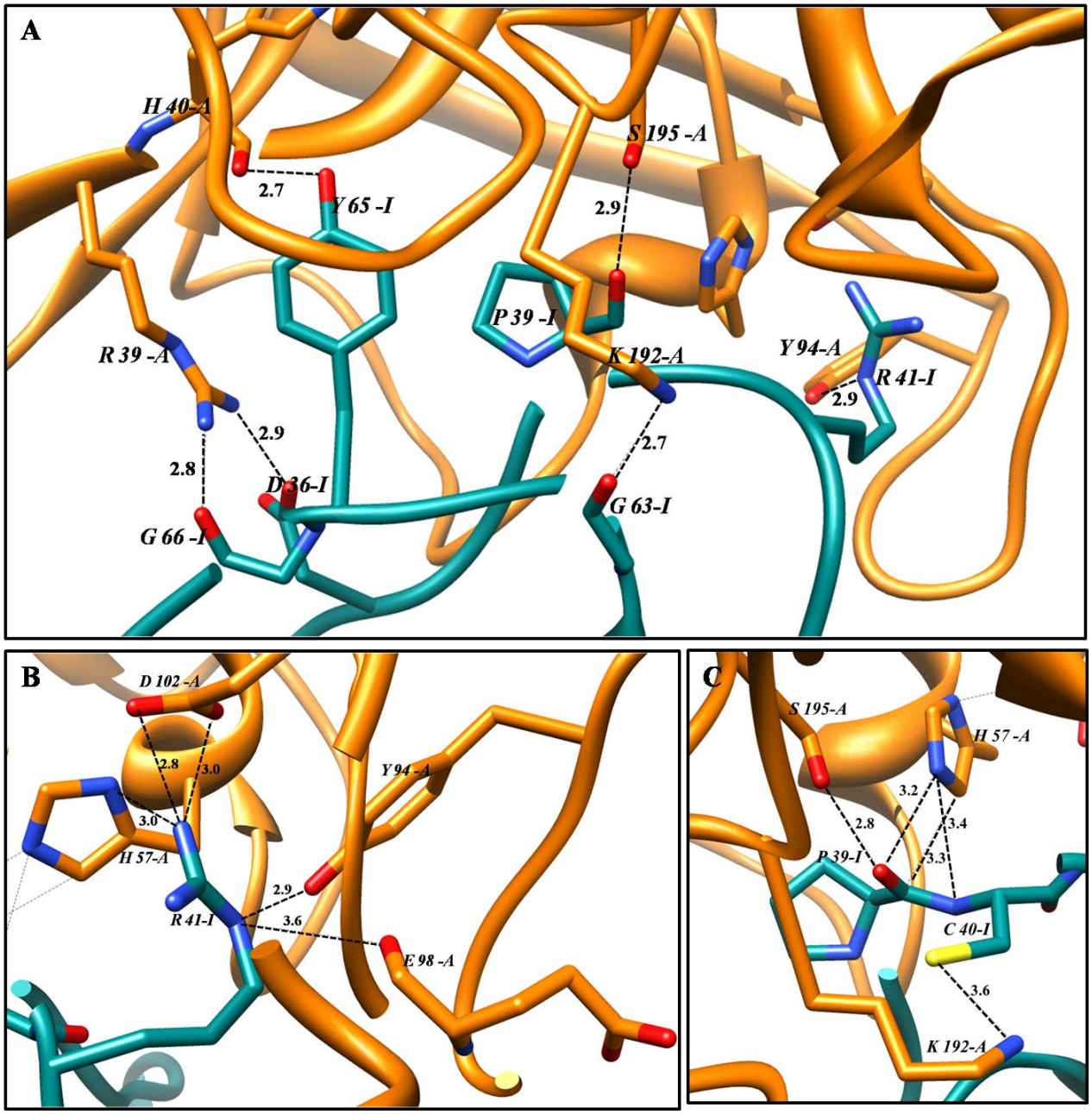

Fig. 65: Intermolecular interactions between tigerin-1 and *pkal 1*. ■ Chain A (*pkal 1*) ■ Chain I (tigerin-1)

The key interactions of the complex are summarized in Table 10. Fig. 65A shows the hydrogen bonding between Pro[39], at P2 site, and active site residue Ser[195] present at the S1 binding pocket of plasma kallikrein. Tigerin-1 interacts with an important residue Lys[192], bordering the S1 site of plasma kallikrein, through its P3 site (Cys [40]) and Gly[63] (present in the secondary binding loop of the inhibitor), Fig. 65A and C. It has been proposed that inhibitors selective for plasma kallikrein can be developed based on specific interactions with Lys[192], as majority of human

trypsin like proteases usually contain glutamine at residue 192 [143]. Fig. 65B shows interactions of the P1 residue Arg[41] with S1 catalytic residues, Asp[102] and His[57] and also with the S2 loop residues Tyr[94] and Glu[98]. The residues Asp[36] and Gly[66] form hydrogen bonds with Arg[39] present at the S1′ of the enzyme.

Table 10: Key intermolecular interactions of tigerin-1 in complex with *pkal 1*

	<----- A T O M 1 ----->					<----- A T O M 2 ----->					
	Atom no.	Atom name	Res name	Res no.	Chain		Atom no.	Atom name	Res name	Res no.	Chain	Distance
1.	248	NH1	ARG	39	A	<-->	109	OD2	ASP	36	I	2.90
2.	248	NH1	ARG	39	A	<-->	398	O	GLY	66	I	2.80
3.	251	NH2	ARG	39	A	<-->	108	OD1	ASP	36	I	2.90
4.	267	O	HIS	40	A	<-->	390	OH	TYR	65	I	2.70
5.	411	NE2	HIS	40	A	<-->	131	O	PRO	39	I	3.20
6.	817	OH	TYR	94	A	<-->	145	NE	ARG	41	I	2.90
7.	859	O	GLU	98	A	<-->	145	NE	ARG	41	I	3.60
8.	1796	NZ	LYS	192	A	<-->	372	O	GLY	63	I	2.70
9.	1820	OG	SER	195	A	<-->	131	O	PRO	39	I	2.80
10.	1796	NZ	Lys	192	A	<-->	133	SG	CYS	40	I	3.60

4.10.3: Molecular docking of tigerin-3 with trypsin

Fig. 66 shows the intermolecular interactions of the catalytic complex. The key interactions at the protein inhibitor interface are summarized in table 11.

Table 11: Key intermolecular interactions of tigerin-3 in complex with trypsin

	<----- A T O M 1 ----->					<----- A T O M 2 ----->					
	Atom no.	Atom name	Res name	Res no.	Chain		Atom no.	Atom name	Res name	Res no.	Chain	Distance
1.	131	OG1	THR	37	I	<-->	189	OH	TYR	39	A	2.80
2.	161	ND2	ASN	41	I	<-->	218	SG	CYS	42	A	3.22
3.	161	ND2	ASN	41	I	<-->	354	O	HIS	57	A	3.32
4.	402	O	CYS	64	I	<-->	1163	OG1	THR	149	A	2.90
5.	178	NH2	ARG	42	I	<-->	1539	OD2	ASP	189	A	3.20
6.	178	NH2	ARG	42	I	<-->	1549	O	SER	190	A	2.63
7.	178	NH2	ARG	42	I	<-->	1546	OG	SER	190	A	2.70
8.	165	O	ASN	41	I	<-->	1569	N	GLY	193	A	2.80
9.	165	O	ASN	41	I	<-->	1587	OG	SER	195	A	3.00
9.	175	NH1	ARG	42	I	<-->	1741	O	GLY	219	A	2.60

Fig. 66A shows that Asn[41] at P1 site forms hydrogen bonds with the active site residues Ser[195] and His[57] at the S1 pocket of enzyme. In addition to this it also forms a hydrogen bond with back bone nitrogen of Gly[193], facilitating the formation of the oxyanion hole. Arg[42] at P1′ site interacts

with Asp[189] present at the bottom of the catalytic triad. Asn[43] (P2′) side chain points directly into a pocket on the enzyme surface (S3), by forming a hydrogen bond with Ser[96]. Thr[37] (P5) binds to S1′ pocket of enzyme by hydrogen bond formation with Y[39] of trypsin.

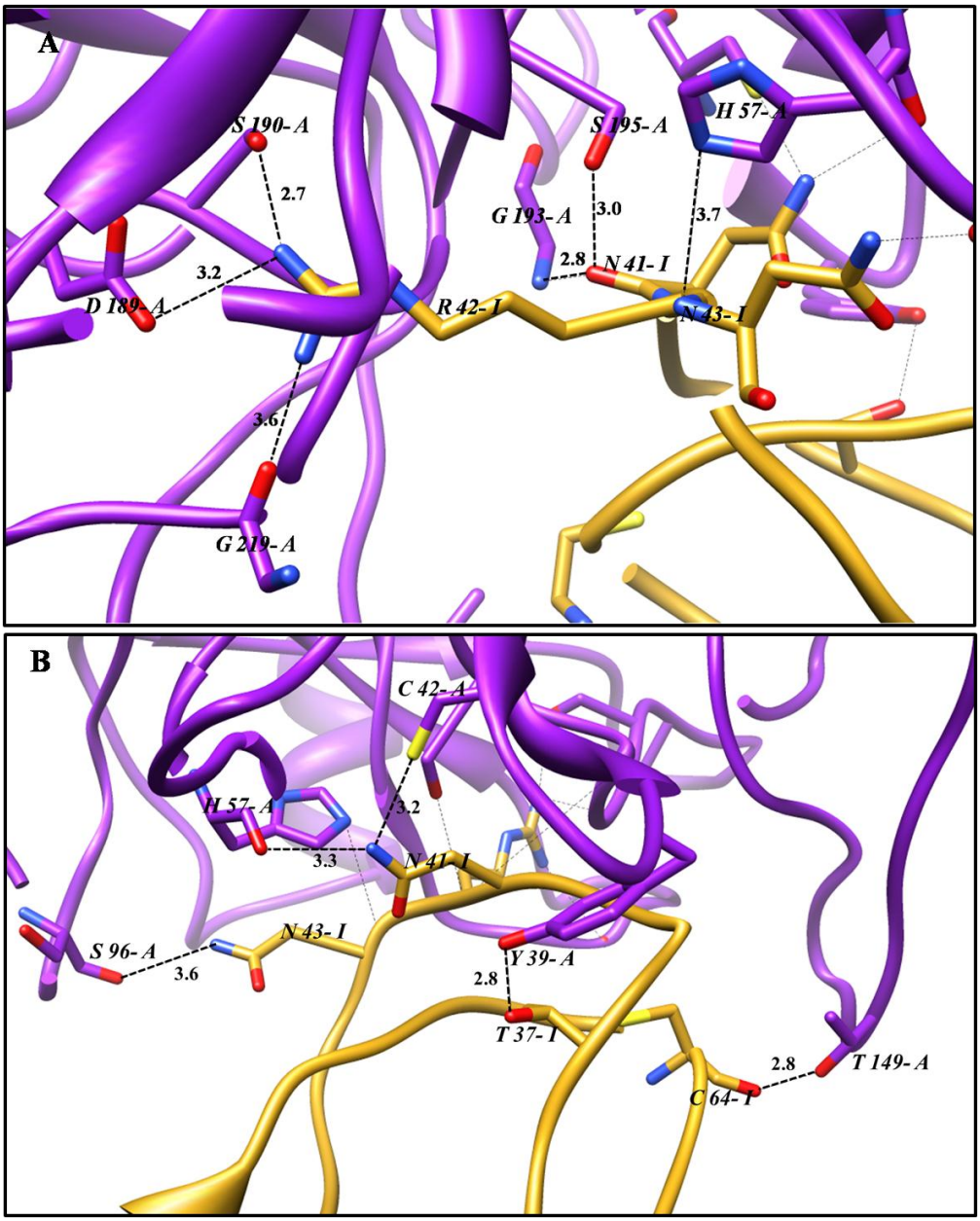

Fig. 66: Intermolecular interactions of tigerin-3 in complex with trypsin; ■ Chain A (trypsin) ■ Chain I (tigerin-3).

4.10.4: Molecular docking of protease inhibitor 1with trypsin

The Fig. 67 shows the interaction of the P1 residue Lys^{17} (equivalent to Lys^{41} in Fig. 62C) with the active site residues of trypsin. Key intermolecular interactions of the complex are given in Table 12.

Table 12: Key intermolecular interactions of protease inhibitor 1 in complex with trypsin

	Atom name	Atom name	Res no.	Chain		Atom no.	Atom name	Res name	Res no.	Chain	Distance
1.	N	GLY	216	E	<-->	95	O	ARG	15	I	3.1
2.	NE2	GLN	192	E	<-->	106	O	CYS	16	I	2.9
3.	OG	SER	195	E	<-->	109	N	LYS	17	I	2.8
4.	O	SER	214	E	<-->	109	N	LYS	17	I	3.3
5.	N	GLY	193	E	<-->	112	O	LYS	17	I	2.3
6.	OG	SER	190	E	<-->	117	NZ	LYS	17	I	2.2
7.	O	PHE	41	E	<-->	123	N	HIS	19	I	3.2
8.	OH	TYR	151	E	<-->	129	ND1	HIS	19	I	3.0
9.	OH	TYR	151	E	<-->	129	ND1	HIS	19	I	3.0

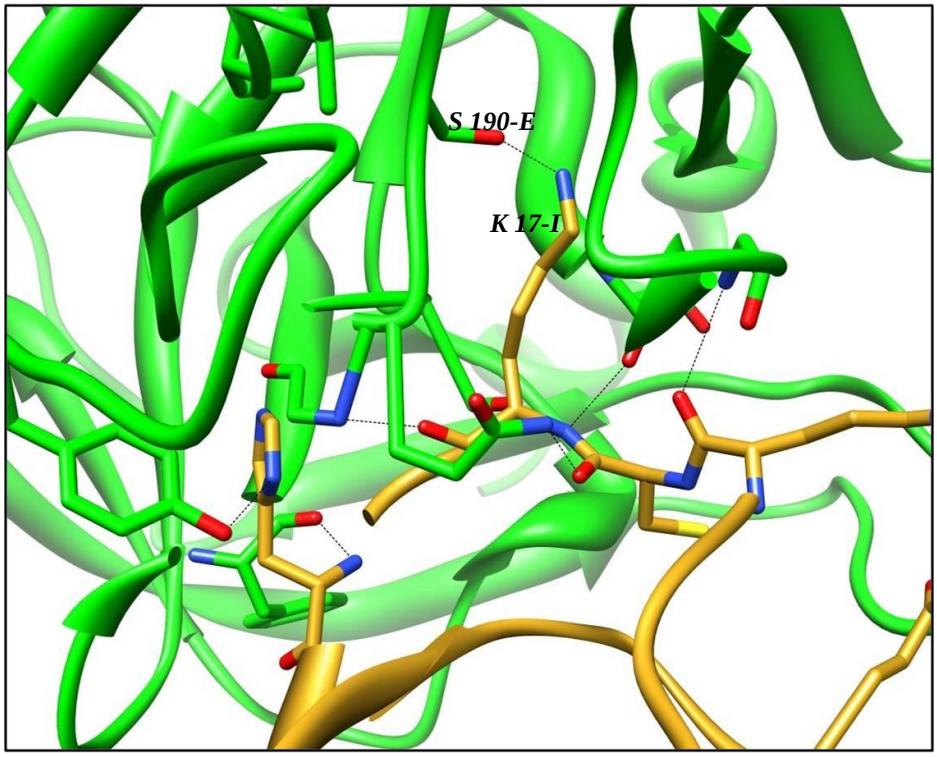

Fig. 67: Illustration of intermolecular interactions of protease inhibitor 1 in complex with trypsin. ■ Chain E (Trypsin) ■ Chain I (protease inhibitor 1)

4.11: Molecular modelling of cytotxin-1 with chymotrypsin

In this work cytotoxin-1 isolated from *Naja mossambica mossambica* was found to inhibit chymotrypsin. Therefore it was interesting to see the possible mode of interaction of cytotoxin-1 with chymotrypsin. The 3D model of cytotoxin-1 was also built by online server SWISS MODEL. The secondary structure of the model consists of 6 β-sheets and is stabilized by four disulfide bridges, Fig. 68.

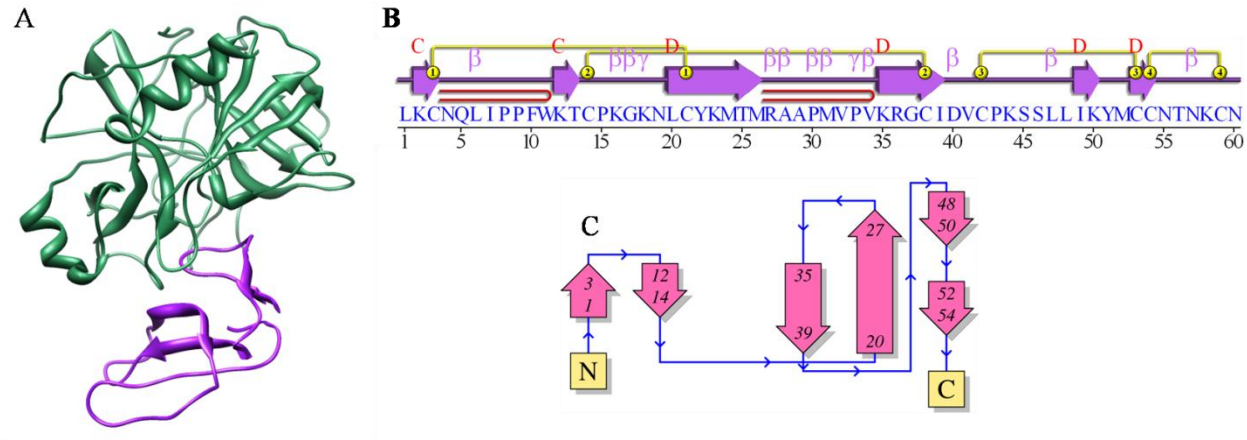

Fig. 68: (A) Catalytic complex of chymotrypsin and cytotoxin-1; (B) Structure-sequence relationship in the polypeptide chain; (C) Topology diagram of cytotoxin-1

The main interactions at the protein-protein interface are illustrated in Fig. 69 and summarized in Table 13.

Table 13: Key intermolecular interactions at the interface of Cytotoxin 1-Chymotrypsin complex

	Atom no.	Atom name	Res name	Res no.	Chain		Atom no.	Atom name	Res name	Res no.	Chain	Distance
1.	473	O	HIS	57	A	<-->	97	N	TRP	11	I	3.14
2.	470	NE2	HIS	57	A	<-->	48	NE2	GLN	5	I	2.94
3.	469	CD2	HIS	56	A	<-->	91	CD2	PHE	10	I	3.60
4.	1279	OH	TYR	146	A	<-->	354	NH2	ARG	36	I	2.68
5.	1701	CB	SER	195	A	<-->	94	CZ	PHE	10	I	3.2
6.	1903	O	SER	218	A	<-->	354	NH2	ARG	36	I	2.57
7.	1908	OG1	THR	219	A	<-->	305	O	MET	31	I	3.04

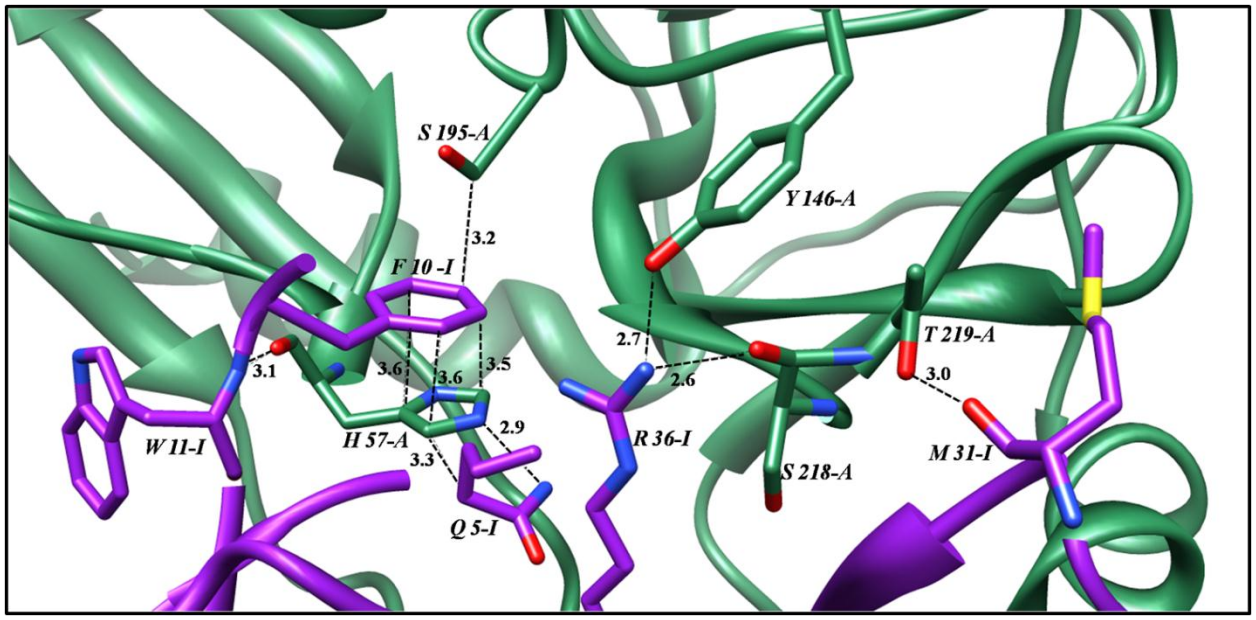

Fig. 69: Key interactions of cytotoxin-1 in complex with chymotryptsin. ■ Chain A (chymotrypsin); ■ Chain I (cytotoxin-1)

The presence of Leu, Met, Phe, Tyr, Trp and Asn at P1 site of the inhibitor tends to inhibit chymotrypsin [145]and references there in. The model of the catalytic complex shows the possible sites of interaction with the protease and illustrates the insertion of the hydrophobic residue Phe^{10} in the S1 pocket of chymotrypsin. Phe^{10} makes extensive hydrophobic interactions with His^{57} and Ser^{195} present at catalytic triad of the active site. Gln^{5} forms a hydrogen bond with His^{57}. Trp^{11} makes a hydrogen bond with His^{57} through its back bone nitrogen. Other residues of cytotoxin-1 are also involved in making hydrogen bonds with surface residues of chymotrypsin further stabilizing the complex, as shown in the Fig. 69. From the model Phe^{10} can be proposed as the P1 site.

4.12: Molecular modelling and docking of selected BPPs with the catalytic C-domain of human ACE

A protein data bank search showed that no crystal structure of snake venom bradykinin potentiating peptide in complex with ACE is available so far. Therefore model complexes of selected BPPs isolated in this work were prepared by molecular modelling and docking using the program SYBYL-X, version 1.3, to predict the binding mode of the snake venom BPP with ACE. C-domain of human ACE is known to be necessary and sufficient for controlling the blood pressure and cardiovascular functions. The tACE is identical to the C-terminal half of somatic

ACE, except for a unique 36-residue sequence making up its amino acid terminus [146]. Hence the crystal structure [147] of tACE in complex with lisinopril (*N*-[(*S*)-1-carboxy-3-phenylpropyl]-Llysyl-L-proline) was used in the model building of complex, and selected as standard structure to compare the model complexes. The structure of tACE adopts an overall ellipsoidal shape, with a central groove that extends for about 30 Å into the molecule and divides the protein into two domains (Fig. 70 A). The surface diagram (Fig. 70 B) of the crystal structure of lisinopril (an analogue of the tripeptide Phe-Lys-Pro) in complex with tACE, shows the buried lisinopril molecule inside the active site.

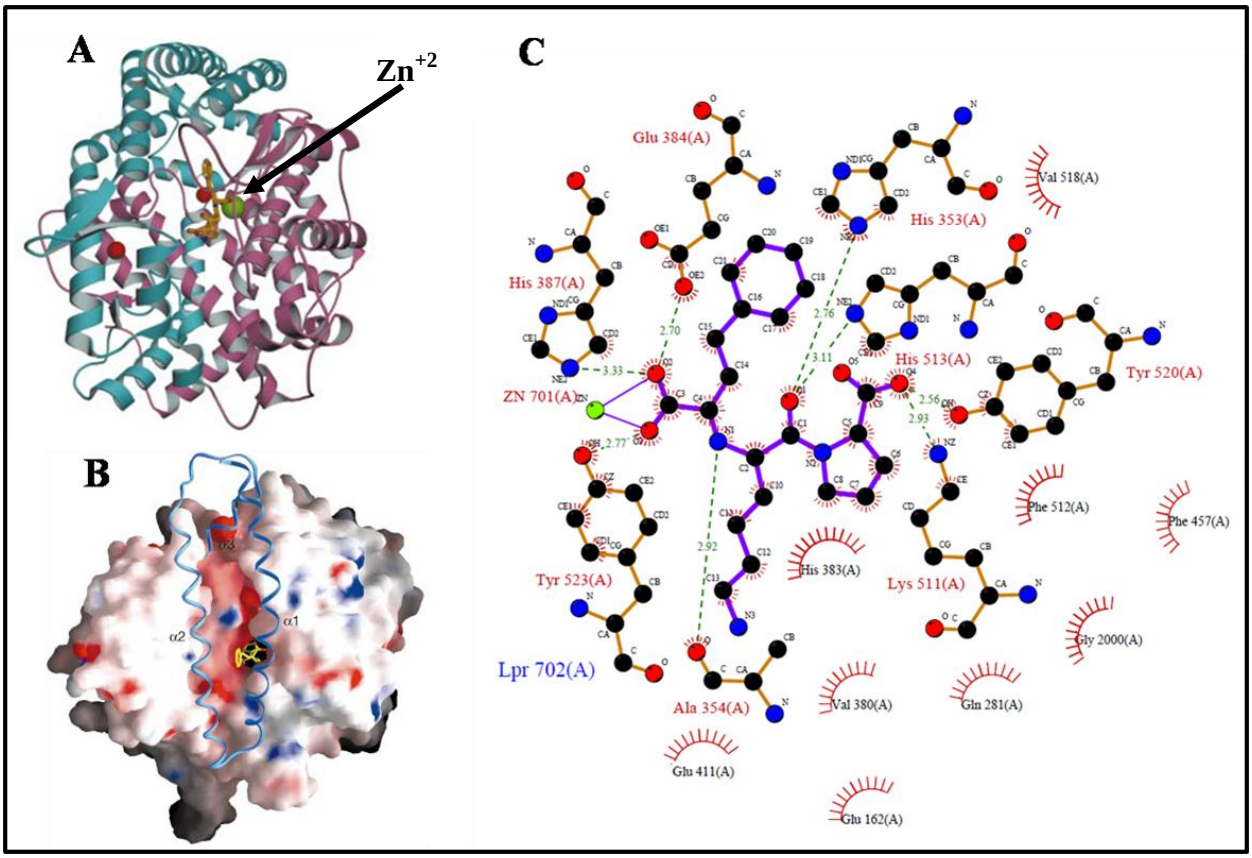

Fig. 70: (A) Ribbon representation of tACE molecule. The active site Zn ion is shown in green color. The bound ligand, lisinopril is shown in yellow color; (B) Molecular surface representation showing the active-site groove. The molecule surface has been sliced to show the groove. The buried lisinopril molecule is shown in yellow color; (C) Ligplot of lisinopril in complex with tACE [147].

The active site of tACE is comprised of the following residues: His^{514}, Tyr 524, Glu^{411}, His^{383}, Asp^{415}, His^{387}, Glu^{384} are present at the Zn^{+2} coordination site. The residues present at and lining

the S1 site are Val^{518}, Phe^{512}, and Ser^{355}, at S1′ site are Glu^{162}, Ala^{354}, Val^{380} and Asp^{377}, at the S2′ site are Tyr^{523}, Phe^{457}, Phe^{527}, Gln^{281} and Thr^{282} [148].

Table 14, shows the BPPs used to prepare models and the resulting energy values given by SYBL-X program, after the formation of BPP- tACE complexes.

Table 14: Selected BPPs isolated in this work used to model the BPP-tACE complex

S.No.	Source of venom	BPP sequence	Average Molecular weight (Da)	Energy value (SYBL-X)
1	*Vipera ammodytes meridionalis*	ZNWPGPKVPP (BPP1)	1101	-1300.0
2		ZNWPGPK (BPP2)	808	-1137.6
3		ZRWPGP (BPP3)	722	-1114.9
4	*Bothrops jararacussu*	RPPHPP (BPP4)	699	-1421.7
5		ZARPPHPPIPP (BPP5)	1188	-994.0
6		ZARPPHPPIPPAP (BPP6)	1356	-1040.4
7		ZGGWPRPGPEIPP (BPP7)	1369	-1216.3
8	*Naja mossambica mossambica*	ZLWPRPQIPP (BPP8)	1213	-1239.0
9		ZQWPPGHHIPP (BPP9)	1275	-1305.9
10		ZLWPRP (BPP10)	778	-1136.0

The intermolecular interactions of the ligand-enzyme model complexes are individually discussed below. In all the complexes, as far as the residue numbering is concerned, an N-terminal pyroglutmate residue is given 0 as number, and the C-terminal carboxylate group is assigned as a separate residue.

Fig. 71A shows the BPP1 ligand (yellow sticks) in complex with tACE. Fig. 71B and C shows that the ligand has penetrated the channel like cavity and the midway slicing of the protein illustrates that the ligand is fit inside the active site cavity making intermolecular interactions with the enzyme. The key intermolecular interactions are also summarized in the table (Fig. 71D). The Lys residue of the peptide forms hydrogen bonded salt bridge with Glu^{376} imparting stability to the complex. The peptide C-terminal proline forms hydrogen bonds with Tyr^{523} present at S2′ site through its carboxylate group and also hydrogen bonds with other active site

residues Glu[384] and His[383] and Ala[354], while in lisinopril the proline carboxlate group binds to Lys[511] and Tyr[513]. The two prolines at the C-terminus form hydrophobic interactions with active site residues His[383], His[513], Phe[512]. The other peptide residues are also involved in important intermolecular interactions like interactions with Asp[453] and other chain residues of the enzyme, which are not present in the lisinopril-tACE complex, possibly due to the small size of the lisinopril, as compared to the BPP1 peptide.

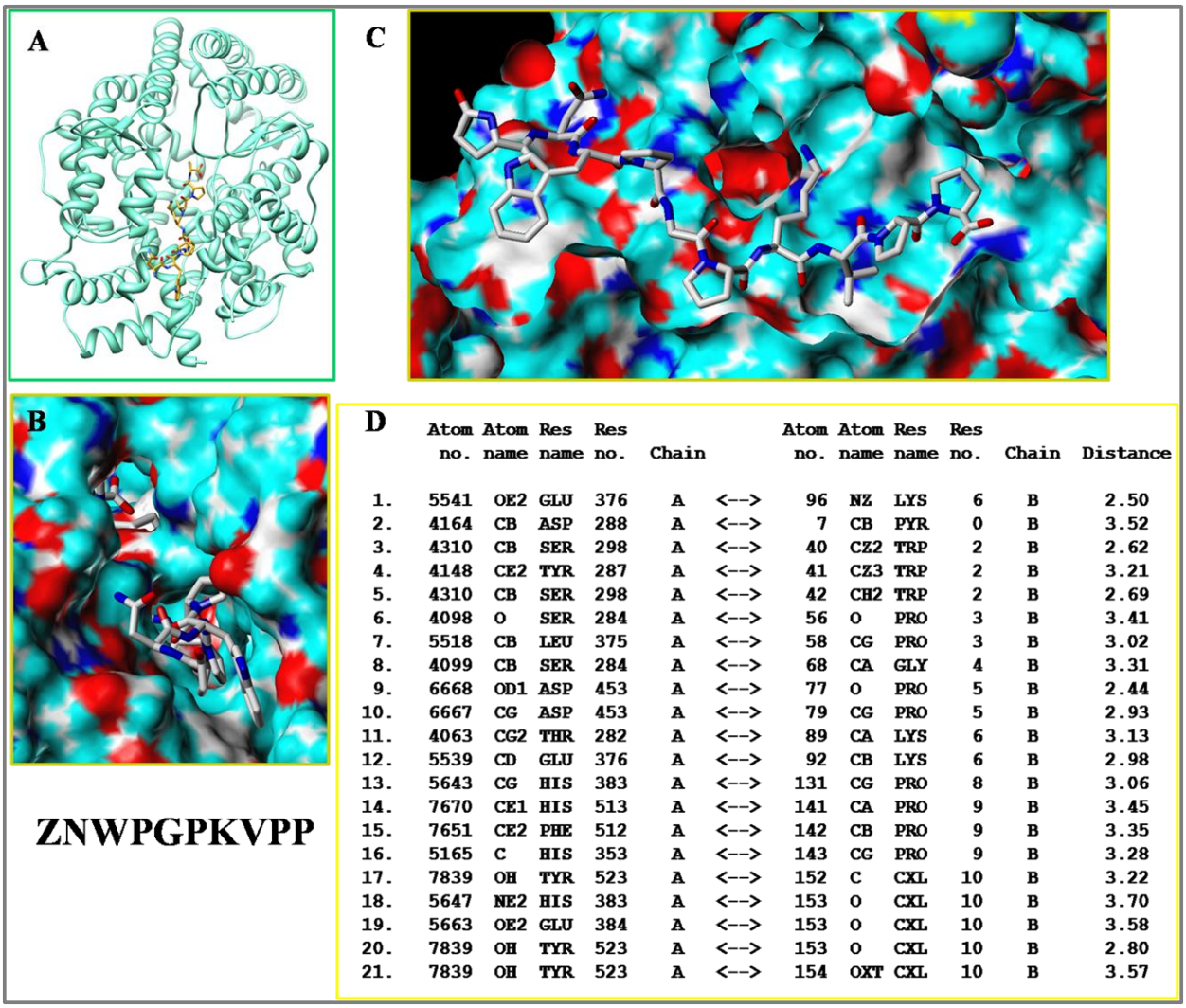

	Atom no.	Atom name	Res name	Res no.	Chain		Atom no.	Atom name	Res name	Res no.	Chain	Distance
1.	5541	OE2	GLU	376	A	<-->	96	NZ	LYS	6	B	2.50
2.	4164	CB	ASP	288	A	<-->	7	CB	PYR	0	B	3.52
3.	4310	CB	SER	298	A	<-->	40	CZ2	TRP	2	B	2.62
4.	4148	CE2	TYR	287	A	<-->	41	CZ3	TRP	2	B	3.21
5.	4310	CB	SER	298	A	<-->	42	CH2	TRP	2	B	2.69
6.	4098	O	SER	284	A	<-->	56	O	PRO	3	B	3.41
7.	5518	CB	LEU	375	A	<-->	58	CG	PRO	3	B	3.02
8.	4099	CB	SER	284	A	<-->	68	CA	GLY	4	B	3.31
9.	6668	OD1	ASP	453	A	<-->	77	O	PRO	5	B	2.44
10.	6667	CG	ASP	453	A	<-->	79	CG	PRO	5	B	2.93
11.	4063	CG2	THR	282	A	<-->	89	CA	LYS	6	B	3.13
12.	5539	CD	GLU	376	A	<-->	92	CB	LYS	6	B	2.98
13.	5643	CG	HIS	383	A	<-->	131	CG	PRO	8	B	3.06
14.	7670	CE1	HIS	513	A	<-->	141	CA	PRO	9	B	3.45
15.	7651	CE2	PHE	512	A	<-->	142	CB	PRO	9	B	3.35
16.	5165	C	HIS	353	A	<-->	143	CG	PRO	9	B	3.28
17.	7839	OH	TYR	523	A	<-->	152	C	CXL	10	B	3.22
18.	5647	NE2	HIS	383	A	<-->	153	O	CXL	10	B	3.70
19.	5663	OE2	GLU	384	A	<-->	153	O	CXL	10	B	3.58
20.	7839	OH	TYR	523	A	<-->	153	O	CXL	10	B	2.80
21.	7839	OH	TYR	523	A	<-->	154	OXT	CXL	10	B	3.57

Fig. 71: BPP1-tACE complex and its key intermolecular interactions.

The ligplot of BPP2-tACE complex is shown in Fig. 72 and key intermolecular interactions are summarized in table 15. The BPP2 peptide lacks a C-terminal proline residue. The lysine carboxylate group of the peptide forms hydrogen bond with His^{383}. The CG of Pro (residue number 5) makes hydrophobic interaction with CE1 of Phe^{527} present at the S2′ site. The peptide interacts with other side chain residues as well to stabilize the complex and less interaction with the known active site residues is observed in this case. The inhibitory activity of this peptide could mainly be ascribed to its interactions with His^{383} at the Zinc binding site.

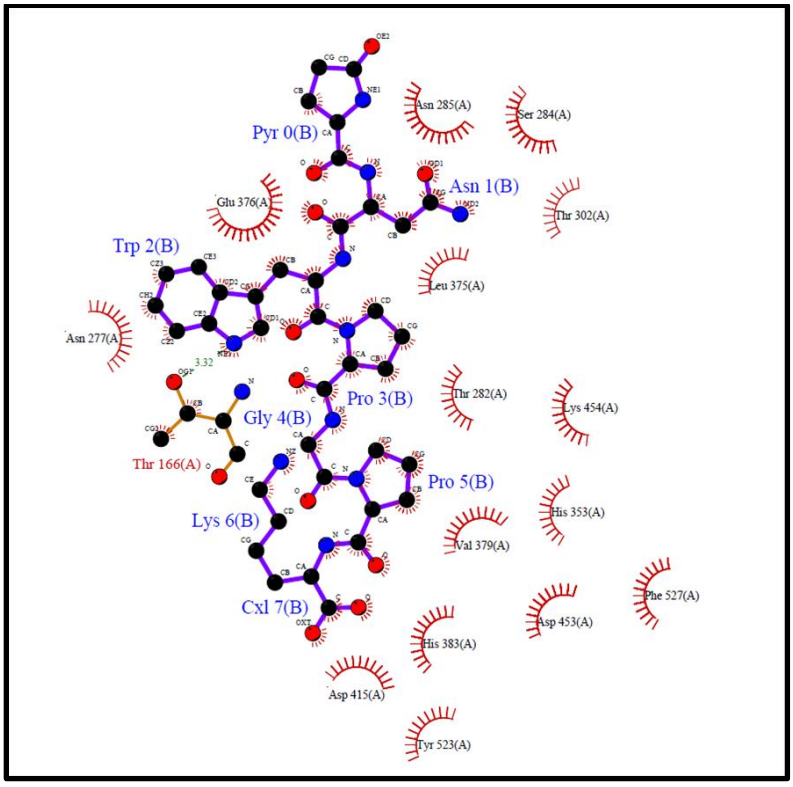

Fig. 72: Ligplot of BPP2 (ZNWPGPK) in complex with human tACE .

Table 15: Key intermolecular interactions of BPP2 in complex with tACE

	Atom No.	Atom Name	Res Name	Res No.	Chain		Atom No.	Atom Name	Res Name	Res No.	Chain	Distance
1	4062	N	ASN	285	A	<-->	3	O	PYR	3	B	3.2
2	4053	C	SER	284	A	<-->	19	CB	ASN	1	B	3.2
3	4054	O	SER	284	A	<-->	21	OD1	ASN	1	B	2.68
4	6625	OD2	ASP	453	A	<-->	56	O	PRO	3	B	2.5
5	4018	OG1	THR	282	A	<-->	67	N	GLY	4	B	3.6
6	5128	NE2	HIS	353	A	<-->	94	NZ	LYS	6	B	2.84
7	5601	CD2	HIS	383	A	<-->	108	C	CXL	7	B	3.4
8	5603	NE2	HIS	383	A	<-->	109	O	CXL	7	B	2.3

The BPP3 peptide is shorter than the previously discussed BPP1 and BPP2. This peptide contains arginine next to pyrogultamate in contrast to BPP1 and BPP2 which contain asparagines at this position.

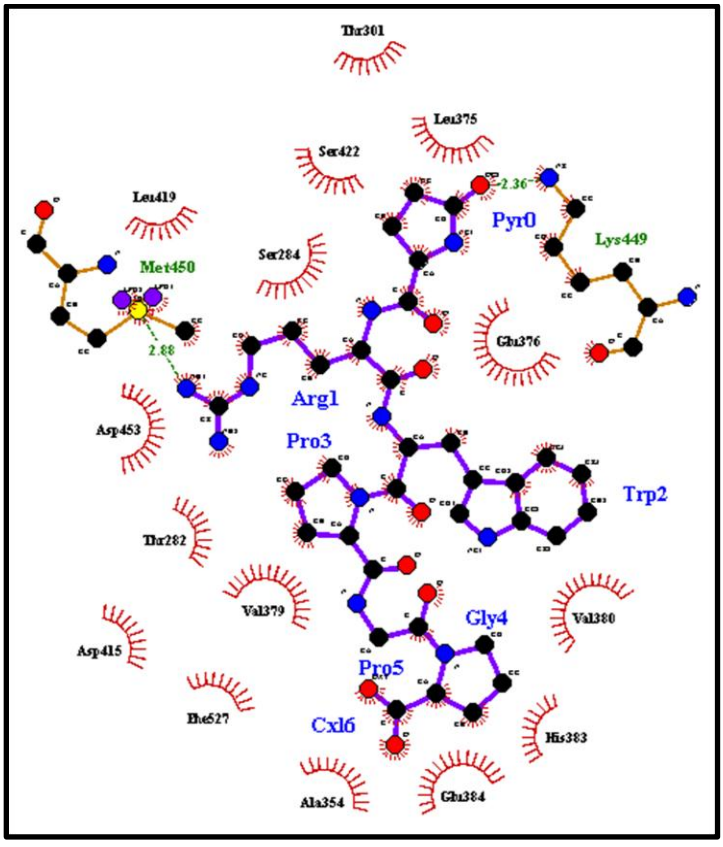

Fig. 73: Ligplot of BPP3 (ZRWPGP) in complex with tACE.

Fig. 73 shows the ligplot of BPP3-tACE complex. The arginine NH_2 group is in distance 2.9 Å with the sulfur atom of Met^{450}. The peptide is although shorter in size compared to BPP2, but is involved in making more interactions with the active site residues, as can be seen from the ligplot (Fig. 73) and key interactions summarized in table 16.

Table 16: Key intermolecular interactions of BPP3-tACE complex

	Atom No.	Atom Name	Res Name	Res No.	Chain		Atom No.	Atom Name	Res Name	Res No.	Chain	Distance
1	5503	N	GLU	376	A	<-->	0	O	PYR	0	B	2.7
2	6644	CB	ASP	453	A	<-->	20	CG	ARG	1	B	2.9
3	6646	OD1	ASP	453	A	<-->	39	N	TRP	2	B	3.3
4	5570	CG1	VAL	380	A	<-->	46	CD2	TRP	2	B	3.6
5	4021	CG2	THR	282	A	<-->	69	CD	PRO	3	B	3.3
6	7886	CZ	PHE	527	A	<-->	67	CB	PRO	3	B	2.9
7	5633	OE2	GLU	384	A	<-->	80	O	GLY	4	B	2.9
8	5615	CD2	HIS	383	A	<-->	85	CA	PRO	5	B	3.5
9	5631	CD	GLU	384	A	<-->	96	C	CXL	6	B	3.3
10	5152	CB	ALA	354	A	<-->	96	C	CXL	6	B	3.1
11	5151	O	ALA	354	A	<-->	97	O	CXL	6	B	2.4
12	5633	OE2	GLU	384	A	<-->	97	O	CXL	6	B	2.9
13	5633	OE2	GLU	384	A	<-->	98	O	OXT	6	B	2.9

BPP4 peptide isolated from *Bothrops jararacussu* venom consists of six residues, and proline constitutes 66 % of this peptide. This peptide also contains a histidine residue which is not present in the BPP peptides isolated from *Vipera ammodytes meridionalis* venom. The liglot of BPP4-tACE complex is shown in Fig. 74. As can be seen from the ligplot of the peptide BBP4, the C-terminal proline interacts with similar residues at the active site as that of proline in lisionopril, for example with Tyr^{520}. The oxygen atom of the carboxylate group present at the c-terminal of the peptide also interacts with $His^{513,}$ while in case of lisinopril the back bone proline oxygen binds at this site. The C-terminal proline shows interactions with residues present at the S2′ site, and appears to be well accommodated in the S2′ site like that of C-terminal proline in lisinopril. The C-terminal proline also makes hydrophobic interactions with Val^{380}, lining the S1′ pocket. The histidine strongly hydrogen bonds to Asp^{415}, present at Zn^{+2} active site. Therefore the presence of histidine at this position in the peptide can be responsible for its potency. The key intermolecular interactions of the BPP4-tACE complex are summarized in table 17.

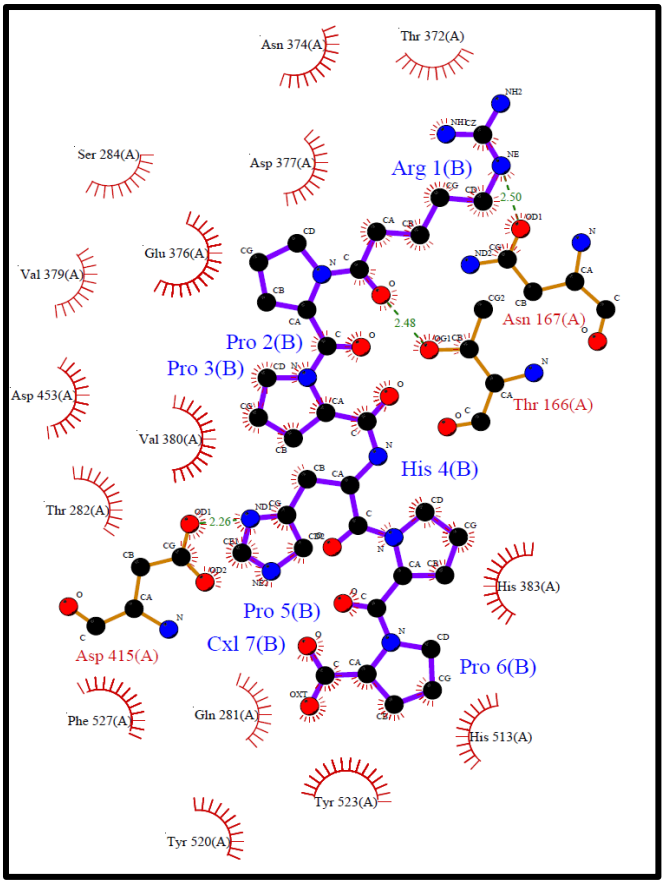

Fig. 74: Ligplot of BPP4 (RPPHPP) in complex with tACE.

Table 17: Key intermolecular interactions of BPP4 in complex with tACE

	Atom No.	Atom Name	Res Name	Res No.	Chain		Atom No.	Atom Name	Res Name	Res No.	Chain	Distance
1	2110	OG1	THR	166	A	<-->	7	O	ARG	1	B	2.5
2	6086	OD1	ASP	415	A	<-->	4	ND1	HIS	4	B	2.3
3	5500	OD1	ASP	377	A	<-->	30	O	PRO	2	B	3.5
4	5541	N	VAL	380	A	<-->	44	O	PRO	3	B	3.2
5	6613	CG	ASP	453	A	<-->	46	CG	PRO	3	B	3.6
6	4009	CG2	THR	282	A	<-->	47	CD	PRO	3	B	3.4
7	60086	OD1	ASP	415	A	<-->	61	ND1	HIS	4	B	2.3
8	6085	CG	ASP	415	A	<-->	63	CE1	HIS	4	B	2.8
9	5542	CA	VAL	380	A	<-->	77	CG	PRO	5	B	3.1
10	7720	CZ	TYR	520	A	<-->	88	CB	PRO	5	B	3.4
11	7614	ND1	HIS	513	A	<-->	99	O	CXL	7	B	3.4
12	7785	OH	TYR	7785	A	<-->	100	OXT	CXL	7	B	2.7

The ligplot of BPP5-tACE complex is shown in Fig. 75. The C-terminal proline of BPP5 forms hydrogen bond to His^{353} and Ala^{354}. The lisinopril proline also forms bond to His^{353}, although through a backbone oxygen. Other important intermolecular interactions are summarized in the table 18.

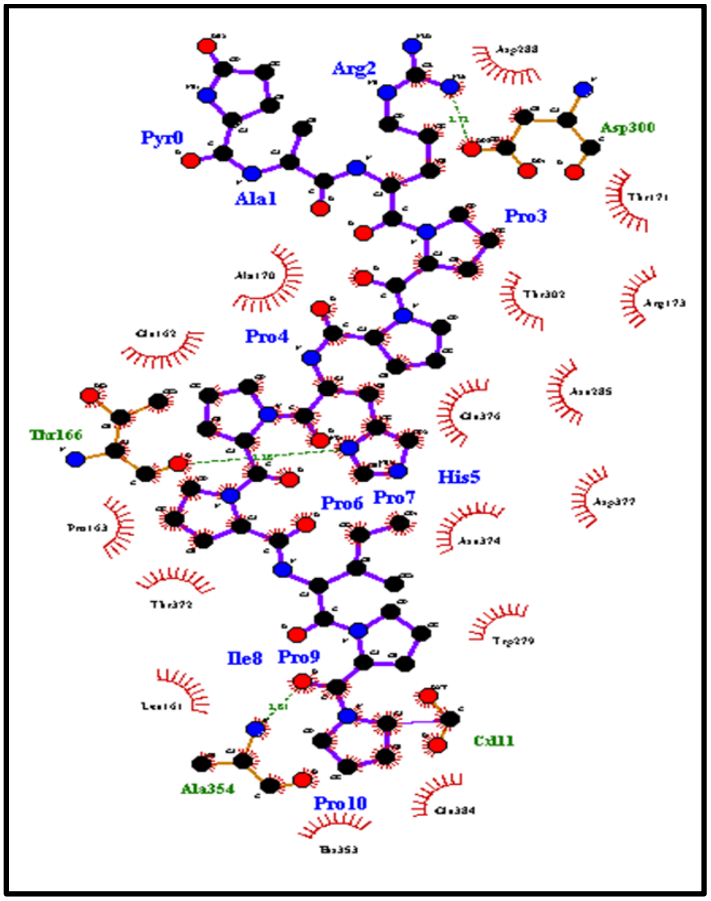

Fig. 75: Ligplot of BPP5 (ZARPPHPPIPP) in complex with tACE.

The ligplot of BPP6-tACE complex is shown in Fig. 76. The key intermolecular interactions with active site residues and other side chain residues are summarized in table 19. The peptide forms five hydrogen bonds and one salt bridge thus stabilizing the complex.

Table 18: Key intermolecular interactions of BPP5-tACE complex

	<----- A T O M 1 ----->					<----- A T O M 2 ----->					
	Atom no.	Atom name	Res name	Res no.	Chain		Atom no.	Atom name	Res name	Res no.	Chain	Distance
1.	4354	OD2	ASP	300	A	<-->	34	NH1	ARG	2	B	2.7
2.	2177	O	THR	166	A	<-->	83	ND1	HIS	5	B	2.3
3.	5195	N	ALA	354	A	<-->	144	O	PRO	9	B	2.8
4.	5184	ND1	HIS	353	A	<-->	169	OXT	CXL	11	B	2.5
5.	4180	CG	ASP	288	A	<-->	29	CB	ARG	2	B	3.2
6.	4354	OD2	ASP	300	A	<-->	34	NH1	ARG	2	B	2.7
7.	2237	C	ALA	170	A	<-->	53	CB	PRO	3	B	2.9
8.	4377	CB	THR	302	A	<-->	67	CB	PRO	4	B	3.0
9.	5522	ND2	ASN	374	A	<-->	80	O	HIS	5	B	3.1
10.	2115	CA	GLU	162	A	<-->	112	CB	PRO	7	B	3.2
11.	2179	OG1	THR	166	A	<-->	122	N	ILE	8	B	3.3
12.	5195	N	ALA	354	A	<-->	144	O	PRO	9	B	2.8
13.	5180	C	HIS	353	A	<-->	167	C	CXL	11	B	3.2
14.	5196	CA	ALA	354	A	<-->	167	C	CXL	11	B	3.6
15.	5184	ND1	HIS	353	A	<-->	168	O	CXL	11	B	3.1
16.	7666	CE2	PHE	512	A	<-->	169	OXT	CXL	11	B	3.49

Table 19: Key intermolecular interactions of BPP6-tACE

	Atom no.	Atom name	Res name	Res no.	Chain		Atom no.	Atom name	Res name	Res no.	Chain	Distance
1.	4348	O	SER	298	A	<-->	35	NH2	ARG	2	B	2.5
2.	4388	OG1	THR	301	A	<-->	80	O	HIS	5	B	2.7
3.	4152	ND2	ASN	285	A	<-->	97	O	PRO	6	B	2.5
4.	2203	OG1	THR	166	A	<-->	125	O	ILE	8	B	2.5
5.	7878	OH	TYR	523	A	<-->	192	OXT	CXL	13	B	2.5
6.	4377	OD1	ASP	300	A	<-->	35	NH2	ARG	2	B	3.6
7.	4388	OG1	THR	301	A	<-->	80	O	HIS	5	B	2.7
8.	4398	CA	THR	302	A	<-->	81	CB	HIS	5	B	3.1
9.	5591	CB	ASP	377	A	<-->	145	CB	PRO	9	B	3.2
10.	5209	CD2	HIS	353	A	<-->	181	CB	PRO	12	B	3.4
11.	5204	C	HIS	353	A	<-->	183	CD	PRO	12	B	3.6
12.	5686	NE2	HIS	383	A	<-->	192	OXT	CXL	13	B	3.6
13.	5222	O	ALA	354	A	<-->	193	O	CXL	13	B	3.3
14.	7878	OH	TYR	523	A	<-->	193	O	CXL	13	B	3.4
15.	4378	OD2	ASP	300	A	<-->	32	NE	ARG	2	B	3.3

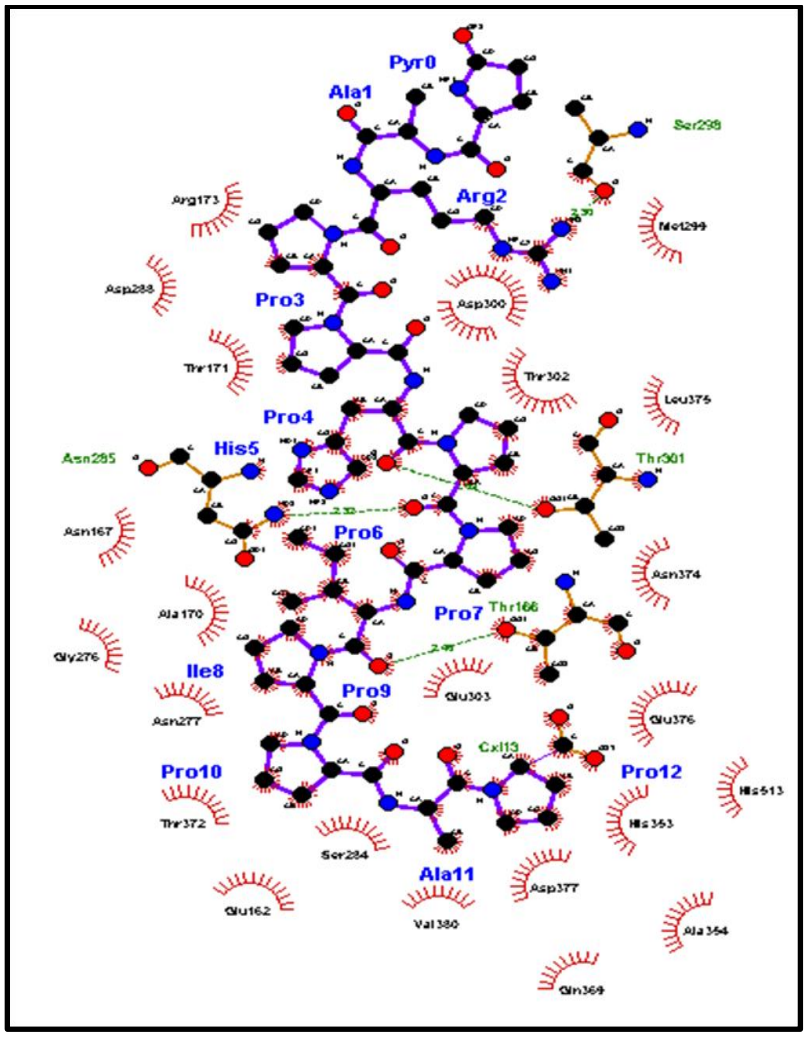

Fig. 76: Ligplot of BPP6 (ZARPPHPPIPPAP) in complex with tACE.

The ligplot of BPP7-tACE complex is shown in Fig. 77. Key intermolecular interactions are summarized in table 20. The carboxylate group has a hydrogen bond with OH group of Tyr^{523} present at the S2′ site. C-terminal Pro forms hydrophobic interactions with His^{353}, His^{513} and Phe^{512}. Other residues of the peptide also form hydrophobic interactions with active site residues and other side chain residues of the peptide.

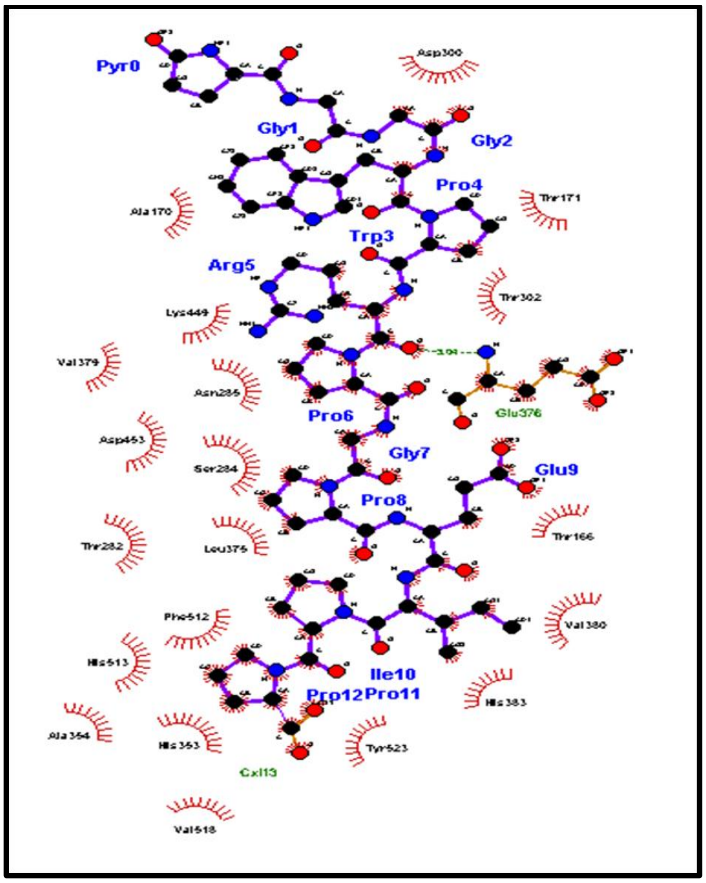

Fig. 77: Ligplot of BPP7 (ZGGWPRPCPEIPP) in complex with tACE.

Table 20: Key intermolecular interactions of BPP7 in complex with tACE

	<----- A T O M 1 ----->					<----- A T O M 2 ----->					
	Atom no.	Atom name	Res name	Res no.	Chain		Atom no.	Atom name	Res name	Res no.	Chain	Distance
1.	5567	N	GLU	376	A	<-->	70	O	ARG	5	B	3.0
2.	4371	CG	ASP	300	A	<-->	24	C	GLY	2	B	3.4
3.	4373	OD2	ASP	300	A	<-->	25	O	GLY	2	B	3.0
4.	4147	ND2	ASN	285	A	<-->	67	N	ARG	5	B	3.1
5.	4133	CB	SER	284	A	<-->	93	C	PRO	6	B	3.1
6.	6703	OD2	ASP	453	A	<-->	112	N	PRO	8	B	3.6
7.	4096	OG1	THR	282	A	<-->	115	O	PRO	8	B	3.6
8.	4095	CB	THR	282	A	<-->	117	CG	PRO	8	B	2.8
9.	6700	CB	ASP	453	A	<-->	117	CG	PRO	8	B	3.0
10.	5634	CG1	VAL	380	A	<-->	142	CA	ILE	10	B	3.4
11.	5679	CD2	HIS	383	A	<-->	147	CG2	ILE	10	B	3.2
12.	5204	CD2	HIS	353	A	<-->	161	CA	PRO	11	B	3.0
13.	5215	CA	ALA	354	A	<-->	165	CG	PRO	11	B	3.3
14.	7773	CG1	VAL	518	A	<-->	176	CB	PRO	12	B	3.5
15.	7697	CA	HIS	513	A	<-->	177	CG	PRO	12	B	3.2
16.	7683	CD2	PHE	512	A	<-->	178	CD	PRO	12	B	3.0
17.	7873	OH	TYR	523	A	<-->	188	OXT	CXL	13	B	3.0

The ligplot of BPP8-tACE complex is shown in Fig. 78. BPP8 isolated from *Naja m. mossambica* venom, consists of ten amino acids. The peptide forms a hydrogen bond with Gln^{281} present at the S2′ site, through residue number 8. The carboxylate group shows hydrophobic interactions with Val^{380}. Other important interactions of the peptide complex are summarized in table 21.

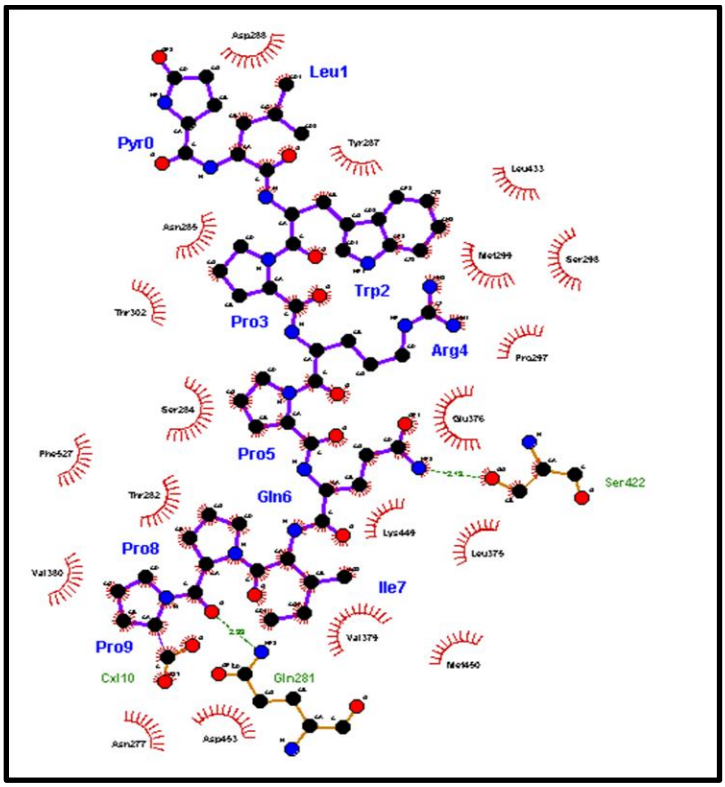

Fig. 78: Ligplot of BPP8 (ZLWPRPQIPP) in complex with tACE.

Table 21: Key intermolecular interactions of BPP8-tACE complex

	<----- A T O M 1 ----->					<----- A T O M 2 ----->					
	Atom no.	Atom name	Res name	Res no.	Chain		Atom no.	Atom name	Res name	Res no.	Chain	Distance
1.	6262	OG	SER	422	A	<-->	118	NE2	GLN	6	B	2.19
2.	4068	NE2	GLN	281	A	<-->	149	O	PRO	8	B	2.99
3.	6688	OD1	ASP	453	A	<-->	113	O	GLN	6	B	2.83
4.	6688	OD1	ASP	453	A	<-->	127	N	ILE	7	B	3.39
5.	6687	CG	ASP	453	A	<-->	128	CA	ILE	7	B	3.64
6.	4083	CG2	THR	282	A	<-->	131	CB	ILE	7	B	3.28
7.	4081	CB	THR	282	A	<-->	132	CG1	ILE	7	B	3.16
8.	4083	CG2	THR	282	A	<-->	132	CG1	ILE	7	B	3.01
9.	4083	CG2	THR	282	A	<-->	134	CD1	ILE	7	B	3.39
10.	7926	CZ	PHE	527	A	<-->	150	CB	PRO	8	B	2.98
11.	5621	CG2	VAL	380	A	<-->	163	CG	PRO	9	B	2.99

The ligplot of BPP9-tACE complex is shown in Fig. 79. The peptide BPP9 also contains histidine residue, which is present in most of the BPP peptides isolated from *Bothrops jararacussu* venom. Both histidine residues 6 and 7 of the peptide form strong hydrogen bonds with Glu^{376} and Glu^{162} respectively. Proline 4 forms a hydrogen bond with Asn^{374} and glycine 5 forms a hydrogen bond with Thr^{166} through their backbone oxygen atom. Isoleucine makes hydrophobic interactions with Gln^{281}. The carboxylate is connected with Glu^{411} and His^{383} close to the Zn^{+2} active site. The two prolines at the C-terminus are involved in hydrophobic interactions with other residues in the active site. The important intermolecular interactions of the complex are summarized in table 22.

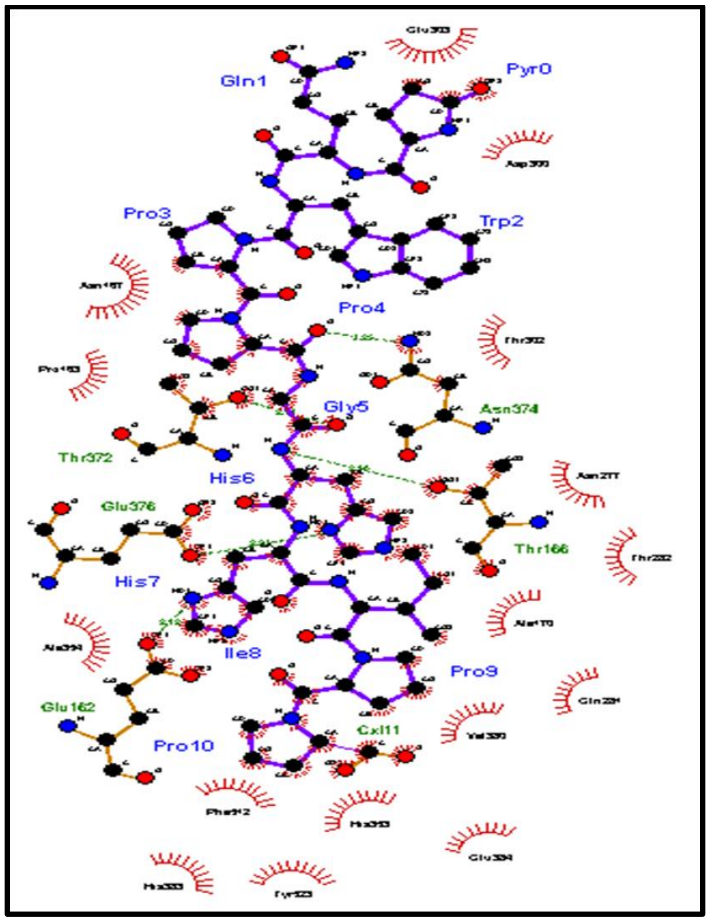

Fig. 79: Ligplot of BPP9 (ZQWPPGHHIPP) in complex with tACE.

Table 22: Key intermolecular interactions of BPP9 in complex with tACE

	<----- ATOM 1 ----->					<----- ATOM 2 ----->					
	Atom no.	Atom name	Res name	Res no.	Chain		Atom no.	Atom name	Res name	Res no.	Chain	Distance
1.	5525	ND2	ASN	374	A	<-->	73	O	PRO	4	B	3.3
2.	2182	OG1	THR	166	A	<-->	91	N	HIS	6	B	3.0
3.	5558	OE1	GLU	376	A	<-->	97	ND1	HIS	6	B	2.2
4.	2125	OE2	GLU	162	A	<-->	114	ND1	HIS	7	B	2.2
5.	2123	CD	GLU	162	A	<-->	112	CB	HIS	7	B	3.5
6.	5202	CB	ALA	354	A	<-->	115	CD2	HIS	7	B	3.1
7.	5182	CA	HIS	353	A	<-->	116	CE1	HIS	7	B	3.1
8.	5183	C	HIS	353	A	<-->	116	CE1	HIS	7	B	3.5
9.	5198	N	ALA	354	A	<-->	117	NE2	HIS	7	B	2.5
10.	5619	CG2	VAL	380	A	<-->	150	CD	PRO	9	B	3.6
11.	7856	CZ	TYR	523	A	<-->	159	CA	PRO	10	B	3.2
12.	7669	CE2	PHE	512	A	<-->	161	CG	PRO	10	B	3.5
13.	5665	NE2	HIS	383	A	<-->	172	OXT	CXL	11	B	3.6
14.	6108	OE1	GLU	411	A	<-->	172	OXT	CXL	11	B	3.0

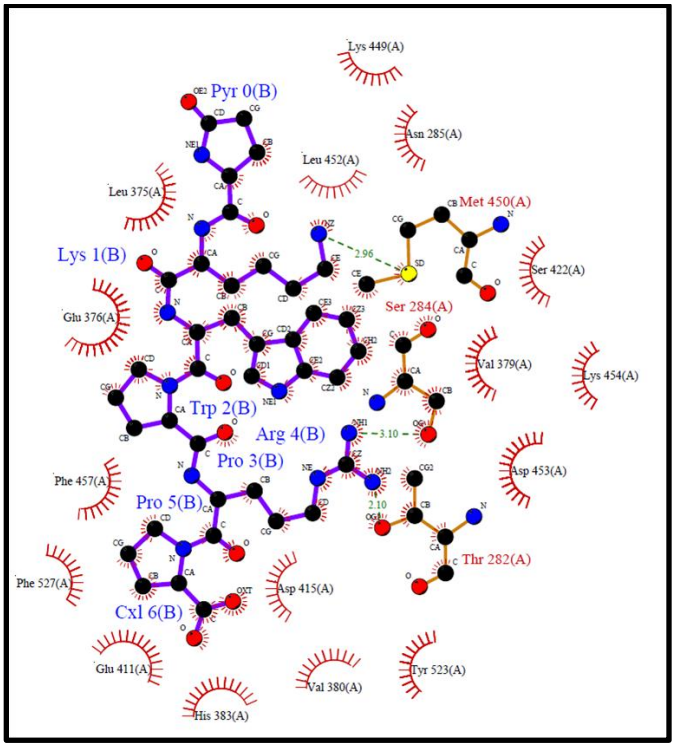

Fig. 80: Ligplot of BPP10 (ZLWPRP) in complex with tACE.

The ligplot of BPP10 in complex with tACE is shown in Fig. 80. The arginine residue of the peptide is strongly hydrogen bonded with Thr^{282} present at the S2′ site. The carboxylate group

forms hydrogen bonds with Glu[411] and His[383]. Other key intermolecular interactions of the complex are summarized in table 23.

Table 23: Key intermolecular interactions of BPP10 in complex with tACE

	Atom No.	Atom Name	Res Name	Res No.	Chain		Atom No.	Atom Name	Res Name	Res No.	Chain	Distance
1	6581	SD	MET	450	A	<-->	23	NZ	LYS	1	B	3.0
2	4021	OG1	THR	282	A	<-->	85	NH2	ARG	4	B	2.2
3	5477	CB	LEU	375	A	<-->	19	CB	LYS	1	B	3.2
4	6640	CE	LYS	454	A	<-->	48	CZ2	TRP	2	B	3.1
5	4021	OG1	THR	282	A	<-->	82	NE	ARG	4	B	3.0
6	6621	N	ASP	453	A	<-->	85	NH2	ARG	4	B	3.4
7	5605	CE1	HIS	383	A	<-->	101	CB	PRO	5	B	3.4
8	5606	NE2	HIS	383	A	<-->	113	OXT	CXL	6	B	3.3
9	6049	OE1	GLU	411	A	<-->	113	OXT	CXL	6	B	2.8

Analysis of the model complexes based on the interactions of the peptide residues with the known active site residues of tACE, and a comparison with the crystal structure of lisinopril-tACE, shows that these peptides are inhibitors of ACE enzyme, as determined by enzyme activity assay also. However the binding strength can vary depending on the length of the peptide and types of the residues present. The peptide model complexes show interactions with other side chain residues of the enzyme, which are absent in lisinopril, possibly because of the small size of this peptide like molecule. The sequence alignment of the peptides used to analyze model complexes, aligned with ClustalW, is shown below.

```
BPP1          -ZNWP--GPKVPP-- 10
BPP2          -ZNWP--GPK----- 7
BPP3          -ZRWP--GP------ 6
BPP8          -ZLWP--RPQIPP-- 10
BPP10         -ZLWP--RP------ 6
BPP4          ---RP-PHPP----- 6
BPP6          -ZARP-PHPPIPPAP 13
BPP5          -ZARP-PHPPIPP-- 11
BPP7          ZGGWPRPGPEIPP-- 13
BPP9          -ZQWP-PGHHIPP-- 11
```

The sequence alignment shows that the BPP peptides have a relatively high content of proline residue. The interpretation of the model complexes explains that proline at the C-terminus is important to guide the peptide through a small channel like cavity of the enzyme to active site, buried deep inside the enzyme. Additional prolines in the sequence also help the peptide to approach the active site. Proline is hydrophobic and a rigid amino acid, and also provides a sharp turning point to the peptide backbone, thereby facilitating the accommodation of the peptide in the active site. Further it can be concluded that peptides longer than 10-11 amino acid might not be very potent inhibitors. Secondly the incorporation of basic residues lysine, arginine and histidine towards the C-terminal can allow the peptides to interact better with the active site residues. Based on these results BPP1, BPP4, BPP5 and BPP9 seem to be good inhibitors, and the BPP4-tACE model complex can be ranked highest of all the studied complexes.

5: General discussion

Comparative analysis of the venom peptidome of the snakes selected from Viperidae, *Vipera ammodytes meridionalis* (Viperinae), *Bothrops jararacussu* (Crotalinae), *Naja mossambica mossambica* (Elapinae) and *Notechis ater niger* (Acanthophiinae) from Elapidae demonstrated the presence of representatives of three protein/peptide families: Kunitz/BPTI, BPPs/NP and three finger toxin. The results and literature data point towards a subfamily-specificity of the Viperidae and Elapidae venom peptides. Peptide fractions of the Viperinae snake venom contain both, a Kunitz type inhibitor and BPPs. The four signals of the Kunitz type inhibitor were attributed to different peptide species (propeptide, mature peptide and dehydrated peptide with pyroglutamate at the N-terminus) of one peptide inhibitor identical to that isolated from the *Vipera ammodytes ammodytes* venom [120] (Table 3). At the same time, all identified peptides from the venom of the Crotalinae snake, with the exception of several proteolytic fragments of metalloproteinases, belong to the family of bradykinin-potentiating peptides (Table 4). The *Naja mossambica mossambica* venom peptidome analysis (Table 5) shows the presence of cytotoxin type three finger toxins, and BPP type peptides, but a lack of Kunitz/BPTI inhibitors. Whereas the peptidic fractions of *Notechis ater niger* contains both Kunitz/BPTI inhibitors and neurotoxin type of three finger toxins in addition to a natriuretic peptide. The published data about the venom peptidome composition of Crotalinae and Viperinae snakes show that in the first case the venom peptide fractions contain BPPs but no Kunitz type inhibitors (with one exception of a very low content, 0.1% and < 0.1% BPTI in the venom of *Sistrurus* rattlesnakes [149]). Thus, BPPs are one of the two major toxic components of the *Bothrops insularis* venom gland (19.7% of the total transcriptome), [150]. Bradykinin-potentiating peptides are also among the most frequent transcripts of the *B. jararaca* venom gland (6.2%) [150]. High contents of hypotensive peptides were found in the venoms of the other Crotalinae snakes as *Lachesis muta* (14.7 % of the venom proteins) [20], *Lachesis stenophrys* (14.6%) [20], *Bothrops alternatus* (8.8%) [151], *Bothriechis nigroviridis* (26.9%) [152], *Bothriechis lateralis* (11.1%) [153], *Bothriechis schlegelii* (13.4%) [153] and *Crotalus simus* (2%) [124]. Small amounts of BPPs (0.8%) were found in the venom of *Bothrops colombiensis* [31].

Kunitz-type inhibitors were identified in the venoms of Viperinae snakes *Vipera ammodytes ammodytes* [120], *Eristocopbis macmaboni* (Leaf-nosed viper) [154], *Bitis gabonica* (Gaboon

viper) [155], *Vipera raddei* [19] and *Vipera ursinii renardi* [156]. Kunitz type inhibitors have been reported in many Australian elapids [136].

The Kunitz type snake venom inhibitors are considered to be involved in inactivation of proteases participating in hemostatic processes [157]. It was supposed that these venom peptides participate in the processes of coagulation, fibrinolysis and inflammation through protease inactivation [158]and references therein. A Kunitz/BPTI inhibitor textilinin has been found to be a potent and selective inhibitor of plasmin, and is under clinical trial for application as an anti bleeding agent [75]. Several Kunitz type protein inhibitors suppress tumour invasion and metastasis [159]. In the present study one of the Kunitz/BPTI inhibitor isolated from *Notechis ater niger* venom and that from *Vipera ammodytes meridionalis* were found to strongly inhibit kallikrein and showed weak inhibition of plasmin.

Among the three finger toxins, cytotoxins have been reported exclusively in the cobra venom [4]. In this study also cytotoxins were found as the main poly peptides present in the venom of *Naja mossambica mossambica*, a cobra snake and the other elapid venom under study contained neurotoxins only, and no cytotoxins could be identified.

All these data suggest differences in the evolution of the two Viperidae and Elapidae subfamilies.

In the present work we demonstrate for the first time possible phosphorylation of a serine residue in snake venom BPPs. Protein phosphorylation is a post-translational modification of proteins with the participation of kinases, which is an important regulatory mechanism [160]. The phosphorylation of BPPs results in addition of phosphate group, which would change the peptide electrostatic charge, and might influence BPP–ACE interactions. This can lead to important changes in the hypotensive effect of the bradykinin-potentiating venom peptides.

The venom peptidome of *Bothrops jararacussu* (Table 4) demonstrates a variety of BPPs due to differences in the C-terminal parts. It was shown that the C-terminus is critical for the interaction of BPPs with their natural targets [161]. Changes in this functionally important segment can lead to differences in the pharmacological effects.

BPPs are natural inhibitors of the angiotensin I-converting enzyme (EC 3.4.15.1) that plays a key role in the blood pressure regulation [162]and references therein. This property makes ACE a pharmacological target for the generation of compounds treating hypertension and cardiovascular diseases. ACE catalyzes the conversion of angiotensin I to the potent vasoconstrictor angiotensin II and the proteolytic degradation of the natural vasodilator bradykinin. BPPs block the formation of angiotensin II and its blood pressure elevating action. At the same time, the breakdown of bradykinin is prevented and its vasodilatory properties support the decrease of the blood pressure [163]. Vasodilatory effects of ACE inhibitors were used by the pharmaceutical industry to produce a large number of antihypertensive drugs such as captopril, enalaprilat, ramiprilat, lisinopril, perindoprilat and other derivatives [162] which are currently used as standard treatment of hypertension and congestive heart failure [163]and references therein. However, contemporary synthetic ACE inhibitors can induce serious adverse reactions as renal failure, angioedema, hyperkalaemia, urticaria and other undesirable cutaneous effects [163]. Also, a long term therapy with the above mentioned drugs may result in reduced efficacy of the treatment [162]. A possible reason for the side effects is the relatively low specificity of these drugs or different functions of the angiotensin converting enzyme. ACE contains two independent catalytic domains, the C-terminal being the main site of the angiotensin I hydrolysis [164]. The next generation of ACE inhibitors should act more selectively inhibiting only the N- or C-domain of the enzyme [162]. ACE is multifunctional enzyme acting on a broad spectrum of substrates as a member of the renin-angiotensin-aldosterone system and non-specific inactivation can induce changes in the function of other physiologically active peptides. In this connection novel, more specific ACE inhibitors will be of pharmacological importance. *Bothrops jararacussu* and *Vipera a. meridionalis* venoms are rich sources of such peptides. The peptide analysis presented here demonstrates the presence of a number of possibly new ACE inhibitors in the venoms of the both snakes.

The sequence homology of ACE peptide inhibitors with natriuretic peptides (Tables 3-5) suggests processing of larger precursors. It was shown that BPPs are part of two distinct C-type natriuretic peptide (CNP) precursors found in the venom gland and in the brain of another Crotalinae snake, *Bothrops jararaca* [165]. NPs from the *Dendroaspis angusticeps* (green mamba) venom exert vasodilator and natriuretic/diuretic effects [66]. The natriuretic peptide

family consists of three subfamilies: atrial NPs and brain NPs, which activate the natriuretic peptide receptor A, and C-type NPs activating the natriuretic peptide receptor B [166].

The effects of the NPs are mediated through the activation of the receptors A and B. It can be supposed that at least some of the identified BPPs result from processing of NP precursors. The homology between BPPs and precursors of natriuretic peptides from venoms of Viperidae and Elapidae snakes suggests structural similarities between ACE inhibitors of the first snake family and the respective part of the NP precursors from the venom of the second family.

These toxin homologies in snake genera, that are quite distant both from the phylogenetic and geographical point of view, are quite remarkable and suggest that these peptides must have appeared at an early stage during the evolutionary process while the fairly high homology rates indicate that a selective pressure must be acting, preserving the BPPs and the natriuretic peptides as vital components of the snake's arsenal.

Cytotoxins are known to cause cell lysis by forming pores in the cell membrane. In the present study, cytotoxin 1 isolated from *Naja mossambica mossambica* venom was found to strongly inhibit chymotrypsin and 20S proteasome. To the best of my knowledge it is a first study of a cytotoxin to demonstrate such an inhibitory activity towards chymotrypsin. Hence it is proposed that cytotoxin-1 is able to translocate itself inside the cell and disturbs the cellular processes by inhibiting a vital catalytic machinery of the cell, the 20S proteasome. Inhibition of 20S proteasome could be one of the mechanisms involved in the cytotoxin mediated cell death. The internalization of cell is supported by other studies as well [133, 134].

Conclusion

Snake venom peptide analysis demonstrates subfamily (Viperinae/Crotalinae and Elapinae/ Acanthophiinae), specificity of the venom peptidome composition in the snake family Viperidae and Elapidae. In contrast to the Crotalinae venoms, the venom peptidome of the Viperinae snakes contains Kunitz type inhibitors. The peptide composition of Acanthophiinae venom contains Kunitz type inhibitors while the Elapinae venom lacks it. Secondly Elapinae venom contains cytotoxin type of three finger toxins as compared to Acanthophiinae. Phosphorylation of a serine residue in BPPs, demonstrated for a first time in the case of *Bothrops jararacussu* venom peptides, can play an important role in the regulation of the BPP–ACE interactions. There is a homology between venom BPPs from a Viperidae snake and venom NPs from Elapidae snakes. The Kunitz/BPTI inhibitors of *Vipera a. Meridionalis* and *Notechis ater niger* are also homologous to each other. The presence of Kunitz/BPTI inhibitors among the venom of both families (Viperidae and Elapidae) indicates that this type of peptide was incorporated into the venom before the divergence of the two families. However disappearance of the peptide at the subfamily level indicates further recruitment events, in which the Kunitz/BPTI type of peptides were selectively retained in the snake venom depending on the environment of the snake. The inhibitory activity of cytoxin 1 towards chymotrypsin and 20S proteasome leads to an inference that cytotoxin 1 can enter the cell, and inhibit 20S proteasome, thereby aiding in the cell lysis, by inhibiting this catalytic machinery. However further investigations are required to understand the mechanism of action of this toxin. The tripeptide metalloproteinase inhibitors isolated from *Vipera a. meridionalis* are also proposed to be involved in preventing the auto digestion of the venom gland as reported in earlier studies. The venoms under study are rich sources of novel inhibitors. In addition to the enzyme inhibition experiments, the crystal structure of a complex of *Agkistrodon bilineatus* peptide-StmPr1 and the model complexes support this notion. The methods optimized in this work provide a basis to isolate pharmacologically active compounds from other snake venoms, and also exemplifies how these bioactive molecules may be characterized at a functional level.

Future work

The results of this work can be used to design further projects. A few examples are:

- Synthesis of snake venom BPP peptides and X-ray crystallographic studies of their complexes with human ACE. The complex structures may reveal new specific active site binding pockets of the enzyme. The complex structures might help to better understand the nature of the enzyme and lead to the design more specific drug.
- Two plasma kallikrein inhibitors have been isolated in this work. To date no crystal structure complex of Kunitz/BPTI-plasma kallikrein is available in protein data bank. The expression of these Kunitz/BPTI inhibitors, enzyme kinetic studies, and subsequent preparation of crystal complexes could lead to the design of selective inhibitors of plasma kallikrein. Selective inhibitors of plasma kallikrein are of interest to treat disease states related to increased levels of this enzyme in the blood for example hereditary angioedema and septicaemia and septic shock.
- As the analytical methods for the purification and characterization of snake venom peptides have been optimized, further investigation of the snake venom peptidome might lead to the discovery of novel bioactive molecules.

References

[1] A. Tu, Snake venoms: General background and composition, in: *Venoms: Chemistry and molecular biology*, John Wiley & Sons, New York, 1998, pp. 1-19.

[2] S. Liu, F. Yang, Q. Zhang, M.Z. Sun, Y. Gao, S. Shao, "Anatomical" view of the protein composition and protein characteristics for Gloydius shedaoensis snake venom via proteomics approach, *Anat Rec (Hoboken)*, 294 (2011) 273-282.

[3] J. Meier, K.F. Stocker, Biology and distributuion of venomous snakes of medical importance and the composition of snake venom, in: W.J. Meier J (Ed.) *Handbook of clinical toxicology of animal venoms and proteins*, CRC Press, Boca Raton, Florida, 1995, pp. 367-412.

[4] R.M. Kini, Molecular moulds with multiple missions: Functional sites in three-finger toxins, *Clinical and Experimental Pharmacology and Physiology*, 29 (2002) 815-822.

[5] D. Georgieva, M. Ohler, J. Seifert, M. von Bergen, R.K. Arni, N. Genov, C. Betzel, Snake venomic of Crotalus durissus terrificus--correlation with pharmacological activities, *J Proteome Res*, 9 (2010) 2302-2316.

[6] D. Georgieva, R.K. Arni, C. Betzel, Proteome analysis of snake venom toxins: pharmacological insights., *Expert review of proteomics*, 5 (2008) 787-797.

[7] T.S. Kang, D. Georgieva, N. Genov, M.T. Murakami, M. Sinha, R.P. Kumar, P. Kaur, S. Kumar, S. Dey, S. Sharma, A. Vrielink, C. Betzel, S. Takeda, R.K. Arni, T.P. Singh, R.M. Kini, Enzymatic toxins from snake venom: structural characterization and mechanism of catalysis, *Febs J*, 278 (2011) 4544-4576.

[8] M. Ohno, R. Menez, T. Ogawa, J.M. Danse, Y. Shimohigashi, C. Fromen, F. Ducancel, S. Zinn-Justin, M.H. Le Du, J.C. Boulain, T. Tamiya, A. Menez, Molecular evolution of snake toxins: is the functional diversity of snake toxins associated with a mechanism of accelerated evolution?, *Progress in nucleic acid research and molecular biology*, 59 (1998) 307-364.

[9] H.L. Gibbs, L. Sanz, J.E. Chiucchi, T.M. Farrell, J.J. Calvete, Proteomic analysis of ontogenetic and diet-related changes in venom composition of juvenile and adult Dusky Pigmy rattlesnakes (Sistrurus miliarius barbouri), *J Proteomics*, 74 (2011) 2169-2179.

[10] P. James, Protein identification in the post-genome era: the rapid rise of proteomics, *Quarterly reviews of biophysics* 4 (1997) 279-331.

[11] M.R. Wilkins, K.L. Williams, R.D. Appel, D.F. Hochstrasser, Proteome Research: New Frontiers in Functional Genomics., Springer, 1997.

[12] B. Lomonte, P. Rey-Suarez, W.C. Tsai, Y. Angulo, M. Sasa, J.M. Gutierrez, J.J. Calvete, Snake venomics of the pit vipers Porthidium nasutum, Porthidium ophryomegas, and Cerrophidion godmani from Costa Rica: toxicological and taxonomical insights, *J Proteomics*, 75 (2012) 1675-1689.

[13] J.W. Fox, S.M. Serrano, Exploring snake venom proteomes: multifaceted analyses for complex toxin mixtures, *Proteomics*, 8 (2008) 909-920.

[14] J.J. Calvete, Proteomic tools against the neglected pathology of snake bite envenoming, Expert review of proteomics, 8 (2011) 739-758.

[15] J. Nawarak, S. Sinchaikul, C.Y. Wu, M.Y. Liau, S. Phutrakul, S.T. Chen, Proteomics of snake venoms from Elapidae and Viperidae families by multidimensional chromatographic methods, *Electrophoresis*, 24 (2003) 2838-2854.

[16] P. Juarez, L. Sanz, J.J. Calvete, Snake venomics: characterization of protein families in Sistrurus barbouri venom by cysteine mapping, N-terminal sequencing, and tandem mass spectrometry analysis, *Proteomics*, 4 (2004) 327-338.

[17] I.H. Tsai, Y.H. Chen, Y.M. Wang, Comparative proteomics and subtyping of venom phospholipases A2 and disintegrins of Protobothrops pit vipers, *Biochim Biophys Acta*, 1702 (2004) 111-119.

[18] A.T. Ching, M.M. Rocha, A.F. Paes Leme, D.C. Pimenta, D.F.M. de Fatima, S.M. Serrano, P.L. Ho, I.L. Junqueira-de-Azevedo, Some aspects of the venom proteome of the Colubridae snake Philodryas olfersii revealed from a Duvernoy's (venom) gland transcriptome, *FEBS Lett*, 580 (2006) 4417-4422.

[19] L. Sanz, N. Ayvazyan, J.J. Calvete, Snake venomics of the Armenian mountain vipers Macrovipera lebetina obtusa and Vipera raddei, *J Proteomics*, 71 (2008) 198-209.

[20] L. Sanz, J. Escolano, M. Ferretti, M.J. Biscoglio, E. Rivera, E.J. Crescenti, Y. Angulo, B. Lomonte, J.M. Gutierrez, J.J. Calvete, Snake venomics of the South and Central American Bushmasters. Comparison of the toxin composition of Lachesis muta gathered from proteomic versus transcriptomic analysis, *J Proteomics*, 71 (2008) 46-60.

[21] A.F. Paes Leme, E.S. Kitano, M.F. Furtado, R.H. Valente, A.C. Camargo, P.L. Ho, J.W. Fox, S.M. Serrano, Analysis of the subproteomes of proteinases and heparin-binding toxins of eight Bothrops venoms, *Proteomics*, 9 (2009) 733-745.

[22] S.L. Rocha, A.G. Neves-Ferreira, M.R. Trugilho, A. Chapeaurouge, I.R. Leon, R.H. Valente, G.B. Domont, J. Perales, Crotalid snake venom subproteomes unraveled by the antiophidic protein DM43, *J Proteome Res*, 8 (2009) 2351-2360.

[23] R.H. Valente, P.R. Guimaraes, M. Junqueira, A.G. Neves-Ferreira, M.R. Soares, A. Chapeaurouge, M.R. Trugilho, I.R. Leon, S.L. Rocha, A.L. Oliveira-Carvalho, L.S. Wermelinger, D.L. Dutra, L.I. Leao, I.L. Junqueira-de-Azevedo, P.L. Ho, R.B. Zingali, J. Perales, G.B. Domont, Bothrops insularis venomics: a proteomic analysis supported by transcriptomic-generated sequence data, *J Proteomics*, 72 (2009) 241-255.

[24] S.C. Wagstaff, L. Sanz, P. Juarez, R.A. Harrison, J.J. Calvete, Combined snake venomics and venom gland transcriptomic analysis of the ocellated carpet viper, Echis ocellatus, *J Proteomics*, 71 (2009) 609-623.

[25] S.T. Chatrath, A. Chapeaurouge, Q. Lin, T.K. Lim, N. Dunstan, P. Mirtschin, P.P. Kumar, R.M. Kini, Identification of novel proteins from the venom of a cryptic snake Drysdalia coronoides by a combined transcriptomics and proteomics approach, *J Proteome Res*, 10 (2011) 739-750.

[26] J. Fernandez, A. Alape-Giron, Y. Angulo, L. Sanz, J.M. Gutierrez, J.J. Calvete, B. Lomonte, Venomic and antivenomic analyses of the Central American coral snake, Micrurus nigrocinctus (Elapidae), *J Proteome Res*, 10 (2011) 1816-1827.

[27] A. Alape-Giron, L. Sanz, J. Escolano, M. Flores-Diaz, M. Madrigal, M. Sasa, J.J. Calvete, Snake venomics of the lancehead pitviper Bothrops asper: geographic, individual, and ontogenetic variations, *J Proteome Res*, 7 (2008) 3556-3571.

[28] V. Nunez, P. Cid, L. Sanz, P. De La Torre, Y. Angulo, B. Lomonte, J.M. Gutierrez, J.J. Calvete, Snake venomics and antivenomics of Bothrops atrox venoms from Colombia and the Amazon regions of Brazil, Peru and Ecuador suggest the occurrence of geographic variation of venom phenotype by a trend towards paedomorphism, *J Proteomics*, 73 (2009) 57-78.

[29] Y. Angulo, J. Escolano, B. Lomonte, J.M. Gutierrez, L. Sanz, J.J. Calvete, Snake venomics of Central American pitvipers: clues for rationalizing the distinct envenomation profiles of Atropoides nummifer and Atropoides picadoi, *J Proteome Res*, 7 (2008) 708-719.

[30] A. Alape-Giron, M. Flores-Diaz, L. Sanz, M. Madrigal, J. Escolano, M. Sasa, J.J. Calvete, Studies on the venom proteome of Bothrops asper: perspectives and applications, *Toxicon*, 54 (2009) 938-948.

[31] J.J. Calvete, A. Borges, A. Segura, M. Flores-Diaz, A. Alape-Giron, J.M. Gutierrez, N. Diez, L. De Sousa, D. Kiriakos, E. Sanchez, J.G. Faks, J. Escolano, L. Sanz, Snake venomics and antivenomics of Bothrops colombiensis, a medically important pitviper of the Bothrops atrox-asper complex endemic to Venezuela: Contributing to its taxonomy and snakebite management, *J Proteomics*, 72 (2009) 227-240.

[32] R.A. Guercio, A. Shevchenko, J.L. Lopez-Lozano, J. Paba, M.V. Sousa, C.A. Ricart, Ontogenetic variations in the venom proteome of the Amazonian snake Bothrops atrox, *Proteome Sci*, 4 (2006) 11.

[33] A. Zelanis, A.K. Tashima, M.M. Rocha, M.F. Furtado, A.C. Camargo, P.L. Ho, S.M. Serrano, Analysis of the ontogenetic variation in the venom proteome/peptidome of Bothrops jararaca reveals different strategies to deal with prey, *J Proteome Res*, 9 (2010) 2278-2291.

[34] A. Zelanis, A.K. Tashima, A.F. Pinto, A.F. Leme, D.R. Stuginski, M.F. Furtado, N.E. Sherman, P.L. Ho, J.W. Fox, S.M. Serrano, Bothrops jararaca venom proteome rearrangement upon neonate to adult transition, *Proteomics*, 11 (2011) 4218-4228.

[35] J.J. Calvete, P. Juarez, L. Sanz, Snake venomics. Strategy and applications, *Journal of mass spectrometry*: JMS, 42 (2007) 1405-1414.

[36] J.M. Gutierrez, D. Williams, H.W. Fan, D.A. Warrell, Snakebite envenoming from a global perspective: Towards an integrated approach, *Toxicon*, 56 (2010) 1223-1235.

[37] D. Williams, J.M. Gutierrez, R. Harrison, D.A. Warrell, J. White, K.D. Winkel, P. Gopalakrishnakone, The Global Snake Bite Initiative: an antidote for snake bite, *Lancet*, 375 (2010) 89-91.

[38] K. Kulkeaw, W. Chaicumpa, Y. Sakolvaree, P. Tongtawe, P. Tapchaisri, Proteome and immunome of the venom of the Thai cobra, Naja kaouthia, *Toxicon*, 49 (2007) 1026-1041.

[39] J.M. Gutierrez, L. Sanz, J. Escolano, J. Fernandez, B. Lomonte, Y. Angulo, A. Rucavado, D.A. Warrell, J.J. Calvete, Snake venomics of the Lesser Antillean pit vipers Bothrops caribbaeus and Bothrops lanceolatus: correlation with toxicological activities and immunoreactivity of a heterologous antivenom, *J Proteome Res*, 7 (2008) 4396-4408.

[40] G.P. Espino-Solis, L. Riano-Umbarila, B. Becerril, L.D. Possani, Antidotes against venomous animals: state of the art and prospectives, *J Proteomics*, 72 (2009) 183-199.

[41] H.L. Gibbs, L. Sanz, J.J. Calvete, Snake population venomics: proteomics-based analyses of individual variation reveals significant gene regulation effects on venom protein expression in Sistrurus rattlesnakes, *Journal of molecular evolution*, 68 (2009) 113-125.

[42] J.M. Gutierrez, B. Lomonte, G. Leon, A. Alape-Giron, M. Flores-Diaz, L. Sanz, Y. Angulo, J.J. Calvete, Snake venomics and antivenomics: Proteomic tools in the design and control of antivenoms for the treatment of snakebite envenoming, *J Proteomics*, 72 (2009) 165-182.

[43] J.J. Calvete, Antivenomics and venom phenotyping: A marriage of convenience to address the performance and range of clinical use of antivenoms, *Toxicon*, 56 (2010) 1284-1291.

[44] J.J. Calvete, L. Sanz, P. Cid, P. de la Torre, M. Flores-Diaz, M.C. Dos Santos, A. Borges, A. Bremo, Y. Angulo, B. Lomonte, A. Alape-Giron, J.M. Gutierrez, Snake venomics of the Central American rattlesnake Crotalus simus and the South American Crotalus durissus complex points to neurotoxicity as an adaptive paedomorphic trend along Crotalus dispersal in South America, *J Proteome Res*, 9 (2010) 528-544.

[45] C. Correa-Netto, R. Teixeira-Araujo, A.S. Aguiar, A.R. Melgarejo, S.G. De-Simone, M.R. Soares, D. Foguel, R.B. Zingali, Immunome and venome of Bothrops jararacussu: a proteomic approach to study the molecular immunology of snake toxins, *Toxicon*, 55 (2010) 1222-1235.

[46] C. Correa-Netto, L. Junqueira-de-Azevedo Ide, D.A. Silva, P.L. Ho, M. Leitao-de-Araujo, M.L. Alves, L. Sanz, D. Foguel, R.B. Zingali, J.J. Calvete, Snake venomics and venom gland transcriptomic analysis of Brazilian coral snakes, Micrurus altirostris and M. corallinus, *J Proteomics*, 74 (2011) 1795-1809.

[47] D. Georgieva, J. Seifert, M. Ohler, M. von Bergen, P. Spencer, R.K. Arni, N. Genov, C. Betzel, Pseudechis australis venomics: adaptation for a defense against microbial pathogens and recruitment of body transferrin, *J Proteome Res*, 10 (2011) 2440-2464.

[48] T. Momic, F.T. Arlinghaus, H. Arien-Zakay, J. Katzhendler, J.A. Eble, C. Marcinkiewicz, P. Lazarovici, Pharmacological aspects of Vipera xantina palestinae venom, *Toxins (Basel)*, 3 (2011) 1420-1432.

[49] P. Rey-Suarez, V. Nunez, J.M. Gutierrez, B. Lomonte, Proteomic and biological characterization of the venom of the redtail coral snake, Micrurus mipartitus (Elapidae), from Colombia and Costa Rica, *J Proteomics*, 75 (2011) 655-667.

[50] J.J. Calvete, A. Perez, B. Lomonte, E.E. Sanchez, L. Sanz, Snake venomics of Crotalus tigris: the minimalist toxin arsenal of the deadliest Neartic rattlesnake venom. Evolutionary Clues for generating a pan-specific antivenom against crotalid type II venoms, *J Proteome Res*, 11 (2012) 1382-1390.

[51] D.C. Koh, A. Armugam, K. Jeyaseelan, Snake venom components and their applications in biomedicine, *Cellular and molecular life science*: CMLS, 63 (2006) 3030-3041.

[52] A. Gomes, P. Bhattacharjee, R. Mishra, A.K. Biswas, S.C. Dasgupta, B. Giri, Anticancer potential of animal venoms and toxins, *Indian J Exp Biol*, 48 (2010) 93-103.

[53] P.F. Reid, Alpha-cobratoxin as a possible therapy for multiple sclerosis: A review of the literature leading to its development for this application, *Critical Reviews In immunology*, 27 (2007) 291-302.

[54] B.G. Fry, K. Roelants, D.E. Champagne, H. Scheib, J.D. Tyndall, G.F. King, T.J. Nevalainen, J.A. Norman, R.J. Lewis, R.S. Norton, C. Renjifo, R.C. de la Vega, The toxicogenomic multiverse: convergent recruitment of proteins into animal venoms, *Annual review of genomics and human genetics*, 10 (2009) 483-511.

[55] F. Mari, J. Tytgat, Natural peptide toxins, in: L. Mander, H.W. Liu (Eds.) *Comprehensive Natural Products Chenistry II: Chemistry and Biology 2.*, Elsevier, Oxford, 2010, pp. 511-538.

[56] S. Mouhat, B. Jouirou, A. Mosbah, M. De Waard, J.M. Sabatier, Diversity of folds in animal toxins acting on ion channels, *Biochem J*, 378 (2004) 717-726.

[57] R.J. Lewis, M.L. Garcia, Therapeutic potential of venom peptides, *Nat Rev Drug Discov*, 2 (2003) 790-802.

[58] A.M. Pimenta, M.E. De Lima, Small peptides, big world: biotechnological potential in neglected bioactive peptides from arthropod venoms, *J Pept sci*, 11 (2005) 670-676.

[59] J.J. Calvete, Venomics: Digging into the evolution of venomous systems and learning to twist nature to fight pathology, *Journal of Proteomics*, 72 (2009) 121-126.

[60] K.K. Ng, J.R. Vane, Some properties of angiotensin converting enzyme in the lung in vivo, *Nature*, 225 (1970) 1142-1144.

[61] M.A. Ondetti, N.J. Williams, E.F. Sabo, J. Pluscec, E.R. Weaver, O. Kocy, Angiotensin-converting enzyme inhibitors from the venom of Bothrops jararaca. Isolation, elucidation of structure, and synthesis, *Biochemistry*, 10 (1971) 4033-4039.

[62] D.W. Cushman, M.A. Ondetti, Design of angiotensin converting enzyme inhibitors, *Nature* medicine, 5 (1999) 1110-1113.

[63] W.C. Hodgson, G.K. Isbister, The application of toxins and venoms to cardiovascular drug discovery, *Curr Opin Pharmacol*, 9 (2009) 173-176.

[64] Y. Zhang, J.B. Wu, G.Y. Yu, Z.M. Chen, X.D. Zhou, S.W. Zhu, R. Li, Y. Zhang, Q.M. Lu, A novel natriuretic peptide from the cobra venom, *Toxicon*, 57 (2011) 134-140.

[65] H. Schweitz, P. Vigne, D. Moinier, C. Frelin, M. Lazdunski, A New Member of the Natriuretic Peptide Family Is Present in the Venom of the Green Mamba (Dendroaspis-Angusticeps), *Journal of Biological Chemistry*, 267 (1992) 13928-13932.

[66] D.G. Johns, Z.H. Ao, B.J. Heidrich, G.E. Hunsberger, T. Graham, L. Payne, N. Elshourbagy, Q. Lu, N. Aiyar, S.A. Douglas, Dendroaspis natriuretic peptide binds to the natriuretic peptide clearance receptor, *BIOCHEMICAL AND BIOPHYSICAL RESEARCH COMMUNICATIONS*, 358 (2007) 145-149.

[67] O. Lisy, J.G. Lainchbury, H. Leskinen, J.C. Burnett, Jr., Therapeutic actions of a new synthetic vasoactive and natriuretic peptide, dendroaspis natriuretic peptide, in experimental severe congestive heart failure, *Hypertension*, 37 (2001) 1089-1094.

[68] F. Ducancel, Endothelin-like peptides, *Cellular and molecular life sciences*: CMLS, 62 (2005) 2828-2839.

[69] J. Patocka, V. Merka, V. Hrdina, R. Hrdina, Endothelins and sarafotoxins: peptides of similar structure and different function, *Acta Medica (Hradec Kralove)*, 47 (2004) 157-162.

[70] A. Scaloni, E. Di Martino, N. Miraglia, A. Pelagalli, R. Della Morte, N. Staiano, P. Pucci, Amino acid sequence and molecular modelling of glycoprotein IIb-IIIa and fibronectin receptor iso-antagonists from Trimeresurus elegans venom, *Biochem J*, 319 (Pt 3) (1996) 775-782.

[71] J.J. Calvete, Structure-function correlations of snake venom disintegrins, *Current pharmaceutical design*, 11 (2005) 829-835.

[72] E.E. Sanchez, A. Rodriguez-Acosta, R. Palomar, S.E. Lucena, S. Bashir, J.G. Soto, J.C. Perez, Colombistatin: a disintegrin isolated from the venom of the South American snake

(Bothrops colombiensis) that effectively inhibits platelet aggregation and SK-Mel-28 cell adhesion, Archives of toxicology, 83 (2009) 271-279.

[73] Y. Wang, J. Hong, X. Liu, H. Yang, R. Liu, J. Wu, A. Wang, D. Lin, R. Lai, Snake cathelicidin from Bungarus fasciatus is a potent peptide antibiotics, *PloS One*, 3 (2008) e3217.

[74] W. Chen, B. Yang, H. Zhou, L. Sun, J. Dou, H. Qian, W. Huang, Y. Mei, J. Han, Structure-activity relationships of a snake cathelicidin-related peptide, BF-15, *Peptides*, 32 (2011) 2497-2503.

[75] S.T. Earl, P.P. Masci, J. de Jersey, M.F. Lavin, J. Dixon, Drug development from Australian elapid snake venoms and the Venomics pipeline of candidates for haemostasis: Textilinin-1 (Q8008), Haempatch (Q8009) and CoVase (V0801), *Toxicon*, 59 (2012) 456-463.

[76] O. Bogin, Venom Peptides and their Mimetics as Potential Drugs, *Modulator*, (2005) 14-20.

[77] M.A. Thayer, Improving peptides, *Chem. Eng. News*, 89 (2011) 13-20.

[78] G.F. King, Venoms as a platform for human drugs: translating toxins into therapeutics, *Expert Opin Biol Th*, 11 (2011) 1469-1484.

[79] B.G. Fry, W. Wuster, S.F. Ryan Ramjan, T. Jackson, P. Martelli, R.M. Kini, Analysis of Colubroidea snake venoms by liquid chromatography with mass spectrometry: evolutionary and toxinological implications, *Rapid communications in mass spectrometry*: RCM, 17 (2003) 2047-2062.

[80] J.J. Calvete, L. Sanz, Y. Angulo, B. Lomonte, J.M. Gutierrez, Venoms, venomics, antivenomics, *FEBS Lett*, 583 (2009) 1736-1743.

[81] B.G. Fry, N.G. Lumsden, W. Wuster, J.C. Wickramaratna, W.C. Hodgson, R.M. Kini, Isolation of a neurotoxin (alpha-colubritoxin) from a nonvenomous colubrid: evidence for early origin of venom in snakes, *Journal of molecular evolution*, 57 (2003) 446-452.

[82] B.G. Fry, W. Wuster, R.M. Kini, V. Brusic, A. Khan, D. Venkataraman, A.P. Rooney, Molecular evolution and phylogeny of elapid snake venom three-finger toxins, *Journal of molecular evolution*, 57 (2003) 110-129.

[83] B.G. Fry, W. Wuster, Assembling an arsenal: origin and evolution of the snake venom proteome inferred from phylogenetic analysis of toxin sequences, *Mol Biol Evol*, 21 (2004) 870-883.

[84] B.G. Fry, From genome to "venome": molecular origin and evolution of the snake venom proteome inferred from phylogenetic analysis of toxin sequences and related body proteins, *Genome Res*, 15 (2005) 403-420.

[85] M. Li, B.G. Fry, R.M. Kini, Putting the brakes on snake venom evolution: the unique molecular evolutionary patterns of Aipysurus eydouxii (Marbled sea snake) phospholipase A2 toxins, *Mol Biol Evol*, 22 (2005) 934-941.

[86] B.G. Fry, N. Vidal, J.A. Norman, F.J. Vonk, H. Scheib, S.F. Ramjan, S. Kuruppu, K. Fung, S.B. Hedges, M.K. Richardson, W.C. Hodgson, V. Ignjatovic, R. Summerhayes, E. Kochva, Early evolution of the venom system in lizards and snakes, *Nature*, 439 (2006) 584-588.

[87] B.G. Fry, H. Scheib, L. van der Weerd, B. Young, J. McNaughtan, S.F. Ramjan, N. Vidal, R.E. Poelmann, J.A. Norman, Evolution of an arsenal: structural and functional diversification of the venom system in the advanced snakes (Caenophidia), *Molecular & cellular proteomics*: MCP, 7 (2008) 215-246.

[88] N. Vidal, S.B. Hedges, Higher-level relationships of caenophidian snakes inferred from four nuclear and mitochondrial genes, *Comptes rendus biologies*, 325 (2002) 987-995.

[89] N. Vidal, Colubroid systematics: evidence for an earlyappearance of the venom apparatus followed by extensive evolutionary tinkering., *J. Toxicol. Toxin Rev*, 21 (2002) 21-41.

[90] P. Juarez, I. Comas, F. Gonzalez-Candelas, J.J. Calvete, Evolution of Snake Venom Disintegrins by Positive Darwinian Selection, *Molecular Biology and Evolution*, 25 (2008) 2391-2407.

[91] L.C. Correa, D.P. Marchi-Salvador, A.C. Cintra, S.V. Sampaio, A.M. Soares, M.R. Fontes, Crystal structure of a myotoxic Asp49-phospholipase A2 with low catalytic activity: Insights into Ca2+-independent catalytic mechanism, *Biochim Biophys Acta*, 1784 (2008) 591-599.

[92] D. Georgieva, M. Risch, A. Kardas, F. Buck, M. von Bergen, C. Betzel, Comparative analysis of the venom proteomes of Vipera ammodytes ammodytes and Vipera ammodytes meridionalis, *Journal of Proteome Research*, 7 (2008) 866-886.

[93] B. Branch, *Field Guide to the Snakes and Other Reptiles of Southern Africa*, Ralph Curtis Publishing, 1998.

[94] U.K. Laemmli, Cleavage of structural proteins during the assembly of the head of bacteriophage T4, *Nature*, 227 (1970) 680-685.

[95] H. Schagger, PROTOCOL. Tricine-SDS-PAGE, Nature Protocols, 1 (2006) 16-22.

[96] A.K. Carmona, S.L. Schwager, M.A. Juliano, L. Juliano, E.D. Sturrock, A continuous fluorescence resonance energy transfer angiotensin I-converting enzyme assay, *Nature Protocols*, 1 (2006) 1971-1976.

[97] A. Negm, X-ray structure analysis of a pathogenic bacterial protease from *Stenotrophomonas maltophilia* towards drug discovery, in: Department of Chemistry, University of Hamburg, 2011.

[98] D.N. Georgieva, S. Stoeva, W. Voelter, N. Genov, C. Betzel, Substrate specificity of the highly alkalophilic bacterial proteinase esperase: relation to the x-ray structure, *Current microbiology*, 42 (2001) 368-371.

[99] Y. Li, Y.Q. Qian, W.M. Ma, W.J. Yang, Inhibition Mechanism and the Effects of Structure on Activity of Male Reproduction-Related Peptidase Inhibitor Kazal-Type (MRPINK) of Macrobrachium rosenbergii, *Marine Biotechnology*, 11 (2009) 252-259.

[100] Y.J. Chang, N. Hamaguchi, S.C. Chang, W. Ruf, M.C. Shen, S.W. Lin, Engineered recombinant factor VII Q217 variants with altered inhibitor specificities, *Biochemistry*, 38 (1999) 10940-10948.

[101] Y.M. Choo, K.S. Lee, H.J. Yoon, Y. Qiu, H. Wan, M.R. Sohn, H.D. Sohn, B.R. Jin, Antifibrinolytic role of a bee venom serine protease inhibitor that acts as a plasmin inhibitor, *PloS One*, 7 (2012) e32269.

[102] M.L. Lai, S.W. Chen, Y.H. Chen, Purification and characterization of a trypsin inhibitor from mouse seminal vesicle secretion, *Archives of biochemistry and biophysics*, 290 (1991) 265-271.

[103] S. Nam, D.M. Smith, Q.P. Dou, Ester bond-containing tea polyphenols potently inhibit proteasome activity in vitro and in vivo, *The Journal of biological chemistry*, 276 (2001) 13322-13330.

[104] R. Glas, M. Bogyo, J.S. McMaster, M. Gaczynska, H.L. Ploegh, A proteolytic system that compensates for loss of proteasome function, *Nature*, 392 (1998) 618-622.

[105] K.F. Huang, C.C. Hung, S.H. Wu, S.H. Chiou, Characterization of three endogenous peptide inhibitors for multiple metalloproteinases with fibrinogenolytic activity from the

venom of Taiwan habu (Trimeresurus mucrosquamatus), *Biochem Biophys Res Commun*, 248 (1998) 562-568.

[106] R. Marques-Porto, I. Lebrun, D.C. Pimenta, Self-proteolysis regulation in the Bothrops jararaca venom: The metallopeptidases and their intrinsic peptidic inhibitor, *Comp Biochem Phys C*, 147 (2008) 424-433.

[107] S.M. Lonergan, M.H. Johnson, C.R. Calkins, Improved Calpain Assay Using Fluorescein Isothiocyanate-Labeled Casein, *J Food Sci*, 60 (1995) 72-&.

[108] D.N. Perkins, D.J. Pappin, D.M. Creasy, J.S. Cottrell, Probability-based protein identification by searching sequence databases using mass spectrometry data, *Electrophoresis*, 20 (1999) 3551-3567.

[109] B. Boeckmann, A. Bairoch, R. Apweiler, M.C. Blatter, A. Estreicher, E. Gasteiger, M.J. Martin, K. Michoud, C. O'Donovan, I. Phan, S. Pilbout, M. Schneider, The SWISS-PROT protein knowledgebase and its supplement TrEMBL in 2003, *Nucleic Acids Res*, 31 (2003) 365-370.

[110] B. Ma, K. Zhang, C. Hendrie, C. Liang, M. Li, A. Doherty-Kirby, G. Lajoie, PEAKS: powerful software for peptide de novo sequencing by tandem mass spectrometry, *Rapid communications in mass spectrometry*: RCM, 17 (2003) 2337-2342.

[111] B.W. Matthews, Solvent content of protein crystals, *Journal of molecular biology*, 33 (1968) 491-497.

[112] A.A. Vagin, R.A. Steiner, A.A. Lebedev, L. Potterton, S. McNicholas, F. Long, G.N. Murshudov, REFMAC5 dictionary: organization of prior chemical knowledge and guidelines for its use, *Acta crystallographica. Section D, Biological crystallography*, 60 (2004) 2184-2195.

[113] T. Schwede, J. Kopp, N. Guex, M.C. Peitsch, SWISS-MODEL: An automated protein homology-modeling server, *Nucleic Acids Res*, 31 (2003) 3381-3385.

[114] K. Arnold, L. Bordoli, J. Kopp, T. Schwede, The SWISS-MODEL workspace: a web-based environment for protein structure homology modelling, *Bioinformatics*, 22 (2006) 195-201.

[115] N. Guex, M.C. Peitsch, SWISS-MODEL and the Swiss-PdbViewer: an environment for comparative protein modeling, *Electrophoresis*, 18 (1997) 2714-2723.

[116] S.R. Comeau, D.W. Gatchell, S. Vajda, C.J. Camacho, ClusPro: a fully automated algorithm for protein-protein docking, *Nucleic Acids Res*, 32 (2004) W96-99.

[117] D. Kozakov, D.R. Hall, D. Beglov, R. Brenke, S.R. Comeau, Y. Shen, K. Li, J. Zheng, P. Vakili, I. Paschalidis, S. Vajda, Achieving reliability and high accuracy in automated protein docking: ClusPro, PIPER, SDU, and stability analysis in CAPRI rounds 13-19, *Proteins*, 78 (2010) 3124-3130.

[118] S.R. Comeau, D.W. Gatchell, S. Vajda, C.J. Camacho, ClusPro: an automated docking and discrimination method for the prediction of protein complexes, *Bioinformatics*, 20 (2004) 45-50.

[119] D. Kozakov, R. Brenke, S.R. Comeau, S. Vajda, PIPER: an FFT-based protein docking program with pairwise potentials, *Proteins*, 65 (2006) 392-406.

[120] A. Ritonja, B. Meloun, F. Gubensek, The primary structure of Vipera ammodytes venom trypsin inhibitor I, *Biochim Biophys Acta*, 748 (1983) 429-435.

[121] V. Rioli, B.C. Prezoto, K. Konno, R.L. Melo, C.F. Klitzke, E.S. Ferro, M. Ferreira-Lopes, A.C.M. Camargo, F.C.V. Portaro, A novel bradykinin potentiating peptide isolated from Bothrops jararacussu venom using catallytically inactive oligopeptidase EP24.15, *Febs J*, 275 (2008) 2442-2454.

[122] Y. Komori, H. Sugihara, Characterization of a New Inhibitor for Angiotensin Converting Enzyme from the Venom of Vipera-Aspis-Aspis, *Int J Biochem*, 22 (1990) 767-771.

[123] D. Ianzer, K. Konno, R. Marques-Porto, F.C. Vieira Portaro, R. Stocklin, A.C. Martins de Camargo, D.C. Pimenta, Identification of five new bradykinin potentiating peptides (BPPs) from Bothrops jararaca crude venom by using electrospray ionization tandem mass spectrometry after a two-step liquid chromatography, *Peptides*, 25 (2004) 1085-1092.

[124] L.S. Wermelinger, D.L. Dutra, A.L. Oliveira-Carvalho, M.R. Soares, C. Bloch, Jr., R.B. Zingali, Fast analysis of low molecular mass compounds present in snake venom: identification of ten new pyroglutamate-containing peptides, *Rapid communications in mass spectrometry*: RCM, 19 (2005) 1703-1708.

[125] G.H. Souza, R.R. Catharino, D.R. Ifa, M.N. Eberlin, S. Hyslop, Peptide fingerprinting of snake venoms by direct infusion nano-electrospray ionization mass spectrometry: potential use in venom identification and taxonomy, *Journal of mass spectrometry*: JMS, 43 (2008) 594-599.

[126] M.A. Larkin, G. Blackshields, N.P. Brown, R. Chenna, P.A. McGettigan, H. McWilliam, F. Valentin, I.M. Wallace, A. Wilm, R. Lopez, J.D. Thompson, T.J. Gibson, D.G. Higgins, Clustal W and Clustal X version 2.0, *Bioinformatics*, 23 (2007) 2947-2948.

[127] P.V. Dubovskii, D.M. Lesovoy, M.A. Dubinnyi, Y.N. Utkin, A.S. Arseniev, Interaction of the P-type cardiotoxin with phospholipid membranes, *European journal of biochemistry* / FEBS, 270 (2003) 2038-2046.

[128] A.I. Louw, "Snake venom toxins. The amino acid sequences of three cytotoxin homologues from Naja mossambica mossambica venom.", *Biochim. Biophys. Acta*., (1974) 481-495.

[129] J.M. Peters, W.W. Franke, J.A. Kleinschmidt, Distinct 19 S and 20 S subcomplexes of the 26 S proteasome and their distribution in the nucleus and the cytoplasm, *The Journal of biological chemistry*, 269 (1994) 7709-7718.

[130] A. Ciechanover, Early work on the ubiquitin proteasome system, an interview with Aaron Ciechanover. Interview by CDD, *Cell death and differentiation*, 12 (2005) 1167-1177.

[131] J. Wang, M.A. Maldonado, The ubiquitin-proteasome system and its role in inflammatory and autoimmune diseases, *Cellular & molecular immunology*, 3 (2006) 255-261.

[132] M. Ploug, V. Ellis, Structure-function relationships in the receptor for urokinase-type plasminogen activator. Comparison to other members of the Ly-6 family and snake venom alpha-neurotoxins, *FEBS Lett*, 349 (1994) 163-168.

[133] A.V. Feofanov, G.V. Sharonov, M.V. Astapova, D.I. Rodionov, Y.N. Utkin, A.S. Arseniev, Cancer cell injury by cytotoxins from cobra venom is mediated through lysosomal damage, *Biochem J*, 390 (2005) 11-18.

[134] S.H. Su, S.J. Su, S.R. Lin, K.L. Chang, Cardiotoxin-III selectively enhances activation-induced apoptosis of human CD8+ T lymphocytes, *Toxicology and applied pharmacology*, 193 (2003) 97-105.

[135] L. St Pierre, H. Fischer, D.J. Adams, M. Schenning, N. Lavidis, J. de Jersey, P.P. Masci, M.F. Lavin, Distinct activities of novel neurotoxins from Australian venomous snakes for nicotinic acetylcholine receptors, *Cellular and molecular life sciences*: CMLS, 64 (2007) 2829-2840.

[136] L. St Pierre, S.T. Earl, I. Filippovich, N. Sorokina, P.P. Masci, J. De Jersey, M.F. Lavin, Common evolution of waprin and kunitz-like toxin families in Australian venomous snakes, *Cellular and molecular life sciences*: CMLS, 65 (2008) 4039-4054.

[137] R. Helland, I. Leiros, G.I. Berglund, N.P. Willassen, A.O. Smalas, The crystal structure of anionic salmon trypsin in complex with bovine pancreatic trypsin inhibitor, *European journal of biochemistry* / FEBS, 256 (1998) 317-324.

[138] A.J. Scheidig, T.R. Hynes, L.A. Pelletier, J.A. Wells, A.A. Kossiakoff, Crystal structures of bovine chymotrypsin and trypsin complexed to the inhibitor domain of Alzheimer's amyloid beta-protein precursor (APPI) and basic pancreatic trypsin inhibitor (BPTI): engineering of inhibitors with altered specificities, *Protein science*: a publication of the Protein Society, 6 (1997) 1806-1824.

[139] E.K. Millers, M. Trabi, P.P. Masci, M.F. Lavin, J. de Jersey, L.W. Guddat, Crystal structure of textilinin-1, a Kunitz-type serine protease inhibitor from the venom of the Australian common brown snake (Pseudonaja textilis), *Febs J*, 276 (2009) 3163-3175.

[140] J.E. Syka, J.J. Coon, M.J. Schroeder, J. Shabanowitz, D.F. Hunt, Peptide and protein sequence analysis by electron transfer dissociation mass spectrometry, *Proceedings of the National Academy of Sciences of the United States of America*, 101 (2004) 9528-9533.

[141] H.N. Behnken, M. Fellenberg, M.P. Koetzler, R. Jirmann, T. Nagel, B. Meyer, Resolving the problem of chromatographic overlap by 3D cross correlation (3DCC) processing of LC, MS and NMR data for characterization of complex glycan mixtures, *Analytical and bioanalytical chemistry*, 404 (2012) 1427-1437.

[142] L. Quinton, N. Gilles, N. Smargiasso, A. Kiehne, E. De Pauw, An unusual family of glycosylated peptides isolated from Dendroaspis angusticeps venom and characterized by combination of collision induced and electron transfer dissociation, *Journal of the American Society for Mass Spectrometry*, 22 (2011) 1891-1897.

[143] J. Tang, C.L. Yu, S.R. Williams, E. Springman, D. Jeffery, P.A. Sprengeler, A. Estevez, J. Sampang, W. Shrader, J. Spencer, W. Young, M. McGrath, B.A. Katz, Expression, crystallization, and three-dimensional structure of the catalytic domain of human plasma kallikrein, *The Journal of biological chemistry*, 280 (2005) 41077-41089.

[144] A.E. Schmidt, H.S. Chand, D. Cascio, W. Kisiel, S.P. Bajaj, Crystal structure of Kunitz domain 1 (KD1) of tissue factor pathway inhibitor-2 in complex with trypsin. Implications

for KD1 specificity of inhibition, *The Journal of biological chemistry*, 280 (2005) 27832-27838.

[145] Y.Y. He, S.B. Liu, W.H. Lee, J.Q. Qian, Y. Zhang, Isolation, expression and characterization of a novel dual serine protease inhibitor, OH-TCI, from king cobra venom, *Peptides*, 29 (2008) 1692-1699.

[146] M.R. Ehlers, E.A. Fox, D.J. Strydom, J.F. Riordan, Molecular cloning of human testicular angiotensin-converting enzyme: the testis isozyme is identical to the C-terminal half of endothelial angiotensin-converting enzyme, *Proceedings of the National Academy of Sciences of the United States of America*, 86 (1989) 7741-7745.

[147] R. Natesh, S.L. Schwager, E.D. Sturrock, K.R. Acharya, Crystal structure of the human angiotensin-converting enzyme-lisinopril complex, *Nature*, 421 (2003) 551-554.

[148] J.L. Guy, R.M. Jackson, K.R. Acharya, E.D. Sturrock, N.M. Hooper, A.J. Turner, Angiotensin-converting enzyme-2 (ACE2): comparative modeling of the active site, specificity requirements, and chloride dependence, *Biochemistry*, 42 (2003) 13185-13192.

[149] L. Sanz, H.L. Gibbs, S.P. Mackessy, J.J. Calvete, Venom proteomes of closely related Sistrurus rattlesnakes with divergent diets, *J Proteome Res*, 5 (2006) 2098-2112.

[150] D.A. Cidade, T.A. Simao, A.M. Davila, G. Wagner, I.L. Junqueira-de-Azevedo, P.L. Ho, C. Bon, R.B. Zingali, R.M. Albano, Bothrops jararaca venom gland transcriptome: analysis of the gene expression pattern, *Toxicon*, 48 (2006) 437-461.

[151] K.C. Cardoso, M.J. Da Silva, G.G. Costa, T.T. Torres, L.E. Del Bem, R.O. Vidal, M. Menossi, S. Hyslop, A transcriptomic analysis of gene expression in the venom gland of the snake Bothrops alternatus (urutu), *BMC genomics*, 11 (2010) 605.

[152] J. Fernandez, B. Lomonte, L. Sanz, Y. Angulo, J.M. Gutierrez, J.J. Calvete, Snake venomics of Bothriechis nigroviridis reveals extreme variability among palm pitviper venoms: different evolutionary solutions for the same trophic purpose, *J Proteome Res*, 9 (2010) 4234-4241.

[153] B. Lomonte, J. Escolano, J. Fernandez, L. Sanz, Y. Angulo, J.M. Gutierrez, J.J. Calvete, Snake venomics and antivenomics of the arboreal neotropical pitvipers Bothriechis lateralis and Bothriechis schlegelii, *J Proteome Res*, 7 (2008) 2445-2457.

[154] A.R. Siddiqi, Z.H. Zaidi, H. Jornvall, Purification and characterization of a Kunitz-type trypsin inhibitor from Leaf-nosed viper venom, *FEBS Lett*, 294 (1991) 141-143.

[155] I.M. Francischetti, V. My-Pham, J. Harrison, M.K. Garfield, J.M. Ribeiro, Bitis gabonica (Gaboon viper) snake venom gland: toward a catalog for the full-length transcripts (cDNA) and proteins, *Gene*, 337 (2004) 55-69.

[156] I.H. Tsai, Y.M. Wang, A.C. Cheng, V. Starkov, A. Osipov, I. Nikitin, Y. Makarova, R. Ziganshin, Y. Utkin, cDNA cloning, structural, and functional analyses of venom phospholipases A(2) and a Kunitz-type protease inhibitor from steppe viper Vipera ursinii renardi, *Toxicon*, 57 (2011) 332-341.

[157] B.G. Fry, Structure-function properties of venom components from Australian elapids, *Toxicon*, 37 (1999) 11-32.

[158] V. Zupunski, D. Kordis, F. Gubensek, Adaptive evolution in the snake venom Kunitz/BPTI protein family, *FEBS Lett*, 547 (2003) 131-136.

[159] W.M. Chou, W.H. Liu, K.C. Chen, L.S. Chang, Structure-function studies on inhibitory activity of Bungarus multicinctus protease inhibitor-like protein on matrix metalloprotease-2, and invasion and migration of human neuroblastoma SK-N-SH cells, *Toxicon*, 55 (2010) 353-360.

[160] C. Chang, R.C. Stewart, The two-component system. Regulation of diverse signaling pathways in prokaryotes and eukaryotes, *Plant physiology*, 117 (1998) 723-731.

[161] D.C. Pimenta, B.C. Prezoto, K. Konno, R.L. Melo, M.F. Furtado, A.C. Camargo, S.M. Serrano, Mass spectrometric analysis of the individual variability of Bothrops jararaca venom peptide fraction. Evidence for sex-based variation among the bradykinin-potentiating peptides, *Rapid communications in mass spectrometry*: RCM, 21 (2007) 1034-1042.

[162] M. Akif, D. Georgiadis, A. Mahajan, V. Dive, E.D. Sturrock, R.E. Isaac, K.R. Acharya, High-resolution crystal structures of Drosophila melanogaster angiotensin-converting enzyme in complex with novel inhibitors and antihypertensive drugs, *Journal of molecular biology*, 400 (2010) 502-517.

[163] U.M. Steckelings, M. Artuc, T. Wollschlager, S. Wiehstutz, B.M. Henz, Angiotensin-converting enzyme inhibitors as inducers of adverse cutaneous reactions, *Acta dermato-venereologica*, 81 (2001) 321-325.

[164] S. Fuchs, H.D. Xiao, C. Hubert, A. Michaud, D.J. Campbell, J.W. Adams, M.R. Capecchi, P. Corvol, K.E. Bernstein, Angiotensin-converting enzyme C-terminal catalytic domain is the main site of angiotensin I cleavage in vivo, *Hypertension*, 51 (2008) 267-274.

[165] M.A. Hayashi, A.C. Camargo, The Bradykinin-potentiating peptides from venom gland and brain of Bothrops jararaca contain highly site specific inhibitors of the somatic angiotensin-converting enzyme, *Toxicon*, 45 (2005) 1163-1170.

[166] P.J. Best, J.C. Burnett, S.H. Wilson, D.R. Holmes, Jr., A. Lerman, Dendroaspis natriuretic peptide relaxes isolated human arteries and veins, *Cardiovascular research*, 55 (2002) 375-384.

List of chemicals and GHS hazards

Name of the reagent	Provider	CAS-No	GHS hazard	Risk phrases	Safety Phrases
Acetic acid (100 %)	ROTH	64-19-7	H226, H314	10-35	23-26-45
Acetonitrile-HPLC grade	Merck	75-05-8	H225, H302, H312, H319, H332	11-20/21/22-36	16-36/37
Angiotensin converting enzyme from rabbit lung (A6778- 0.25 UN)	Sigma Aldrich	9015-82-1	-	-	-
Abz-FRK (Dnp) P-OH	Aminotech Research and Development, Sao Paulo, Brazil	-	-	-	-
Ammonium persulphate	Carl Roth	7727-54-0	H272, H302, H315, H317, H319, H334; H335	8-22-36/37/38-42/43	22-24-26-37
Ammonium bicarbonate BioUltra	Fluka	1066-33-7	H302	22	
Acrylamide/bisacrylamide solution 40% (19:1), 30%(37.5:1)	Carl Roth	79-06-1	H301, H312, H316, H317, H319, H332, H340, H350, H361f, H372	45-46-20/21-25-48/23/24/25-36/38-43/62	53-26-36/37-45
Bovine Trypsin (T1426-100 mg)	Sigma	9002-07-7	H315, H319, H334, H335	36/37/38-42	22-24-26-36/37
Bromo phenol blue	Biorag	115-39-9	-	-	22-24/25
Bz-phe-val-arg-pNA (I-1150)	Bachem	54799-93-8	-	-	-
Suc-Ala-Ala-Pro-Phe-pNA (L-1400)	Bachem	70967-97-4	-	-	-
Z-D-Arg-Gly-Arg-pNA-HCl (L-2115)	Bachem	113711-77-6	-	-	-
Bz-Arg-pNA (L-1130)	Bachem	21653-40-7	-	-	-
Bz-Pro-Phe-Arg-pNA (L-1545)	Bachem	59188-28-2	-	-	-
Z-Gly-Gly-Leu-AMC (I-1425)	Bachem	97792-39-7	-	-	-
Casein	Sigma	9000-71-9	-	-	-
Chymotrypsin from bovine pancreas (C7762-25 mg)	Sigma	904-07-3	H315, H319, H334, H335	36/37/38-42	22-24-26-36/37
Coomassie brilliant blue	Applichem	6104-59-2	-	-	22-24/25
Dithiothreitol	Sigma	578517	H302, H315, H319, H335	22-36/37/38	26-36
DMSO	Sigma	67-68-5	-	36/37/38	23-26-36

Name of the reagent	Provider	CAS-No	GHS hazard	Risk phrases	Safety Phrases
Factor Xa from bovine plasma (F9302-50 µg)	Sigma	9002-05-5	-	-	-
Formic acid	Sigma Aldrich	64-18-6	H226, H314	35	23-26-45
Hydrochloric acid, 37%	Merck	7647-01-0	H314, H335	34-37	26-36/37/39-45
Iodoacetamide	Sigma Aldrich	144-48-9	H301, H307, H337, H413	25-42/43	22-36/37-45
Isopropanol	Carl Roth	67-63-0	H225, H319, H336	11-36-67	7/6-24/25-26
Kallikrein from human plasma (K2638-50 µg)	Sigma	9001-01-8	-	-	-
Plasmin from human plasma (P1867-150 µg)	Sigma	9001-90-5	-	-	-
20 S Proteasome fraction from rabbit (P3988-25µg)	Sigma	-	-	-	-
Protein marker (SM 1816, SM1891, SM0431)	Fermentas		H302, H312, H315, H319, H335	21/22-36/37/38	-
SDS	Sigma	151-21-3	H228, H302, H311, H315, H319, H335	11-21/22-36/37/38	26-36/37
Sodium hydroxide	Merck	1310-73-2	H314	35	26-37/39-45
Thrombin from human plasma (T6884-100 UN)	Sigma	9002-04-4	H315, H319, H334, H335	-	-
Tris(hydroxymethyl)aminomethane	Carl Roth	76-86-1	H315, H319, H335	36/37/38	26-36
Tricine	Applichem	5704-04-01	-	-	-
Urea	Merck	57-13-6	-	-	-
Water LiChrosolv	Merck	7732-18-5	-	-	-

Acknowledgement

I am thankful to Almighty Allah who has given me the strength and ambition to acquire knowledge and complete this auspicious task.

I am thankful to my parents, my husband Munawar, my kids Ahmad and Amna for their love, care and pray for me and for their continuous encouragement and support to achieve this milestone. Thanks to my brothers Saud and Waqas for their support throughout my work.

I feel honored to express my sincere appreciation and gratitude to my respected supervisor Prof. C. Betzel for his continuous pursuance, consistent encouragement, keen interest, kind and motivating attitude and his most valuable guidance and support to complete this task. I am grateful to him for providing me all the facilities and opportunities for a successful completion of this work.

I am deeply indebted to Dr. P Spencer for his helpful discussions, nice suggestions, technical advice, moral support and encouragement. It was nice to work with him in the lab as he makes science easier by creating a friendly and relaxed environment. I am also grateful to him for generously providing the venom samples. His support was absolutely indispensable.

I endow special thanks to Prof. H. Schlüter, for providing mass spectrometric facilities for peptide analysis, his helpful discussions and interest in my results, his kind and welcoming temperament. Special thanks to all his group members for supporting the mass spectrometric part of my work.

I am very much grateful to Dr. M. Trusch for guiding me with mass spectrometric methods for peptide analysis, closely looking at my results, always welcoming for discussion and encouraging me. Her support greatly facilitated the progress of my work.

Special thanks to Prof. Dr. Genov and Dr. Georgieva for their help in the preparation and discussion of the manuscript.

I shall always cherish the knowledge I gained from all these experienced people during my stay at Germany.

Acknowledgement

My sincere appreciation and thanks to my colleagues and friends, especially Dr. Begum, Dr. Negm and Dr. Rehders for their extended cooperation, timely and precious advice towards successful completion of this work.

At the end I would like to thank the University of Engineering and Technology, Lahore, Pakistan for granting me study leave, HEC, Pakistan and DAAD, Germany for funding my stay here.

Aisha Munawar

Selbstständigkeitserklärung

Hiermit erkläre ich an Eides statt, dass ich die an der Universität Hamburg zur Promotion eingereichte Dissertation mit dem Titel:

"Analysis of the low molecular weight peptides of selected snake venoms"

im Institut für Biochemie des Fachbereichs Chemie der Universität Hamburg unter der Leitung von Herrn Prof. C. Betzel ohne sonstige Hilfe durchgeführt und bei der Abfassung der Dissertation keine anderen als die dort aufgeführten Hilfsmittel benutzt habe.

Ferner versichere ich, dass ich bisher an keiner in- oder ausländischen Universität ein Gesuch um Zulassung zur Promotion eingereicht und weder diese noch eine andere Arbeit als Dissertation vorgelegt habe.

Aisha Munawar

Hamburg, 14thSeptember, 2012